

This is to certify that the

thesis entitled

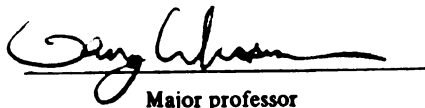
Characterization of Aquifer Heterogeneity and Tracer Test
Simulations by Incorporating Geologic Information in the
Form of Outcrop Analog and Well Core at a Distal and
Medial Outwash Aquifer in Schoolcraft, Michigan

presented by

Susanne Evelyn Biteman

has been accepted towards fulfillment
of the requirements for

Master's degree in Geology



Major professor

Date August 22, 2002

LIBRARY
Michigan State
University

**PLACE IN RETURN BOX to remove this checkout from your record.
TO AVOID FINES return on or before date due.
MAY BE RECALLED with earlier due date if requested.**

[illegible]

CHARACTERIZATION OF AQUIFER HETEROGENEITY AND TRACER TEST
SIMULATIONS BY INCORPORATING GEOLOGIC INFORMATION IN THE
FORM OF OUTCROP ANALOG AND WELL CORE AT A DISTAL AND MEDIAL
OUTWASH AQUIFER IN SCHOOLCRAFT, MICHIGAN

By

Susanne Evelyn Biteman

A THESIS

Submitted to
Michigan State University
In partial fulfillment of the requirements
for the degree of

MASTER OF SCIENCE

Department of Geological Sciences

2002

C
S
F

at

zu

w

S

M

et

et

th

ti

co

co

no

et

si

ABSTRACT

CHARATERIZATION OF AQUIFER HETEROGENEITY AND TRACER TEST SIMULATIONS BY INCORPORATING GEOLOGIC INFORMATION IN THE FORM OF OUTCROP ANALOG AND WELL CORE AT DISTAL AND MEDIAL OUTWASH AQUIFER IN SCHOOLCRAFT, MICHIGAN

by

Susanne Evelyn Biteman

The integration of geostatistics and geologic data in the form of outcrop analogs and well core produced detailed models of aquifer heterogeneity using two methods, zonal kriging and transition probability geostatistics (Carle and Fogg, 1996). This study was conducted at the Schoolcraft Plume A site, located in Kalamazoo County, Michigan. Sediments at this site were deposited as outwash medial and distal to the Kalamazoo Moraine. Using core data from the site and outcrop analog data from nearby sand and gravel pits, the aquifer was separated into major sedimentologic units to preserve abrupt changes in hydraulic conductivity and to better honor the assumption of stationarity. For the first geostatistical method, zonal kriging was used to estimate hydraulic conductivity distribution. After geostatistic estimation all the zones were combined to produce a complete aquifer realization. A non-zonal kriging was also generated using the same conditioning data but without the geologically based zones. Both the zonal kriging and the non-zonal kriging hydraulic conductivity values were used as inputs for three dimensional ground water flow models and transport simulations. The zonal kriging more accurately simulates the migration of an injected tracer pulse.

t

s

i

E

t

s

i

P

b

a

S

m

ACKNOWLEDGEMENTS

I extend my thanks to my advisor Dr. Gary Weissmann who has helped me over the past two years by providing stimulating discussion which have lead me to have a greater knowledge and understanding of the many aspects of hydrogeology. His insightful reviews of this manuscript were greatly appreciated. Committee members Dr. David Hyndman and Dr. Grahame Larson provided much knowledge and experience throughout the different stages of this project. M.S. Phanikumar's help with the groundwater modeling and transport simulations was irreplaceable. I thank Michelle Vit for her help conducting the field work portion of this study. This research was funded in part by Michigan Department of Environmental Quality (Contract # Y40386) and in part by Michigan State University through Dr. Gary Weissmann's set up fund.

I would thank my parents and my brother who have supported me throughout my educational endeavors. I would also like to thank my friends who have experienced graduate school with me, most of all Jennifer Wade, who has been a wonderful friend to me. I am especially grateful to my husband, Adam for his absolute love and support.

TABLE OF CONTENTS

| | |
|---|------------|
| LIST OF TABLES | vii |
| LIST OF FIGURES | x |
| I. INTRODUCTION AND SCOPE OF WORK | 1 |
| INTRODUCTION | 1 |
| PURPOSE OF THE STUDY | 3 |
| THESIS OUTLINE | 5 |
| II. PREVIOUS WORK | 7 |
| GEOLOGY | 7 |
| Regional Bedrock Geology | 7 |
| Glacial History of Southwestern Michigan | 9 |
| General Stratigraphy and Sedimentology of Glaciofluvial Deposit | 12 |
| HYDROGEOLOGY | 20 |
| Regional Hydrogeology | 20 |
| History of Contamination at Plume A | 23 |
| Bioremediation of Plume A | 24 |
| III. INTEGRATION OF SEDIMENTOLOGIC AND HYDROGEOLOGIC PROPERTIES FOR IMPROVED TRANSPORT SIMULATIONS: DETAILED CHARACTERIZATION OF A GLACIAL OUTWASH AQUIFER AT THE SCHOOLCRAFT BIOREMEDIATION SITE, MICHIGAN..... | 25 |
| INTRODUCTION | 26 |
| SITE DESCRIPTION | 28 |
| CORE DESCRIPTIONS | 32 |

| | |
|--|-----------|
| Methods | 32 |
| <i>Core facies interpretation</i> | 34 |
| Schoolcraft Stratigraphic Evaluation | 37 |
| OUTCROP ANALOG | 41 |
| GEOSTATISTICS | 42 |
| GROUNDWATER MODELING AND TRACER TEST SIMULATIONS | 44 |
| RESULTS AND DISCUSSION | 49 |
| CONCLUSTIONS | 51 |
| IV. TRANSITION PROBABILITY GROSTATISTICS | 52 |
| INTRODUCTION | 52 |
| STRATIFICATION OF ZONES | 54 |
| Explanation of Hydrofacies from Categories | 54 |
| Top Zone | 56 |
| Bottom Zone | 61 |
| MARKOV CHAIN MODELS | 64 |
| Top Zone Markov Chain Models | 64 |
| Bottom Zone Markov Chain Models | 69 |
| CONDITIONAL SEQUENTIAL INDICATOR SIMULATION | 77 |
| COMBINING THE ZONES | 77 |
| CONCLUSIONS | 81 |
| V. CONCLUSIONS | 82 |
| DEPOSTIONAL ENVIRONMENT OF THE AQUIFER BELOW SCHOOLCRAFT..... | 82 |
| AQUIFER CHARACTERIZATIONS | 83 |

Kriging Method84

Transition Probability Method84

APPENDIX A. STRATIGRAPHY OF THE SCHOOLCRAFT PLUME A SITE ..86

CORE DATA86

INTERPRETATIONS OF DEPOSITIONAL ENVIRONMENT OF THE
AQUIFER BENEATH SCHOOLCRAFT86

APPENDIX B. OUTCROP ANALOGS123

REFERENCES134

LIST OF TABLES

| | | |
|-----------|---|----|
| TABLE 3.1 | Anisotropy values for vertical K and horizontal K, determined by comparing repacked to non-repacked core..... | 35 |
| TABLE 3.2 | Vertical K (cm/s) of facies vs. sorting from well P18..... | 35 |
| TABLE 3.3 | Horizontal K (cm/s) statistics for the four stratigraphic zones and the non-zonal model..... | 40 |
| TABLE 3.4 | Variogram parameters for zonal krige and non-zonal krige. All variograms fit using exponential model..... | 45 |
| TABLE 4.1 | Mean grain size (GS) in Phi unit, corresponding Wentworth size class (Boggs, 2001), mean standard deviation (SD), sorting based on standard deviation (Boggs, 2001), and number of data points in each zone for the transition probability (T.P.) zones and the four zonal kriging zones. Zone one is the same for the transition probability and zonal krige zones..... | 55 |
| TABLE 4.2 | Proportions of hydrofacies in the top and bottom zone..... | 55 |
| TABLE 4.3 | Hydrofacies and corresponding assigned category for the top zone with high K value, low K value, average K value, and number of points..... | 57 |
| TABLE 4.4 | Hydrofacies and corresponding assigned category for the bottom zone with high K value, low K value, average K value, and number of points..... | 57 |
| TABLE 4.5 | Embedded transition probability matrices for the top zone. These matrices are read as transition probabilities from the row hydrofacies to the column hydrofacies. (hydrofacies labels: PMS, poorly sorted medium sand; PCS, poorly sorted coarse sand; MWFS, moderately to well sorted fine sand; PFS, poorly sorted fine sand; VFS, very fine sand. Other labels: L, mean length. Bold numbers indicate background category with computed values listed in the table.)..... | 66 |
| TABLE 4.6 | Embedded transition probability matrices for the bottom zone. These matrices are read as transition probabilities from the row hydrofacies to the column hydrofacies. (hydrofacies labels: PGVCS, pebbles, gravel and very coarse sand; WMS, well sorted medium sand; PCS, poorly sorted coarse sand; PMS, poorly sorted medium sand; MWFS, moderately to well sorted fine sand. Other labels: L, mean length. Bold numbers | |

| | |
|---|----|
| indicate background category with computed values listed in the table). | 73 |
|---|----|

| | | |
|-----------|---|-----|
| TABLE 4.7 | W.r.t independent transition frequencies matrices for the bottom zone. These matrices are read as independent transition probabilities from the row hydrofacies to the column hydrofacies. (hydrofacies labels: PGVCS, pebbles, gravel and very coarse sand; WMS, well sorted medium sand; PCS, poorly sorted coarse sand; PMS, poorly sorted medium sand; MWFS, moderately to well sorted fine sand. Other labels: L, mean length. Bold numbers indicate background category with computed values listed in the table.)..... | 75 |
| TABLE A.1 | Key for the core descriptions..... | 92 |
| TABLE A.2 | Well D2. X, Y, and Z location, Log K value, mean grain size (determined by sieve analysis), and sorting (determined by standard deviation of grain size (Boggs, 2001))..... | 116 |
| TABLE A.3 | Well D4. X, Y, and Z location, Log K value, mean grain size (determined by sieve analysis), and sorting (determined by standard deviation of grain size (Boggs, 2001))..... | 117 |
| TABLE A.4 | Well D6. X, Y, and Z location, Log K value, mean grain size (determined by sieve analysis), and sorting (determined by standard deviation of grain size (Boggs, 2001))..... | 118 |
| TABLE A.5 | Well D8. X, Y, and Z location, Log K value, mean grain size (determined by sieve analysis), and sorting (determined by standard deviation of grain size (Boggs, 2001))..... | 119 |
| TABLE A.6 | Well D10. X, Y, and Z location, Log K value, mean grain size (determined by sieve analysis), and sorting (determined by standard deviation of grain size (Boggs, 2001))..... | 120 |
| TABLE A.7 | Well D12. X, Y, and Z location, Log K value, mean grain size (determined by sieve analysis), and sorting (determined by standard deviation of grain size (Boggs, 2001))..... | 121 |
| TABLE A.8 | Well D14. X, Y, and Z location, Log K value, mean grain size (determined by sieve analysis), and sorting (determined by standard deviation of grain size (Boggs, 2001))..... | 122 |
| TABLE B.1 | Key for photomosaics..... | 123 |

| | | |
|------------------|--|------------|
| TABLE B.2 | Description of outcrop analog shown in Figure B.5. Bed number, mean grain size, grain size range, sorting, facies, and apparent trends are given..... | 129 |
| TABLE B.3 | Description of outcrop analog shown in Figure B.5. Bed number, mean grain size, grain size range, sorting, facies, and apparent trends are given..... | 131 |
| TABLE B.4 | Description of outcrop analog shown in Figure B.5. Bed number, mean grain size, grain size range, sorting, facies, and apparent trends are given..... | 133 |

LIST OF FIGURES

| | | |
|------------|---|----|
| FIGURE 2.1 | Bedrock map of the Lower Peninsula of Michigan. Kalamazoo County is outlined in black. Modified from Milstein, 1987. Image is presented in color..... | 8 |
| FIGURE 2.2 | Location of Moraines in southwestern Michigan. Notice the interlobate boundary marking the extent of both the Saginaw and Lake Michigan lobes. Kalamazoo County is marked by a bold outline. Modified from Monaghan <i>et al.</i> , 1986..... | 10 |
| FIGURE 2.3 | Till sheets underlying moraines in southwestern Michigan. Modified from Monaghan <i>et al.</i> , 1986..... | 11 |
| FIGURE 2.4 | Figure 2.4. Study areas of Steinmann (1994) and Baresse (1991). Boundary of Prairie Rhonde Fan as described by Steinmann, marked by Steinmann's study area. Modified from Baresse, 1991 and Steinmann, 1994..... | 13 |
| FIGURE 2.5 | Principal bar types and where they form in a stream. Modified from Miall, 1977..... | 16 |
| FIGURE 2.6 | Vertical facies models of Scott-type, Donjeck-type and Bijou Creek type. Modified from Miall, 1977; 1996..... | 17 |
| FIGURE 2.7 | Block diagrams showing the braided stream patterns associated with Scott-type streams (A), Donjeck-type streams (B), and Platte type Streams (C). Modified from Miall, 1985..... | 18 |
| FIGURE 2.8 | Study area of Lipinski (2002) regional model. Lipinski's smaller scale transport model is outlined by the bold rectangle near Schoolcraft. Modified from Lipinski, 2002..... | 22 |
| FIGURE 3.1 | Kalamazoo County Surficial Geology, location of Kalamazoo Moraine and outcrop site used for this study. Modified from Monaghan and Larson, (1982)..... | 29 |
| FIGURE 3.2 | Schoolcraft Plume A site. Location of biocurtian is marked by arrow. Modified from Mayotte (1991)..... | 31 |
| FIGURE 3.3 | Location of delivery wells (D) and monitoring wells (MW) at the Plume A Schoolcraft site..... | 33 |

FIG

FI

FI

FI

FIG

FIG

FIG

FIG

FIGU

FIGU

FIGUR

| | | |
|------------|---|----|
| FIGURE 3.4 | Core description of P18 showing zonal boundaries (marked by arrows) and measured vertical K..... | 38 |
| FIGURE 3.5 | Cross-section of log K data points used for interpolation. Figure 3.5a is transect through the delivery wells, Figure 3.5b is a transect through the down gradient wells (Figure 3.3 for location). Zonal boundaries picked at 16 m bgs, 20 m bgs, and 21 m bgs. Scalebar is in log K (cm/s)..... | 39 |
| FIGURE 3.6 | A portion of the outcrop analog showing the stratigraphic character of the outwash material with a shovel for scale. Image is presented in color.... | 43 |
| FIGURE 3.7 | Zonal (top) and non-zonal (bottom) kriged results. Arrows mark boundaries of zones in zonal kriging. Note that abrupt changes in K are preserved in zonal kriging approach. Scalebar is in log K (cm/s)..... | 46 |
| FIGURE 3.8 | Discretization of grid in plan view, delivery well gallery is located near the center of the grid, marked by light colored squares where discretization is the finest..... | 48 |
| FIGURE 3.9 | Measured tracer test from site (x) with simulated zonal kriging (black line) and simulated non-zonal kriging (gray line)..... | 50 |
| FIGURE 4.1 | Top zone of Schoolcraft site, 1-5 are categories of hydrofacies, corresponds to Table 4.3. Top diamond is high K value, bottom diamond is low K value and middle diamond is mean K value. | |
| FIGURE 4.2 | Cross-section of categories in top zone. Category 1, poorly sorted medium sand (PMS); category 2, poorly sorted coarse sand (PCS); category 3, moderately to well sorted fine sand (MWFS); category 4, poorly sorted fine sand (PFS); category 5, very fine sand (VFS). X axis is depth (m). Image is presented in color..... | 60 |
| FIGURE 4.3 | Bottom zone of Schoolcraft site, 1-5 categories of hydrofacies, corresponds to Table 4.4. Top diamond is high K value, bottom diamond is low K value and middle diamond is mean K value..... | 62 |
| FIGURE 4.4 | Matrix of vertical (z)-direction transition probabilities showing core data as measurements (open circles) and the Markov chain model (solid line) from the core measurements. The diagonal elements represent auto-transition probabilities within each category, and the off diagonal elements represent transition probabilities between categories..... | 63 |
| FIGURE 4.5 | Matrix of perpendicular to flow (y)-direction transition probabilities showing core data as measurements (open circles) and the Markov chain model (solid line) from the core measurements. The diagonal elements | |

represent auto-transition probabilities within each category, and the off diagonal elements represent transition probabilities between categories..68

- FIGURE 4.6 Cross-section of category in bottom zone. Category 1, pebbles, granules and very coarse sand (PGVCS); category 2, poorly sorted medium sand (PMS); category 3 poorly sorted coarse sand (PCS); category 4, poorly sorted medium sand (PMS); category 5, moderately and moderately to well sorted fine sand (MWFS). Image is presented in color.....70
- FIGURE 4.7 Outcrop analog with 0.25 m grid overlay. Image is presented in color...71
- FIGURE 4.8 Matrix of vertical (z)-direction transition probabilities showing core data as measurements (open circles) and the Markov chain model (solid line) from the core measurements. The diagonal elements represent auto-transition probabilities within each category, and the off diagonal elements represent transition probabilities between categories.....72
- FIGURE 4.9 Matrix of perpendicular to flow (y)-direction transition probabilities showing core data as measurements (open circles) and the Markov chain model (solid line) from the core measurements. The diagonal elements represent auto-transition probabilities within each category, and the off diagonal elements represent transition probabilities between categories..76
- FIGURE 4.10 A realization of the Schoolcraft plume A site based on transition probability/ Markov chain geostatistics in two zones. This image is presented in color.....79
- FIGURE 4.11 A realization of the Schoolcraft plume A site based on transition probability/ Markov chain geostatistics in two zones. This image is presented in color.....80
- FIGURE A.1 Location of delivery wells (D), monitoring wells (MW), peizometers (P) and other wells at the Schoolcraft plume A site.
- FIGURE A.2a Core descriptions of well P18. Vertical K measurements shown in second column.....93
- FIGURE A.2b Core descriptions of well P18. Vertical K measurements shown in second column.....94
- FIGURE A.2c Core descriptions of well P18. Vertical K measurements shown in second column.....95
- FIGURE A.2d Core descriptions of well P18. Vertical K measurements shown in second column.....96

| | |
|---|-----|
| FIGURE A.2e Core descriptions of well P18. Vertical K measurements shown in second column..... | 97 |
| FIGURE A.3a Core descriptions of well P6..... | 98 |
| FIGURE A.3b Core descriptions of well P6..... | 99 |
| FIGURE A.4a Core descriptions of well P7..... | 100 |
| FIGURE A.4b Core descriptions of well P7..... | 101 |
| FIGURE A.5a Core descriptions of well P8..... | 102 |
| FIGURE A.5b Core descriptions of well P8..... | 103 |
| FIGURE A.5c Core descriptions of well P8..... | 104 |
| FIGURE A.5d Core descriptions of well P8..... | 105 |
| FIGURE A.5e Core descriptions of well P8..... | 106 |
| FIGURE A.5f Core descriptions of well P8..... | 107 |
| FIGURE A.6a Core descriptions of well P9..... | 108 |
| FIGURE A.6b Core descriptions of well P9..... | 109 |
| FIGURE A.7a Core descriptions of well P11..... | 110 |
| FIGURE A.7b Core descriptions of well P11..... | 111 |
| FIGURE A.8a Core descriptions of well P12..... | 112 |
| FIGURE A.8b Core descriptions of well P12..... | 113 |
| FIGURE A.8c Core descriptions of well P12..... | 114 |
| FIGURE A.8d Core descriptions of well P12..... | 115 |
| FIGURE B.1 Photomosaic of outcrop analog at Azon pit. Yellow lines represent bounding surfaces. Thinner lines represent lower order bounding surfaces. Shovel for scale. Image is presented in color..... | 124 |

FIGURE B.2 Photomosaic of outcrop analog at Azon pit. Yellow lines represent bounding surfaces. Thinner lines represent lower order bounding surfaces. Shovel for scale. Image is presented in color.....125

FIGURE B.3 Photomosaic of outcrop analog at Azon pit. Yellow lines represent bounding surfaces. Thinner lines represent lower order bounding surfaces. All measurements are in centimeters and are shown by pink arrows. Image is presented in color.....126

FIGURE B.4 Photomosaic of outcrop analog at Stadler sand and gravel pit. Yellow lines represent bounding surfaces. Thinner lines represent lower order bounding surfaces. Height of outcrop is approximately 12 meters. Image is presented in color.....127

FIGURE B.5 Photomosaic of outcrop analog at Stadler sand and gravel pit. Yellow lines represent bounding surfaces. Thinner lines represent lower order bounding surfaces. Measurements are in centimeters and are shown by pink arrows. Bed numbers correspond to descriptions given in Table B.2. Image is presented in color.....128

FIGURE B.6 Photomosaic of outcrop analog at Stadler sand and gravel pit. Yellow lines represent bounding surfaces. Thinner lines represent lower order bounding surfaces. Measurements are in centimeters and are shown by pink arrows. Bed numbers correspond to descriptions given in Table B.3. Image is presented in color.....130

FIGURE B.7 Photomosaic of outcrop analog at Stadler sand and gravel pit. Yellow lines represent bounding surfaces. Thinner lines represent lower order bounding surfaces. Measurements are in centimeters and are shown by pink arrows. Bed numbers correspond to descriptions given in Table B.4. Image is presented in color.....132

Chapter One

Introduction and Scope of Work

Introduction

Inaccurate characterizations of aquifer heterogeneity commonly result in simulations of groundwater flow and contaminant transport that are inadequate to fully understand the migration of contaminant plumes. The need to more accurately simulate the migration of fluids has led to better heterogeneity characterization approaches in aquifers through incorporation of more geologic information. Koltermann and Gorelick (1996) stated that in order to accurately model and predict containment transport, we must be able to predict the spatial variability of hydraulic properties. Many studies e.g Borden (Sudicky, 1986); Cape Cod (Hess *et al.*, 1991); Twin Lake (Moltyaner and Killey, 1998; MADE site (Adams and Gelhar, 1992; Boggs *et al.*, 1992; Renfeldt *et al.*, 1992) have shown that the resolution of acquired data necessary for predicting solute transport cannot be achieved by standard subsurface investigation techniques such as pumping tests, flow meter measurements or core analysis. Klingbeil *et al.* (1999) stated that aquifer stress tests by pumping yield parameters at a scale much larger than the typical length of structures in a heterogeneous aquifer. When characterizing an aquifer, focus should be placed on fine scale geologic properties rather than on larger scale hydraulic responses of the wells to accurately predict fluid flow and solute transport (Klingbeil *et al.*, 1999). Weissmann and Fogg (1999) used the geology and stratigraphy as a framework for geostatistical realizations in order to preserve stationarity.

Most geologic information comes from boreholes. Core from boreholes can be described for geologic features, or core can be described using standard engineering geology techniques. Geophysical logs may also be used in boreholes to test resistivity, conductivity, porosity, density and other parameters. Although measurements that come from a borehole may yield enough detailed information to characterize heterogeneity in the vertical direction, the spacing between boreholes is generally too great to yield sufficient information on the heterogeneity in the horizontal direction.

One approach to increasing lateral geologic information is studying an outcrop composed of similar stratigraphy and similar lithologies as the aquifer of interest. This outcrop may be viewed as an analog to the aquifer (“outcrop analog”). Miall, (1985), used outcrop analogs to interpret facies architecture in fluvial settings, however using them as a characterization tool of the subsurface to create a geologic based characterization of an aquifer or reservoir is a relatively new idea.

Many recent researchers have used outcrop analogs as an aid to subsurface characterization of aquifers and reservoirs (Davis *et al.*, 1993; Davis *et al.*, 1997; Robinson and McCabe, 1997; Anderson *et al.*, 1999; Bersezio *et al.*, 1999; Klingbeil *et al.*, 1999; and Hornung and Aigner, 1999). Anderson *et al.* (1999) quantified the spatial distribution of hydrofacies in braided stream deposits using two approaches 1) a small scale outcrop analog and 2) a large scale model of a medial braided stream deposit. In both approaches, three-dimensional images showing interconnectedness of high K units were used as inputs to a groundwater flow model and flow paths were analyzed by following the transport of particles. They found that particles that were uniformly distributed at the up gradient end of the model were clustered along preferential flow

paths during transport, showing that connection among high permeability facies is a critical factor in hydrogeological investigations involving solute transport. Bersezio *et al.* (1999) found strong anisotropic behavior in two-dimensional groundwater models based on an outcrop analog exposure in a delta environment, which was attributed to the layering of sedimentologic units. Davis *et al.* (1993) suggested that architectural elements may provide a role in evaluating aquifer heterogeneity at the scale of meters. Davis *et al.* (1997) used three different meter scale outcrops to demonstrate that fluvial bounding surfaces provide a good geological basis for conceptualizing and modeling heterogeneity in alluvial deposits. Klingbeil *et al.* (1999) defined 5 hydrofacies from 23 lithofacies at an outcrop analog composed primarily of gravel. These hydrofacies were to be used in subsequent hydrogeological analysis. Hornung and Aigner (1999) characterized an aquifer using fluvial architectural elements (Miall, 1985, 1996) on a large alluvial plain outcrop analog. Nine architectural elements were recognized in their study, and information collected in this study provided a database for subsequent fluid flow simulations. Robinson and McCabe (1997) measured geometries of sand and shale bodies in a braided fluvial environment, generated a three-dimensional stratigraphic model of the reservoir, and simulated flow through the model. They found that flood deposits affected flow in the simulation by having sufficient thickness and lateral extent to compartmentalize reservoir flow units and increase vertical flow tortuosity.

Purpose of the study

The purpose of this study was to apply stratigraphic methods of aquifer characterization of Weissmann and Fogg (1999) to a smaller scale in a glacial outwash

setting. This method uses stratigraphic breaks identified in core to define zones of similar deposits and model heterogeneity within the stratigraphic framework. This is important because it provides a framework to better honor the stationary assumption. The mean and standard deviation of the zones is more spatially consistent within the zones than in the entire aquifer. This method also better preserves abrupt changes in K that would commonly be smoothed with traditional geostatistics.

This method was implemented at the Schoolcraft Plume A site, located in the village of Schoolcraft southwest of Kalamazoo in Kalamazoo County, Michigan. The Schoolcraft Plume A site is located in a 27 m thick sand and gravel aquifer that overlies a regional till layer that acts as an aquitard, with a water table at 4.5 m below ground surface. Seven contaminant plumes (A-G) have been identified in the Schoolcraft area. The focus of this project is a transect across the down gradient end of plume A, at the site of the Schoolcraft bioaugmentation project (Hyndman *et al.*, 2000; Dybas *et al.*, 2002). Plume A is roughly 1.2 km long and 90 m wide, and extends from 8 to 26.5 m below ground surface (Hyndman *et al.*, 2000). This study site was selected for this project for the following reasons: 1) much closely spaced core data is available, 2) hydrologic and injected tracer test measurements exist for the site, 3) it is a site of ongoing groundwater investigation, and 4) detailed characterization approaches are needed to improve previous groundwater flow models and transport simulations.

The main approach used to characterize aquifer heterogeneity at the Schoolcraft site was zonal kriging, which is a method where the aquifer parameters are kriged within zones of similar geology. The mean and standard deviation of K is more spatially consistent within each zone, thereby better honoring the stationarity assumption. To test

the effects of zonal kriging, a non-zonal krige distribution of K was estimated using the same conditioning data but without dividing the data into stratigraphically based zones. Transition probability geostatistics was used as another method to characterize the heterogeneity. Both the zonal krige and the transition probability geostatistics methods were used within a stratigraphic framework provided by core descriptions, with lateral correlation lengths supplemented by measured data from outcrop analogs. Stratigraphic breaks in core identifying major bounding surfaces were used to define stratigraphic zones used in zonal kriging. To test the hypothesis that a better aquifer characterization would lead to a better tracer test comparison, both the zonal and non-zonal kriged aquifer characterizations were used as inputs to groundwater flow models and tracer test simulations. A closer match of the simulated tracer to the measured tracer breakthrough from field tracer tests indicates a positive test of the hypothesis. Running tracer simulations through the transition probability geostatistics results was beyond the scope of this thesis.

Thesis outline

This document is divided into four main sections with subsequent appendices:

- The first section, covered by chapter two, describes the bedrock and glacial geology of the study region. A brief review is given of previous hydrological studies in Kalamazoo County, specifically in the Schoolcraft Aquifer, and the history of contamination and bioremediation of Plume A.
- The second section, covered by chapter three, presents an approach to incorporate geostatistical estimation into a stratigraphic framework utilizing zonal kriging to better represent aquifer characterization. Using a high-

resolution three-dimensional flow model and transport simulation, simulation of an injected tracer pulse was improved. This chapter forms a manuscript that has been submitted for publication (Biteman, *et al. submitted*).

- The third section, covered by chapter four, applies a transition probability / Markov chain approach in a stratigraphic framework to simulate the distribution of K. The stratigraphy provides a framework in which the K distribution can be simulated while better honoring the stationarity assumption.
- The fourth section, covered by chapter five, reviews the overall conclusions of the work conducted for this thesis.
- Subsequent appendices are attached and list core descriptions, outcrop analog photomosaics and descriptions, and data tables that were used / collected in this study.

Chapter 2

Previous Work

Geology

Regional Bedrock Geology

Kalamazoo County overlies the southwestern rim of the Michigan basin. The Michigan Basin is nearly 5 km deep with a radius of approximately 250 km (Howell and van der Pluijm, 1990). The Michigan Basin reveals a number of subsidence reactivations and cessations (Sleep and Sloss, 1978). Howell and van der Pluijm (1999) cite evidence to support their theory that episodes of different types of subsidence occurred from the Cambrian to Pennsylvanian to form the Michigan Basin. The Mississippian Marshall Formation subcrops in the most northeastern corner of Kalamazoo County and the Mississippian Coldwater Shale Formation subcrops over the remainder of Kalamazoo County (figure 2.1) (Forstater and Sorensen, 1982). In the early Mississippian, the Coldwater Shale was deposited as a fine grained mud in an off shore environment and at the close of the early Mississippian, a reduction of the seas caused much of southern Michigan to become a beach environment (Dorr and Eschman, 1970). The Marshall Formation was deposited at this time and is composed of the Marshall Sandstone and Napoleon Sandstone. The Coldwater Shale is blue-gray in color and contains small amounts of limestone, dolomite, siltstone and sandstone (Martin, 1957). The bedrock which subcrops under Schoolcraft consists of a limestone facies of the Coldwater Shale. The surface of the limestone slopes gently towards the northwest (Mayotte, 1991).

Bedrock Geology of Lower Peninsula

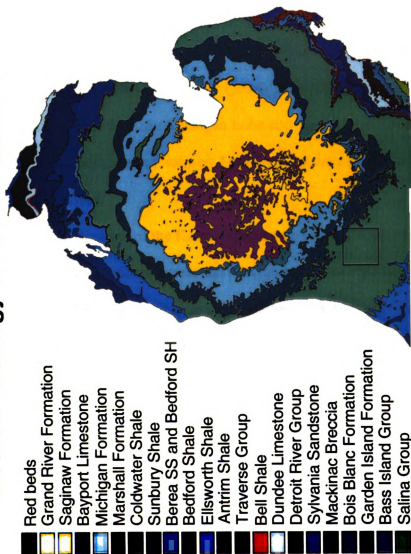


Figure 2.1. Bedrock map of the Lower Peninsula of Michigan. Kalamazoo County is outlined in black. Modified from Milstein, 1987. Image is presented in color.

Glacial History of Southwestern Michigan

With the exception of recent alluvial deposits, the sediments that overlie bedrock in Kalamazoo County were deposited in the last glacial episode, the late Wisconsinan, as the Laurentide Ice Sheet retreated. Researchers believe that both the Saginaw and Michigan Lobes of the Laurentide Ice Sheet contributed to surficial deposits in Kalamazoo County (Monahan and Larson, 1982; Monahan *et al.*, 1986; Monahan and Larson, 1986; Finkbeiner, 1994). Finkbeiner (1994) stated that the county is located within a reentrant between the Lake Michigan Lobe and the Saginaw Lobe. Figure 2.2 shows the location of moraines in southwest Michigan and the extent of both the Saginaw and Lake Michigan Lobes.

The prominent features of the Kalamazoo Moraine are the main reason that so many authors believe a significant retreat and readvance occurred before its formation (Finkbeiner, 1994). The presence of lacustrine sediments between the Ganges and Saugatuck Tills implies that a significant retreat of the Lake Michigan Lobe occurred between the formation of the Tekonsha Moraine and the Sturgis-Kalamazoo Morainic System (Monaghan *et al.*, 1986). Monaghan *et al.* (1986) showed contrasting mineralogy of clays within different till units and concluded that the Saugatuck, Ganges and Glenn Shores tills are unlikely to represent till facies of the same advance. An east-west cross-section through southwestern Michigan summarizes the correlations of Moraine and underlying till unit as proposed by Monaghan *et al.* (1986) (Figure 2.3).

Outwash deposited as meltwater from the glacier compose approximately two thirds of the surficial deposits in Kalamazoo County. Studies by Straw (1991) and Steinman (1994) presented descriptions of the outwash fans in Kalamazoo County. The

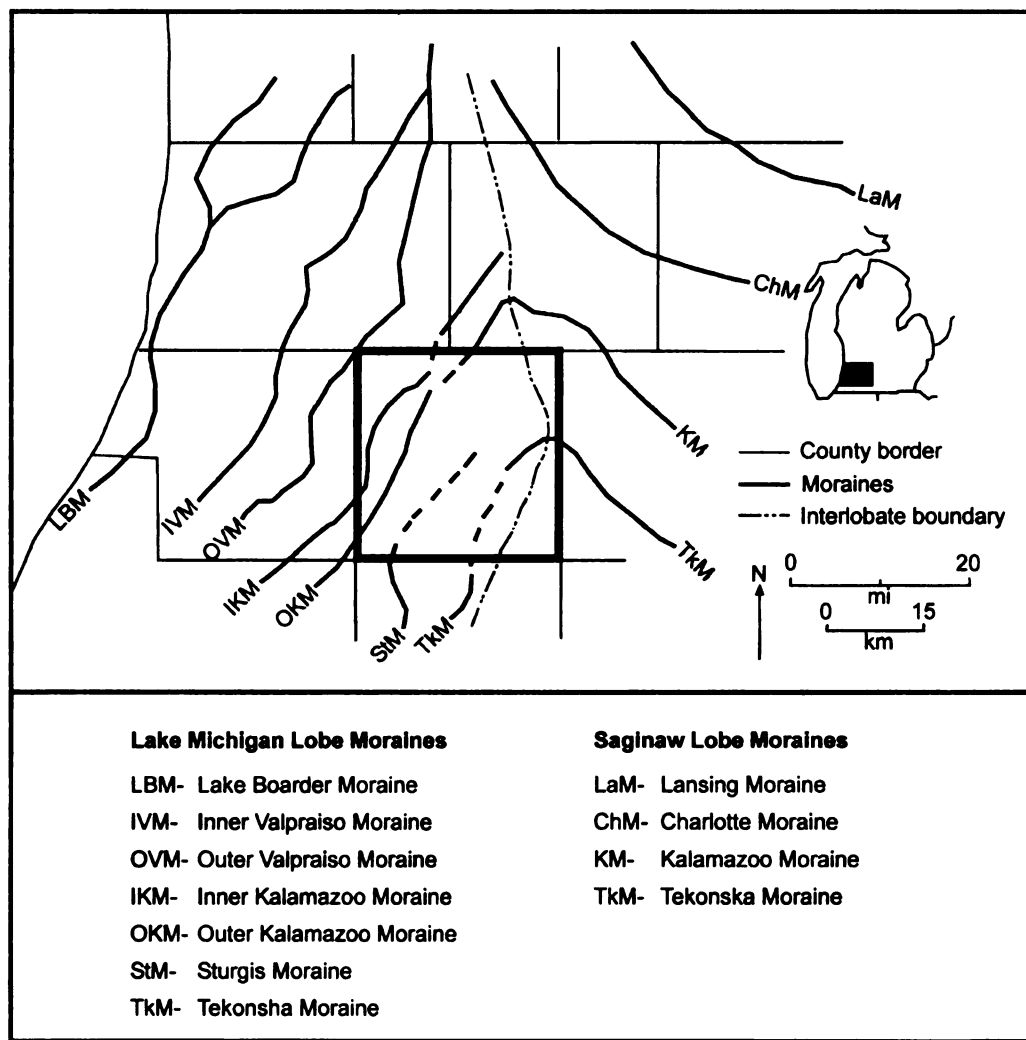


Figure 2.2. Location of Moraines in southwestern Michigan. Notice the interlobate boundary marking the extent of both the Saginaw and Lake Michigan lobes. Kalamazoo County is marked by a bold outline. Modified from Monaghan *et al.*, 1986.

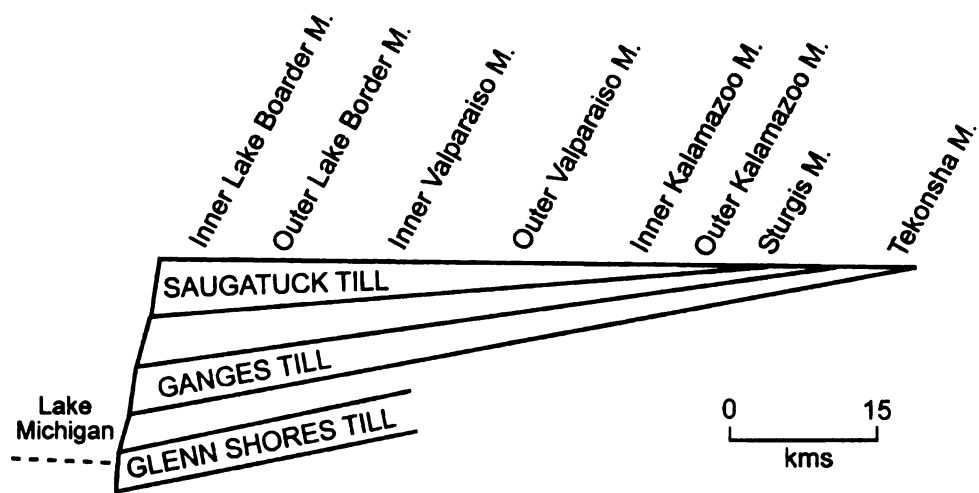


Figure 2.3. Till sheets underlying moraines in southwestern Michigan. Modified from Monaghan *et al.*, 1986.

city of Schoolcraft lies within the Prairie Rhonde Fan, described by Steinman (1994). The Prairie Rhone Fan was deposited when meltwater and outwash broke through a narrow breach in the Kalamazoo Moraine near Paw Paw Lake and deposited the material from braided streams throughout Prairie Rhonde and Schoolcraft Townships Steinman (1994) (Figure 2.4).

General Stratigraphy and Sedimentology of Glaciofluvial Deposits

Streams that are fed from glacial meltwater carry enormous quantities of detrital sediment, most of which is deposited in broad alluvial plains called sandar or sandurs (Icelandic: “sand plains”, singular sandur) (Smith, 1985). Two different kinds of sandur were recognized by Kingstrom (1962) – valley sandar and plain sandur. Valley sandur occur within well defined valley walls, are usually formed by one main channel and are commonly associated with individual cirque or valley glaciers. In North America, valley sandur are called valley trains. Plain sandar are broad and unconfined when compared to valley sandar; they are formed by the coalescence of many braided streams that deposit sediment to form extensive alluvial plains. They are usually associated with large ice sheets and are common features of the Pleistocene landscape of North America (Smith, 1985). Plain sandur are commonly called outwash plains.

Krigstrom (1962) recognized three rather distinct zones of sandar related to distance from the ice margin, 1) proximal, 2) intermediate and 3) distal. Meltwater flow in the proximal zone is confined to only a few main channels that are relatively deep and narrow. Incision of proximal channels into alluvium is common and is likely a result of slope adjustment to a normal hydraulic and sediment-load regimen. The intermediate

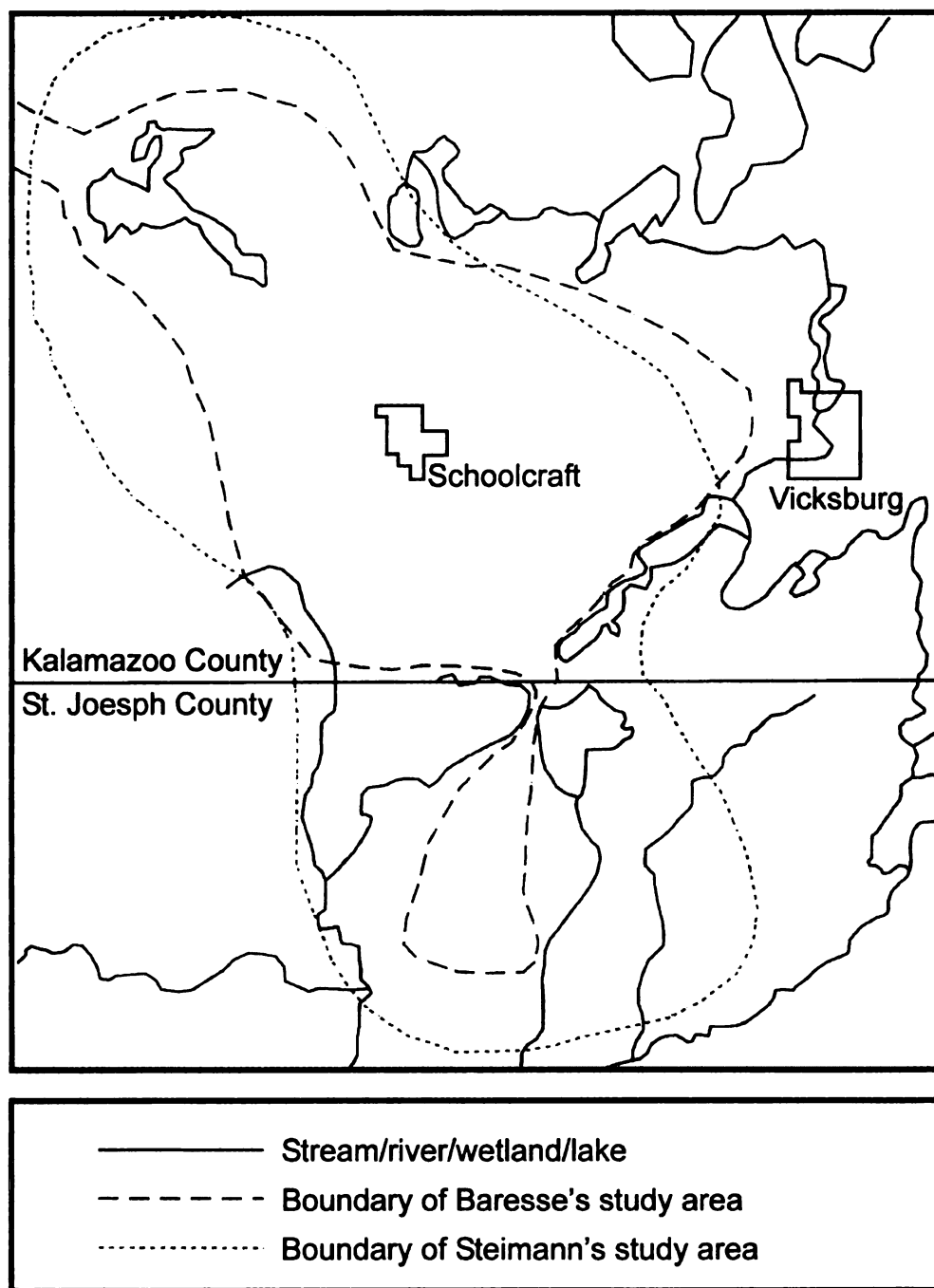


Figure 2.4. Study areas of Steinmann (1994) and Baresse (1991). Boundary of Prairie Rhonde Fan as described by Steinmann, made by Steinmann's study area. Modified from Baresse, 1991 and Steinmann, 1994.

zone is characterized by networks of wide, shallow distinct channels that shift frequently. Abandoned channels are prominent during normal discharge. In the distal zone, channels become shallower and poorly defined. At periods of high discharge, flow may merge into a single sheet.

The streams responsible for sandur are typically braided (Benn and Evans 1998). Braided streams are characterized by high width to depth ratios, steep slopes, abundant bedload, cohesionless banks, fluctuating discharge and generally low sinuositities (Benn and Evans, 1998; Miall, 1977). At least nine variables interact to determine the nature of the resulting braided stream channel: 1) discharge amount, 2) discharge variability, 3) sediment load, 4) grain size of sediment load, 5) width, 6) depth, 7) velocity, 8) slope and 9) bed roughness (Leopold and Wolman 1957). Braiding is developed by sorting action as a stream leaves behind particle sizes that it is unable to transport. Deposition of the coarser bed load causes mid-channel bars to form (Boggs, 1987). Repeated bar formation and channel branching generate a braided network of bars and channels over the stream bed (Leopold and Wolman 1957).

There are three main bar types found in braided stream systems 1) longitudinal, comprising crudely bedded gravel sheets, 2) transverse to linguoid, consisting of sand or gravel and formed by downstream avalanche-face progradation and 3) point or side bars, formed by bedform coalescence and chute and swale development in areas of low energy (Miall, 1977). Longitudinal bars are mid-channel bars that form when the coarsest part of the stream load is deposited as stream flow wanes (Boggs, 1987). They are diamond shaped in plan view with the long axis in the parallel to flow direction. They are bounded on either side by active channels and may therefore have partially eroded margins. Bars

formed in gravel are most common, although some sand bars show similar morphology (Miall, 1977). The internal structure in longitudinal bars is weak horizontal bedding commonly with imbrication (Miall, 1996). Common in sandy streams transverse and linguoid bars are also called 2-D and 3-D dunes, respectively. 2-D dunes are formed under lower flow velocities than 3-D dunes for any grain size (Ashley, 1990). The internal structure in 2-D dunes is characterized by planar tabular cross-bedding while the internal structure of 3-D dunes is characterized by trough cross-bedding (Ashley, 1990). Point and side bars are genetically the same as lateral bars, they form in areas of low energy, such as the inside of a meander (Miall, 1977). Although point bars are usually thought to occur in meandering streams, they may also occur in braided streams (Miall, 1977). The internal structure in lateral, point and side bars is complex, and may include planar-tabular cross-bedding, trough cross-bedding, ripple cross-lamination, coarse-grained lag deposits, and fine-grained drape and fill deposits (Miall, 1977). Figure 2.5 shows the location and geometries of bars within braided streams.

Miall (1977) proposed four vertical models that can develop under varying conditions of bedload and discharge, these are 1) Scott-type, 2) Donjeck-type, 3) Platte type and 4) Bijou Creek-type (Figure 2.6 and 2.7). The Scott-type is characteristic of proximal, gravelly rivers and consists of mainly longitudinal bars gravels with sand lenses formed by infill of channels and scours during low water (Miall, 1977). The Donjeck-type, characteristic of medial streams, may be dominated by either sand or gravel, and consists of fining upward cycles of variable scale. Longitudinal-bar deposits, linguoid-bar deposits, channel-floor dune deposits, bar-top and overbank deposits all may be important (Miall, 1977). The Platte-type model, representative of distal streams, is

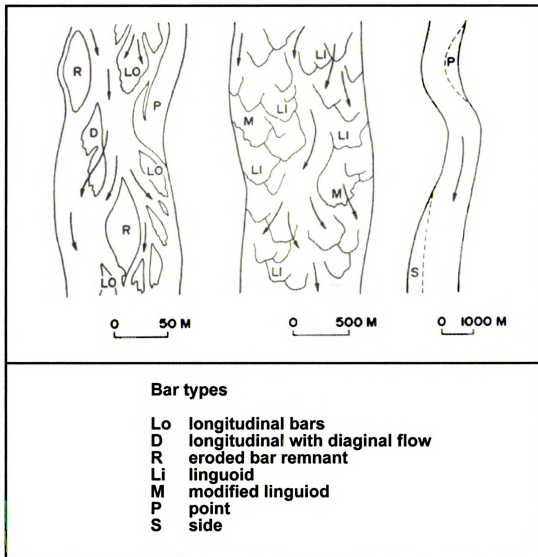


Figure 2.5. Principal bar types and where they form in a stream. Modified from Miall, 1977.

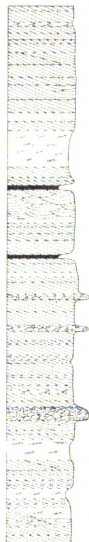
Scott-type



Donjeck-type



Platte-type

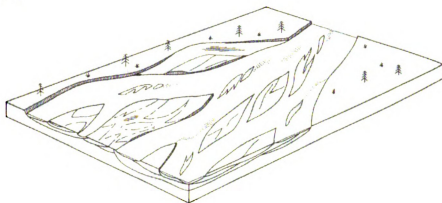


Bijou Creek-type

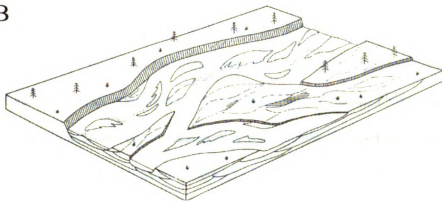


Figure 2.6. Vertical facies models of Scott-type, Donjeck-type, Platte-type and Bijou Creek-type. Modified from Miall, 1977; 1996.

A



B



C

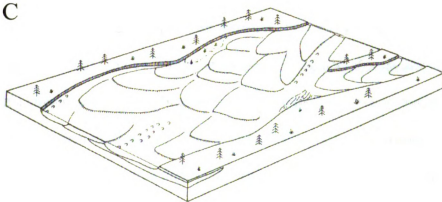


Figure 2.7. Block diagrams showing the braided stream patterns associated with Scott-type streams (A), Donjeck-type streams (B), and Platte type Streams (C). Modified from Miall, 1985.

characterized by linguoid and transverse bars that generate largely cross-bedded, sandy deposits (Miall, 1977). There is no well developed cyclicity, although some fining upward sequences may be identified (Boggs, 1987). Bijou Creek-type deposits consist of horizontally laminated sand and a lesser amount of sand showing planar cross-bedding and ripple cross-lamination (Miall, 1977). Deposits are formed during flash flood, and each flood event is represented by a fining upward sequence (Miall, 1977).

There is no absolute indicator that can be used to estimate proximity to source in braided stream environments (Miall, 1977). However, grain size is one of the best parameters that shows downstream variation. Thus, grain size is useful in measuring proximity (Miall, 1977). Mean and maximum grain size tend to decrease down stream at a rate that varies depending on stream power (Miall, 1977). Smith (1985) stated that grain size tends to decrease down-sandar in an approximately exponential way, but, the rate of diminution varies significantly between sandar. Smith (1985) suggested that this is probably a reflection of different aggradation rates. The coarsest gravel in the system is moved infrequently and only for short distances, during high energy flows, whereas finer grained material can be transported progressively farther during any time or flow event. If a stream is degrading, little or no downstream fining occurs because sediments that enter the system must leave it (Smith, 1985). If a stream is aggrading, the coarse sediments will be buried before they are transported far. Thus the faster they are buried (i.e. the higher the rate of aggradation), the shorter their final distance can be, resulting in a downstream-fining gradient proportional to the aggradation rate (Norman, 1985).

Hydrogeology

Regional Hydrogeology

Groundwater studies have been conducted within the Kalamazoo outwash plain by Barrese (1991), Steinmann (1994), with subsequent results presented by Kehew *et al.* (1996), Hyndman *et al.* (2000) and Lipinski (2002). Barrese (1991) divided the Schoolcraft Aquifer, into two flow systems based on geochemical results. A northern flow system located north of the Spring Creek-Government Marsh and a southern flow system located south of the Spring Creek-Government Marsh (figure 2.4). Barrese (1991) defined the Schoolcraft aquifer as ranging in saturated thickness from 230 feet to 200 feet, the base of the aquifer is defined as the top of the Coldwater Shale. He stated that the aquifer is composed of sand, gravel and diamicton. Three aquifer stress tests by pumping conducted near the village of Schoolcraft yielded calculated hydraulic conductivity (K) values ranging from 3.6×10^{-2} cm/s to 5.2×10^{-2} cm/s (Barrese, 1991). Maps of groundwater elevation near the village of Schoolcraft show groundwater flowing generally southeast.

Steinmann (1994) used newly installed monitoring wells, county well logs, gamma ray logs, head measurements, flow nets, slug tests, and aquifer stress tests by pumping to characterize the geologic and hydrologic conditions of the aquifer below Schoolcraft. Steinmann's study area was similar to Barrese's (1991) (figure 2.4). Steinmann (1994) used tritium data and flow nets to support the conclusion of two separate ground water flow systems, where horizontal flow dominates the region with the exception of limited recharge and discharge areas. K values were calculated from three aquifer stress tests by pumping conducted near the village of Schoolcraft. Calculated K

values are 3.8×10^{-2} cm/s, 3.9×10^{-2} cm/s and 5.0×10^{-2} cm/s based on estimated saturated thicknesses of 152.5 feet, 168 feet, and 130 feet respectively. Steinmann (1994) stated that the regional gradient ranges from 0.0022 to 0.0012, depending on location within the Prairie Rhonde fan. Groundwater flow direction is down fan or southeast. Kehew *et al.* (1996) published much of Barrese (1991) and Steinmann (1994) results, focusing on the area within the Prairie Rhonde fan.

Hyndman *et al.* (2000) studied a small area within the Schoolcraft Aquifer where they developed a bioremediation system that degrades carbon tetrachloride, discussed in more depth below. Small scale groundwater and transport models were developed to predict the migration of tracer. This aquifer is composed of 27 meters of glaciofluvial sediment overlying a regional clay layer with a water table at approximately 4.5 m below ground surface (bgs). 220 core segments from 7 wells were analyzed for K. The average K value was approximately 2.7×10^{-2} cm/s and a log (K) variance of 0.12, highest K values are at the base of the aquifer. The gradient is 0.0011 and flow is to the southeast.

Lipinski (2002) built a regional scale model with boundaries based primarily on surface water bodies in the vicinity of Schoolcraft, Michigan (figure 2.8). In this model, Lipinski (2002) used regional geological studies to build a three layer model 60 to 90 m thick. Two layers representing outwash were separated by a third layer that represented a discontinuous till. K values used in this model were taken from previous studies. Lipinski (2002) also constructed a smaller scale groundwater model and reactive transport simulation around plume G based on head results from the regional model (figure 2.8). This model was approximately 27 meters thick and represented the upper unit of outwash. A clay layer at the base of the aquifer marks the bottom of the model.

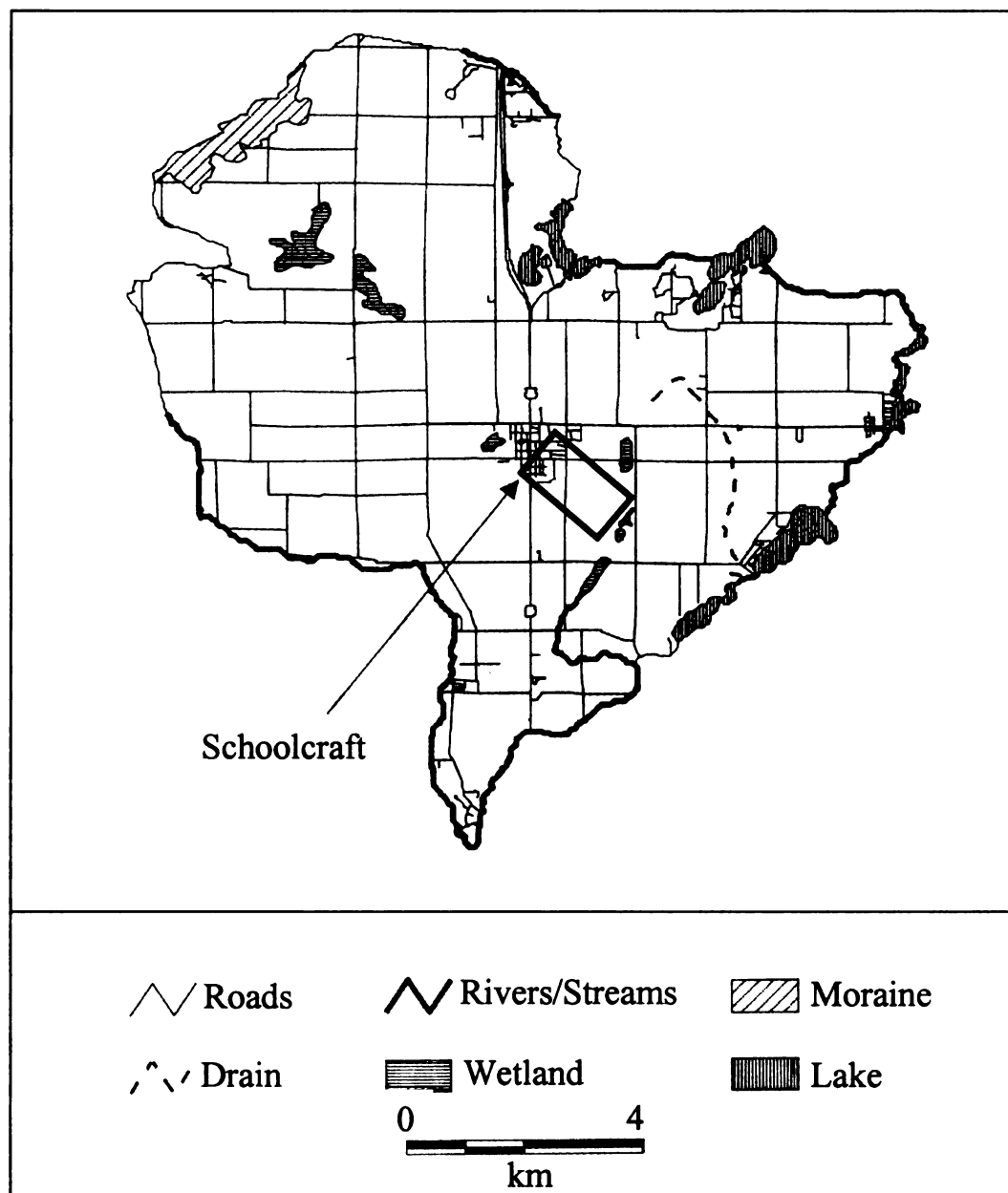


Figure 2.8. Study area of Lipinski (2002) regional model. Lipinski's smaller scale transport model is outlined by the bold rectangle near Schoolcraft. Modified from Lipinski, 2002.

The gradient of the water table is approximately 0.0012 near Schoolcraft and flow is to the southeast.

History of Contamination at Plume A

A history of the contamination source at plume A, located in Schoolcraft, Michigan, is given by Mayotte (1991) and is briefly described here. In 1986, significant concentrations of carbon tetrachloride and trichloroethene were detected in ground water quality samples obtained from residential wells just outside the village of Schoolcraft. Water quality data revealed that the contamination most likely originated at the Countymark Incorporated facility (Mayotte, 1991). The data also indicate that chloroform and 1,1,1-trichloroethane are minor constituents of the plume. At the date of Mayotte's report, the plume was known to extend 1128 m down gradient of the Countrymark property and was present throughout most of the saturated thickness of the aquifer.

Mayotte (1991) reported that evidence obtained by the Michigan Department of Natural Resources indicates that carbon tetrachloride was used as a fire retardant, as a transport agent for carbon disulfide, and as an insecticide applied to grain silos on the Countrymark property. It is believed that carbon tetrachloride and other solvents were stored in bulk in above ground storage tanks located near the silos. Throughout the history of the facility, contaminants leaked from the silos and/or storage tanks and infiltrated the vadose zone and the ground water (Mayotte, 1991).

Bioremediation of Plume A

Bioremediation studies at Plume A focused on the design and implementation of a delivery well system for bioaugmentation (Hyndman *et al.*, 2000; Dybas *et al.*, 2002). Bioaugmentation is a process that involves the addition of microbes and the necessary nutrients to sustain them in an aquifer. The researchers designed a system where water was allowed to flow passively through a treatment zone, or biocurtain, where injected bacteria attach to the sediments degrade carbon tetrachloride. A row of delivery wells spaced one-meter apart and screened across the vertical extent of contamination were installed. Ground water is periodically extracted from alternating delivery wells, amended with the chemicals needed to support bioremediation, and then the amended water is injected into adjacent wells. An intermittent feeding schedule maintains adequate biomass to efficiently remove contaminants without significant reduction to aquifer conductivity. This biocurtain has proven to be 97% effective (Hyndman, *et al.*, 2000).

To better understand the heterogeneity at the Schoolcraft plume A site, core from 11 wells were collected and either sieved, measured for K value on a constant head permeameter, described for sedimentologic features, or a combination of these. A full scale field tracer test was conducted in November 1997, using Fluorescein and Bromide as relatively conservative tracers to verify to the researchers that their selected pumping strategy would provide roughly the expected extraction well concentrations and to evaluate the fate of fluid pumped through the delivery well gallery (Hyndman *et al.*, 2000).

Chapter 3

Integration of Sedimentologic and Hydrologic Properties for Improved Transport Simulations: Detailed Characterization of a Glacial Outwash Aquifer at the Schoolcraft Bioremediation Site, Michigan

(Note: This chapter forms a manuscript that has been submitted to SEPM for publication and was authored by BITEMAN, S.E., HYNDMAN, D.W., PHANIKUMAR, M.S., and WEISSMANN, G.S., Dept. of Geological Sciences, Michigan State University, East Lansing, MI, 48824)

Abstract: Traditional geostatistical approaches for estimating hydraulic conductivity values fail to reflect sharp contrasts that occur at boundaries between different stratigraphic units, thus limiting the accuracy of contaminant transport models. We present a novel approach to incorporate geostatistical simulation into a stratigraphic framework to better represent aquifer heterogeneity. The approach was developed and tested at the Schoolcraft Bioremediation Site in Southwestern Michigan, where detailed aquifer property estimates were needed to accurately simulate multicomponent reactive transport and to design an effective bioremediation strategy. The sediments at the site were deposited as outwash medial and distal to the Kalamazoo Moraine, and consist of primarily fine to medium sands with interbedded gravels and silts. A series of 18-meter long continuous cores were collected in the vicinity of the 210 square meter biocurtain injection zone. These cores were assessed for sedimentologic character, grain size distribution, porosity, and hydraulic conductivity values. Sedimentologic character and correlation lengths from outcrop analogs in the same outwash unit supplemented the

site's core data. Based on the core data, the aquifer was separated into major sedimentologic units to preserve abrupt natural changes in conductivity, and the conductivity values were then geostatistically interpolated within each stratigraphic unit to better preserve stationarity. The stratigraphically-based conductivity and porosity estimates were used as inputs to a high-resolution three-dimensional flow and transport model of the region. The model with stratigraphic interpolation provided improved transport predictions for an injected tracer pulse.

Introduction

In recent years, the need to more accurately predict contaminant migration has focused efforts to develop novel aquifer characterization approaches, such as those that incorporate geological information. In the Northeastern and upper Midwestern United States, many aquifers for domestic and agricultural uses are composed of unconsolidated Quaternary glacial sediments. These aquifers have a high risk of point and non-point source contamination due to their generally unconfined nature. Glacial deposits typically have moderate to high levels of heterogeneity, which often complicates transport predictions within these environments. Contaminants follow subsurface preferential flow paths, such as paleo-river channels, flowing faster and in slightly different directions than the regional groundwater flow. Without an understanding of the depositional setting and the geometries of heterogeneities, an accurate characterization of the aquifer is unlikely.

Since the distribution of sedimentologic heterogeneities is directly related to the distribution of hydraulic conductivity (K) and other aquifer properties, stratigraphic complexities should be incorporated into heterogeneity models. This concept has lead to

sedimentologic research for estimating the heterogeneity of hydrologic properties (e.g., Webb and Anderson, 1996; Carle *et al.*, 1997; Davis *et al.*, 1997). Traditional geostatistical methods that interpolate between hydrologic property estimates without considering stratigraphy commonly misrepresent a site's geology by not honoring the stationarity assumption and smoothing the data rather than preserving abrupt conductivity changes (Weissmann and Fogg, 1999).

The need to improve simulation of fluid and solute migration has led to characterization approaches in aquifers and petroleum reservoirs that incorporate more geologic information. Eschard *et al.* (1998) and Weissmann and Fogg (1999) used the geology and stratigraphy as a framework for geostatistical realizations in order to better preserve stationarity. While outcrop analogs have been used to interpret facies architecture (Miall, 1985), there is a renewed interest in such subsurface characterization tools to estimate aquifer hydrologic properties (Davis *et al.*, 1997; Anderson *et al.*, 1999; Bersezio *et al.*, 1999; Hornung and Aiger, 1999; Klingbeil *et al.*, 1999). Facies distributions can be measured on outcrop analogs and can be applied to anisotropic variograms, as has been applied at a small scale by Davis *et al.* (1997) to interpret bounding surfaces.

In this paper, we present a method to better characterize aquifer heterogeneity through separate geostatistical interpolation within zones of similar sedimentologic character. Within each zone, geologic information distinct to that zone was used to estimate the lateral correlation lengths. Each hydrostratigraphic zone was then kriged separately to estimate that zone's K field. The different zonal conductivity estimates were then merged to create a single K field. By dividing the data into geologically based

zones of similar sedimentologic character, where the mean and standard deviation of K are distinct from other zones, stationarity is much more likely to be honored. Additionally, K values are estimated (kriged) separately by zone, thereby preserving the natural abrupt changes in K across bounding surfaces. Core from the site yielded stratigraphic and sedimentologic data that was used to identify zones. In addition, core material was used to measure horizontal and vertical K values using constant head permeameters, with dense vertical information but relatively sparse horizontal information. To supplement the common lack of information to accurately estimate the horizontal correlation parameters, measurements from outcrop analogs were used to evaluate K distributions, facies distributions, and width to thickness ratios. Our results show that the transport simulations based on the stratigraphically-based model more closely match measured tracer concentrations at the site.

Site Description

The Schoolcraft site is composed of glaciofluvial sands and gravels that were deposited as water drained away from a retreating ice margin. The ice margin later stagnated long enough for sediments to accumulate and form the Kalamazoo Moraine. The moraine, located west of Kalamazoo, was deposited in the last glacial episode (late Wisconsinan), and trends northeast-southwest (Figure 1). The glaciofluvial sediments are coarsest near the glacier where braided rivers had the highest energy as they flowed southeastward away from the ice margin. The energy of the rivers decreased with distance from the ice margin. Thus the further the glacier retreated, the finer the sediments that were deposited at any location. Subsurface sediments at the Schoolcraft

Kalamazoo County Surficial Geology

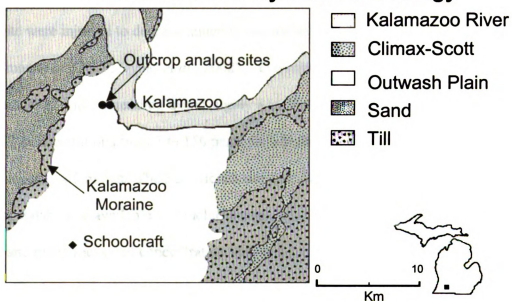


Figure 3.1. Kalamazoo County Surficial Geology, location of Kalamazoo Moraine and outcrop site used for this study. Modified from Monaghan and Larson, (1982).

site are composed of gravels at the base of the aquifer, fining upward to medium and fine sands with some interbedded very fine silty sands. This is the typical fining outward and upward succession present in glacial outwash systems, as described by Miall (1977).

The Schoolcraft Plume A study site is located within an unconfined aquifer composed of a 27.5 m thick sequence of glaciofluvial sediments that lie directly over a regional clay-rich till that acts as an aquitard in Schoolcraft, Michigan. Plume A is the location of a carbon tetrachloride (CT) bioaugmentation experiment, where microbes and substrate were injected to degrade aqueous and sorbed phase contaminants (Figure 2) (Hyndman *et al.*, 2000; Dybas *et al.*, 2002). The contaminant plume is about 1.2 km long and 90 m wide, extending from roughly 8 to 26.5 m below ground surface (bgs), with CT concentrations from 5 to 150 parts per billion (ppb). The water table at this site lies at roughly 4.5 m bgs. The Schoolcraft site was chosen for this study because a large existing database is available that includes core descriptions, K measurements from many wells, and many measured concentration histories collected during tracer tests.

The bioaugmentation system at this site was designed as a series of closely spaced recirculation wells for delivery of microbes and nutrients. The spacing and flow rates were chosen by minimizing the total design and operation cost using a flow and transport model coupled to an optimization routine (Hyndman, *et al.* 2000). A portion of the contaminant plume flows passively into the treatment zone or “biocurtain,” where microbes degrade the CT. Groundwater is periodically extracted from alternating delivery wells, amended with the chemicals needed to support bioremediation, and then injected into adjacent wells. An intermittent feeding schedule maintains adequate biomass to efficiently remove contaminants without significantly reducing the aquifer

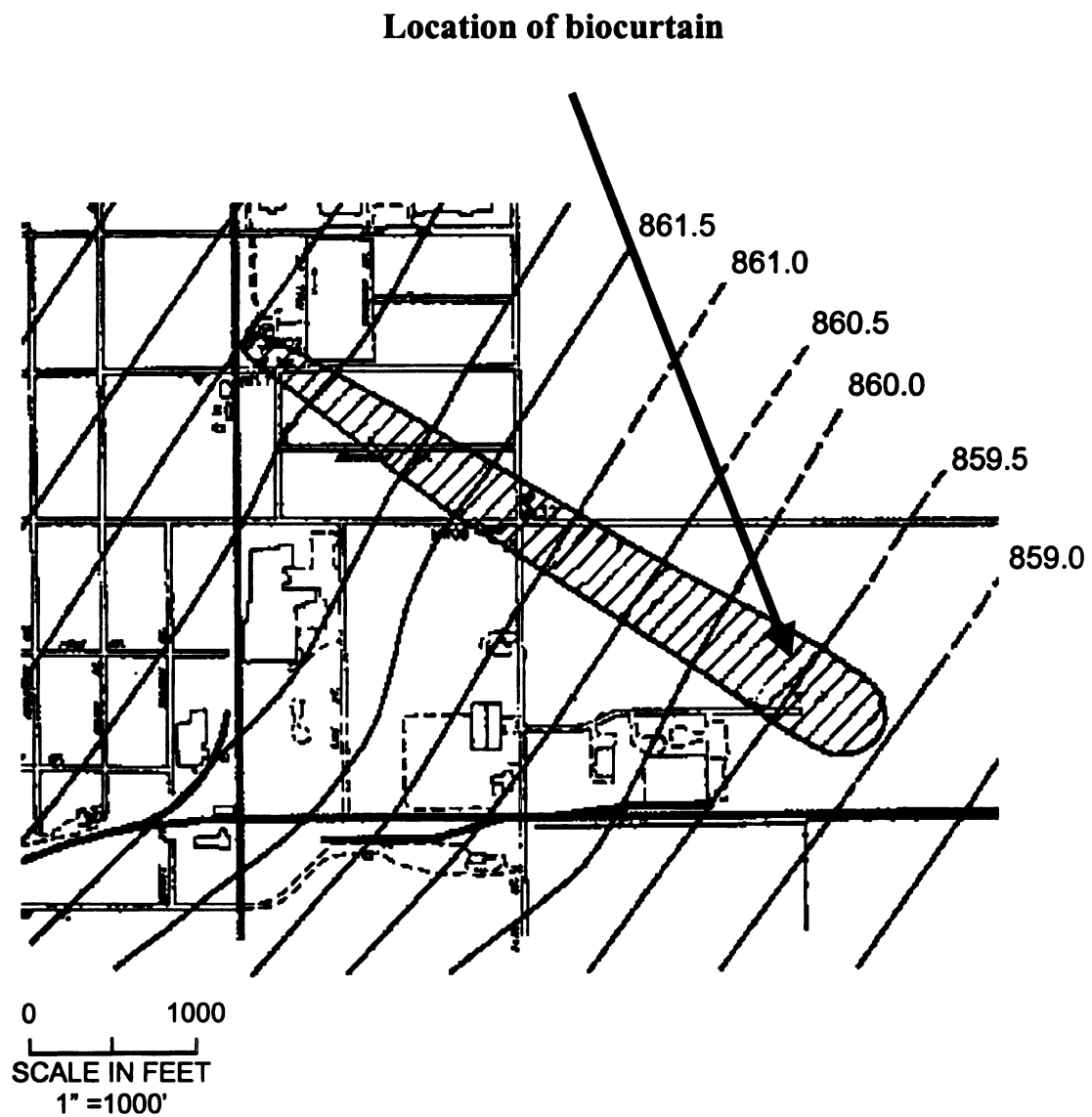


Figure 3.2. Schoolcraft Plume A site. Location of biocurtain is marked by arrow. Modified from Mayotte (1991).

conductivity. This biocurtain has proven to be greater than 97% effective at removing aqueous phase contaminants (Hyndman, *et al.*, 2000), and effective at removing sorbed phase CT in the biocurtain region over greater than 4 years of operation (Dybas *et al.*, 2002).

Core Descriptions

Methods

We evaluated core from seven of the 15 delivery wells in the biocurtain (D2, D4, D6, D8, D10, D12 and D14), spaced 2m apart in a transect perpendicular to flow, and from wells P6, P7 P8, and P18, located approximately 2-3 m downgradient of the biocurtain (see Figure 3). These cores were collected in 1.5 m sections using the Waterloo continuous core sampler that advances a core barrel ahead of an auger string. A vacuum sealed core liner minimized sediment loss. Sediment from each core except well P18 was sieved for grain size distribution, repacked to its original volume, flushed with carbon dioxide, and tested for K values on a constant head permeameter. For this study we assumed that these repacked K values were representative of local horizontal K. Core segments from P18 were cut into 15.2 cm sections, flushed with carbon dioxide, saturated with water from below over a 4-8 hour period, and then tested for vertical hydraulic conductivity values using a constant head permeameter. Each core segment was weighed while saturated, photographed and described for sedimentologic characteristics, dried and reweighed to estimate porosity, then sieved for the grain size distribution. Additionally, core from wells P6, P7, P8, and P18 were described for geologic properties including grain size, sorting and stratigraphic bedding character and grain size trends.

Vertical K values were measured from P18. To obtain horizontal K, vertical K to

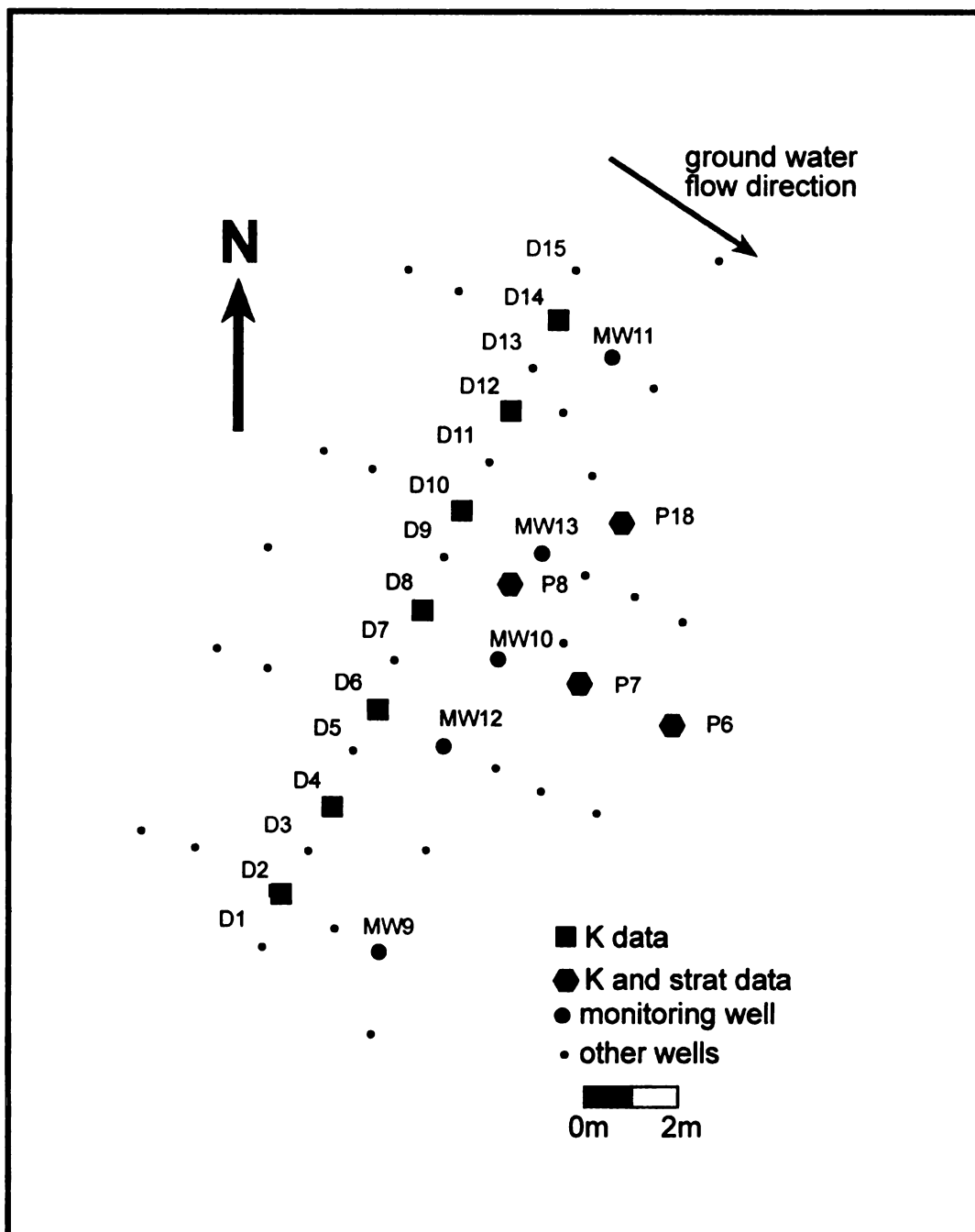


Figure 3.3. Location of delivery wells (D) and monitoring wells (MW) at the Plume A Schoolcraft site.

horizontal K anisotropy factors were applied to the vertical K values. The average K anisotropy factor of each zone was calculated as the ratio of the average vertical K values from undisturbed vertical core samples (well P18) to average horizontal K (assumed equivalent to the repacked K from D2 to D14 samples). The values were 0.72, 0.81, 0.73, 0.75, for zones 1 to 4 respectively, the average across all the zones was 0.74 (Table 3.1).

Core facies interpretation

Six facies were interpreted from the core: 1) massively bedded to finely laminated very fine sand, 2) massively bedded medium to coarse sand, 3) massively bedded fine sand, 4) cross-stratified fine sand, 5) cross-stratified medium to coarse sand and 6) cross-stratified gravel.

The *massively bedded to finely laminated very fine sand* facies is moderately well sorted with a high abundance (16%) of silt and clay. Grain sizes for this facies ranged from medium sand to clay. Vertical K was only measured on one sample from this facies due to lack of available material, with a measured value of 1.45×10^{-3} cm/s (Table 3.2).

The *massively bedded medium to coarse sand* facies is well, moderately-well or poorly sorted. Vertical K values range from 1.14×10^{-2} to 1.82×10^{-2} cm/s in the poorly sorted samples. Vertical K was only measured on one well sorted sample and one moderately to well sorted sample; the values were 1.38×10^{-2} cm/s and 2.40×10^{-2} cm/s

The *massively bedded fine sand* facies is well to moderately-well sorted, with coarse sand to silt grain sizes. Vertical K values in the well sorted sand range from 8.62×10^{-3} to 1.61×10^{-2} cm/s, while vertical K values in the moderately to well sorted fine sand respectively (Table 3.2). Grain size for this facies ranged from pebbles to very fine

| | vertical to horizontal |
|------------|---------------------------|
| zone four | 1.25 |
| zone three | 1.27 |
| zone two | 1.19 |
| zone one | 1.28 |
| average | 1.26 |

Table 3.1. Anisotropy values for vertical K and horizontal K, determined by comparing repacked to non-repacked core.

SORTING

| | | well | moderately well | moderately | poorly | very poorly |
|----------------------------|----------------|----------|--------------------|------------|----------|-------------|
| F A C I E S | low | | | | 1.14E-02 | |
| | average | 1.38E-02 | 2.40E-02 | | 1.57E-02 | |
| | high | | | | 1.82E-02 | |
| | no. of samples | 1 | 1 | | 3 | |
| | low | 8.62E-03 | 4.35E-03 | | | |
| | average | 1.23E-02 | 1.01E-02 | | | |
| | high | 1.61E-02 | 1.62E-02 | | | |
| | no. of samples | 5 | 11 | | | |
| | low | | 1.45E-03 | | | |
| | average | | | | | |
| | high | | | | | |
| | no. of samples | | | | | |
| | low | | | 1.78E-02 | 2.62E-02 | 3.50E-03 |
| | average | | | | 3.85E-02 | |
| | high | | | | 5.08E-02 | |
| | no. of samples | | | 1 | 2 | 1 |
| | low | 2.84E-03 | 3.28E-03 | | 1.50E-03 | |
| | average | 6.67E-03 | 4.46E-03 | 7.20E-03 | 3.62E-03 | |
| | high | 1.25E-02 | 5.00E-03 | | 5.36E-03 | |
| | no. of samples | 7 | 3 | 1 | 4 | |
| | low | | | | | 2.40E-02 |
| | average | | | | | |
| | high | | | | | |
| | no. of samples | | | | | 1 |

Table 3.2. Vertical K (cm/s) of facies vs. sorting from well P18.

sands. range from 4.35×10^{-3} to 1.62×10^{-2} cm/s. Generally, the better sorted the massively bedded fine sand, the greater the K value (Table 3.2).

The *cross-stratified fine sand* facies is well to poorly sorted, and vertical K values generally increased with better sorting (Table 3.2). Grain sizes for this facies ranged from pebbles to silt. Vertical K values of the well sorted fine sand ranged from 2.84×10^{-3} to 1.25×10^{-2} cm/s. Vertical K values of the moderately well sorted fine sand ranged from 3.28×10^{-3} to 5.00×10^{-3} cm/s. The moderately sorted sand had a vertical K value of 7.20×10^{-3} cm/s and the poorly sorted fine sand had a vertical K value of 3.50×10^{-3} cm/s.

Cross-stratified medium to coarse sand facies is moderately, poorly or very poorly sorted. Grain size for this facies ranged from pebbles to very fine sand. Moderately sorted medium to coarse sand had a vertical K value of 1.78×10^{-2} cm/s. Cross-stratified medium to coarse sand with poor sorting had vertical K values of 2.62×10^{-2} and 5.08×10^{-2} cm/s. The very poorly sorted medium to coarse sand had a vertical K value of 3.50×10^{-3} m/s (Table 3.2).

The *cross-stratified gravel* facies is very poorly sorted with a vertical K value of 2.40×10^{-2} cm/s (Table 3.2). Grain size for this facies ranged from pebbles to very fine sand.

The *massively bedded to finely laminated very fine sand* facies was interpreted as abandoned channel fill, commonly found in distal outwash facies (Donjeck and Platte type, as described by Miall, 1977). All other massively bedded sand facies were interpreted as having been deposited during high discharge when flow becomes less channelized and forms a large sheet. It is also possible that the stratification is too subtle to be identified at the core scale, or core collection disturbed the subtle cross-

stratification. All cross-stratified facies were interpreted as channel bar deposits in a braided stream environment. In all facies, a larger grain sizes indicate either greater stream energy and/or a more proximal location of the glacier.

Schoolcraft Stratigraphic Evaluation

Three stratigraphic breaks were identified in the cores, which provided a framework of four zones for K interpolation (Figure 3.4). Stratigraphic breaks were identified in cores as one or more of the following: 1) an erosional surface, 2) abrupt changes in mean grain size and 3) abrupt changes in sedimentary structures.

Additionally, the same four zones were apparent in the measured K distribution: zone 1 – a high K zone at the base of the section ($K_{\text{average}} = 5.44 \times 10^{-2}$ cm/s), zone 2 – a small low K unit ($K_{\text{average}} = 1.56 \times 10^{-2}$ cm/s), zone 3 – a medium high K unit ($K_{\text{average}} = 3.2 \times 10^{-2}$ cm/s) and zone 4 – a medium low K unit ($K_{\text{average}} = 1.38 \times 10^{-2}$ cm/s) at the top of the section (Figure 5). Table 3.3 lists the statistics of K values for each zone.

Zone 1 (21-27.4 m bgs) is located at the base of the aquifer and is generally composed of the *cross-stratified gravel*, *cross-stratified coarse sand* and *cross-stratified medium to coarse sand* facies. Zone 2 (21-20 m bgs) is composed of *massively bedded fine sand* facies and *finely laminated very fine sand* facies. The very fine sand facies comprises a low K area that was identified within this zone in three delivery wells (D8, D10 and D12) and in three down-gradient wells (P8, P7 and P18). Zone 3 (16-20 m bgs) is composed of *massively bedded fine sand* facies and the *massively bedded medium to coarse sand* facies. Zone 4 (16-8 m bgs) consists of the *cross-stratified fine sand* facies with *cross-stratified medium to coarse sand* facies at the erosional base of the zone. Pilot

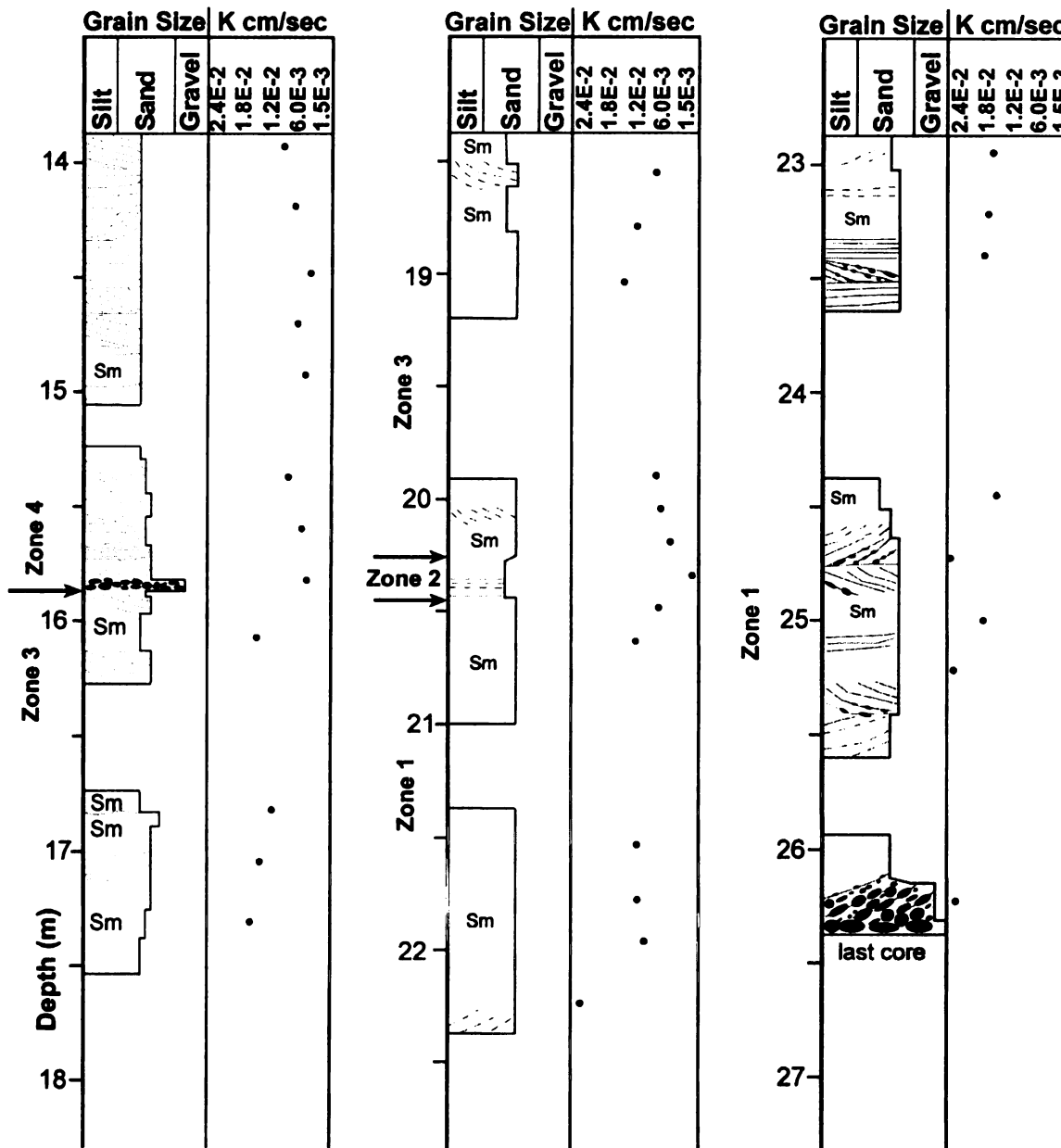


Figure 3.4. Core description of P18 showing zonal boundaries (marked by arrows) and measured vertical K.

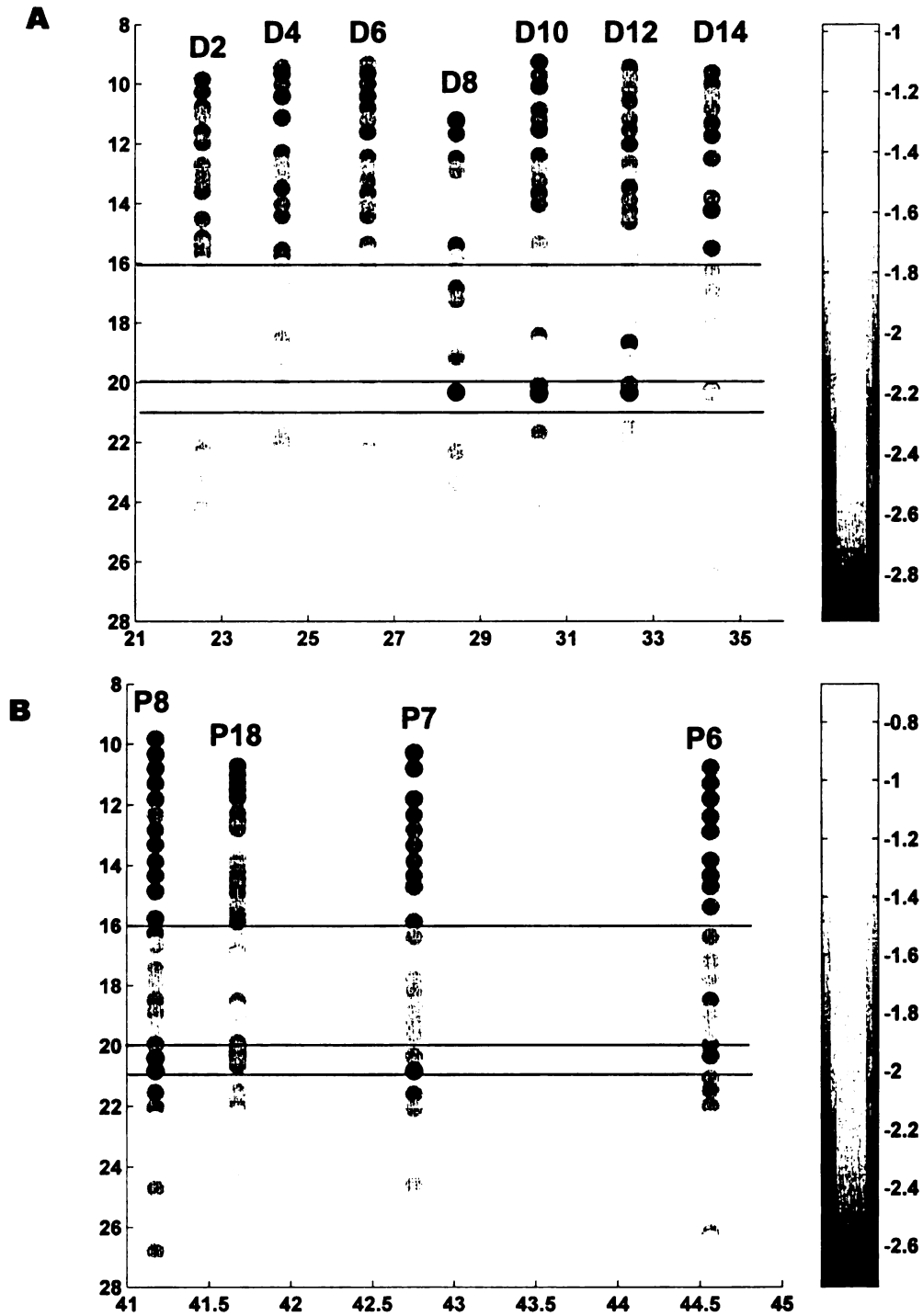


Figure 3.5a and 3.5b. Cross-section of log K data points used for interpolation. Figure 3.5a is a transect through the delivery wells, Figure 3.5b is a transect through the down gradient wells (Figure 3.3 for location). Zonal boundaries picked at 16 m bgs, 20 m bgs and 21 m bgs, identifying 4 zones. Scalebar is in log K (cm/s).

| | zone 1 | zone 2 | zone 3 | zone 4 | all zones |
|--------------------|----------|----------|----------|----------|-----------|
| mean | 5.44E-02 | 1.56E-02 | 3.20E-02 | 1.38E-02 | 3.07E-02 |
| median | 5.28E-02 | 1.74E-02 | 3.12E-02 | 1.27E-02 | 2.59E-02 |
| standard deviation | 2.90E-02 | 1.11E-02 | 9.40E-03 | 5.40E-03 | 2.43E-02 |
| no. of data points | 106 | 25 | 82 | 133 | 346 |

Table 3.3. Horizontal K (cm/s) statistics for the the four stratigraphic zones and the non-zonal model.

studies indicated that sediments above 8 m bgs did not have CT contamination, and were, therefore, not included in this study.

Outcrop Analog

Cores at this site provided an excellent sampling of vertical distributions for K analysis, but lateral data was limited even with the closely spaced cores from this site. To supplement the limited lateral core data, outcrop analogs were used to evaluate lateral variability of hydraulic conductivity at the site and to aid in the interpretation of bounding surface geometries. The excavation of sand and gravel pits in the Kalamazoo moraine outwash deposits exposed unconsolidated outcrops that could be analyzed for facies distribution, channel size, bed thickness, and lateral bed variability.

Outcrop analogs to the Schoolcraft Plume A site (Figure 3.1) were selected based on: 1) location within the same outwash complex, 2) comparable distance from the Kalamazoo Moraine, 3) grain size, 4) bed thickness and 5) sedimentary structures. Using these criteria, the analog sites and the Schoolcraft site appear to have been deposited under a similar energy conditions in the same type of environment. Once the analog sites were chosen, beds and lithofacies were identified, measured and then drawn and labeled on photo mosaics (Appendix B). Samples for horizontal K and grain size distributions were collected by inserting 15.2 cm long brass sleeves in lateral and vertical rows within chosen facies of the outcrop. These samples were tested for hydraulic and sedimentologic properties using similar methods as core from well P18. Width to thickness ratios of facies units for this study were estimated using the sand and gravel pit measurements that compared most closely to the grain size, bed thickness and bedding

structures of the core (Figure 3.6). The sand and gravel pit that was most similar to sediments at the Schoolcraft site is composed of *cross-stratified gravel facies*, *cross-stratified medium to coarse sand facies* and some *cross-stratified fine sand facies*. Width to thickness ratios were estimated for bed sets from the outcrop analog to be an average of 7.7:1. This ratio corresponds well to published data by Robinson and McCabe (1997), who reported trough cross bed sets have an average width to thickness ratio of 8.5:1 to 10.4:1. It was not possible to measure the bed lengths, since the outcrop is two dimensional and bed lengths at the site are longer than the scale of the outcrop. No published data were available on the bed width, depth and length ratios, likely for the reason stated above.

Geostatistics

We use the stratigraphic zones identified at the Schoolcraft site as geologic regions for geostatistical interpolation. For each zone, experimental variograms were developed to estimate the correlation lengths in the vertical, parallel to paleoflow, and perpendicular to paleoflow directions. Variogram parameters were estimated using horizontal log K values measured from core samples. Log K data were used instead of K in this and other geostatistical analysis because hydraulic conductivity values for this site are more log-normally distributed than normally distributed (Hoeksema and Kitanidis, 1985). The parameters for the vertical correlation length were estimated to fit the experimental variogram. Because horizontal data are sparse, the horizontal, perpendicular to flow correlation length structures were determined using the 7.7:1 width to thickness ratio measured from outcrop analog. The horizontal, parallel to flow



Figure 3.6. A portion of the outcrop analog showing the stratigraphic character of the outwash material with a shovel for scale. Image is presented in color.

correlation length structures were extended as far as Groundwater Modeling System (GMS3.1, BYU, 2000) would allow, approximately 18 m. Yet, we believe this is shorter than the true parallel-to-flow correlation length based on the outcrop analogs and the nature of these fluvial deposits. Table 3.4 summarizes the sill, nugget, parallel to flow range, perpendicular to flow range, and vertical range for each stratigraphic unit. Using the estimated variogram models and conditioning data, we generated a three-dimensional K field for each hydrostratigraphic zone using ordinary kriging. The four zones were then merged to create a final K field surrounding the biocurtain area. This zonal kriged field preserved abrupt K changes, especially noticeable at approximately 20-21 m depth in zone 2 (Figure 3.5).

In addition to the zonal kriged results, a K field was estimated by kriging without the zonal boundaries to evaluate the influence of the additional geologic information. For this model, the variogram range was set at 18.0 (to be consistent with the zonal kriging). The nugget, sill, and range in all three orthogonal directions were fit to the experimental variograms based on the core data (Table 3.4). In a visual comparison, the zonal kriged field had significantly more horizontal bedding-like features than the traditional kriged field, which had smoother features with less horizontal continuity. Additionally, the low K area, (20-21 m bgs), interpreted as an abandoned channel fill, is much larger and diffuse in the non-zonal kriged case than suggested by the core data (Figure 3.5).

Groundwater Modeling and Tracer Test Simulation

We used the three-dimensional groundwater flow model MODFLOW-96 (McDonald and Harbaugh, 1988; Harbaugh and McDonald, 1996) to compute the flow

| | nugget | Sill | parallel to flow | Range perpendicular to flow | vertical |
|-----------------|--------|-------|------------------|--------------------------------|----------|
| non-zonal model | 0.011 | 0.065 | 18.0 | 6.84 | 2.700 |
| zonal model | | | | | |
| zone 1 | 0.012 | 0.026 | 18.3 | 2.61 | 0.353 |
| zone 2 | 0.027 | 0.21 | 17.7 | 4.09 | 0.531 |
| zone 3 | 0.0017 | 0.020 | 18.0 | 8.33 | 1.081 |
| zone 4 | 0.0053 | 0.024 | 18.4 | 12.51 | 1.619 |

Table 3.4. Variogram parameters for zonal kriging and non-zonal kriging. All variograms fit using exponential model.

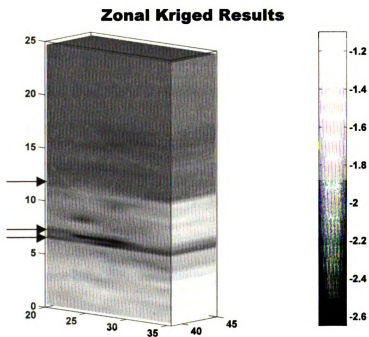
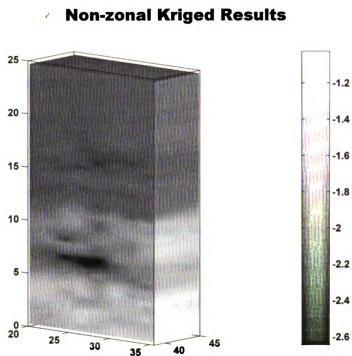


Figure 3.7. Zonal (top) and non-zonal (bottom) kriged results. Arrows mark boundaries of zones in zonal kriging. Note that abrupt changes in K are preserved in zonal kriging approach. Scalebar is in log K (cm/s).

and heads for the region. Constant head boundaries were used in the flow direction to provide a gradient of 0.0011 based on regional head measurements (Figure 3.2). The model domain is a rectangular region 101.5 m wide (Y) by 57.2 m long (X) by 27.4 m in depth (Z). We discretized this region using a computational grid with 136 (Y) x 86 (X) x 44 (Z) cells (Figure 3.8). The delivery well gallery is located at the center of the computational domain such that fine cells (20 cm x 20 cm) approximately equal to the size of the well boreholes surround the delivery wells. Cell size increased in a geometric progression away from the well gallery. The resolution in the vertical direction varies and is discretized most finely around the low conductivity zone located at approximately 20-21 m bgs (Table 5).

During the tracer test, a conservative tracer (bromide) was injected into the seven even-numbered wells and extracted from the eight odd-numbered wells for the first five hours. During the next hour the same pumping rate was used in a flow reversal phase where tracer was extracted from the even wells and injected into the odd wells. We used the reactive transport code RT3D (Clement and Jones, 1998; Clement, 1997) to simulate three-dimensional tracer transport through the site. Since the injected bromide concentration changed during the tracer test, we divided the five-hour interval in the transport model into three stress periods with different concentrations, 18, 14, and 17 ppm respectively. The one hour flow reversal phase was simulated with a single stress period where injected concentrations were 23.5 ppm. The last stress period in this simulation represents a 20-day natural gradient period with no pumping. The differences in hydraulic conductivity across the vertical extent of the aquifer, cause proportional differences in the flux through different layers of the well bore. To represent this

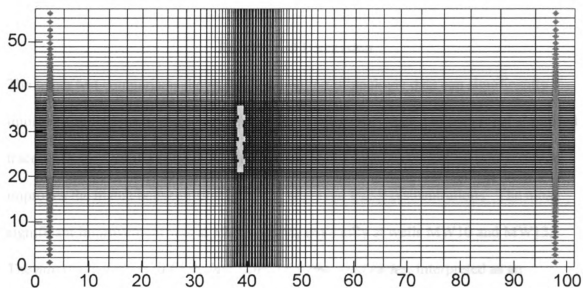


Figure 3.8. Discretization of grid in plan view, delivery well gallery is located near the center of the grid, marked by light colored squares, where discretization is the finest.

| layers | thickness of layer (m) |
|----------|------------------------|
| 1 | 5.4 |
| 2 to 7 | 1.0 |
| 7 to 26 | 0.50 |
| 26 to 34 | 0.25 |
| 34 to 44 | 0.50 |

Table 3.5. Vertical discretization of layers.

behavior, we used a conductivity-weighted average to compute the fluxes for the injection and extraction wells.

Results and Discussion

The tracer test comparison shows that the addition of geologic data can significantly improve simulations in some localities while in others the zonal and non-zonal simulated tracers are very similar (Figure 9). In most cases, the hydrostratigraphic interpretation improves the match between simulated and observed tracer concentrations. The most significant improvement was at 19.8 m depth, especially at wells MW10 and MW13. The *massively bedded to finely laminated very fine sand facies*, interpreted as an abandoned channel fill, is present at this depth over about half of the simulation area. The core descriptions and K data place this channel fill through delivery wells 8, 10, and 12. MW13 and MW10 are located downgradient from delivery wells 10 and 8 respectively (figure 3). MW10 and MW13 are the most affected by the addition of geologic data because this is where the low K channel fill is located. At the same depth with no evidence for the low K abandoned channel fill, tracer simulations MW11 and MW12 respond similarly for both types of kriging. No core was recovered from well D2 at this depth, however, the measured tracer breakthrough at MW9 is very similar to the measured data from MW13, suggesting another possible abandoned channel fill at this location.

At most other depths, the comparison between tracer tests simulated in the zonal and traditional kriging simulations are very similar. Slight improvements are made in MW10, and MW13 at depth 22.9 m, and MW10 and MW11 at depth 16.8 m, and MW11

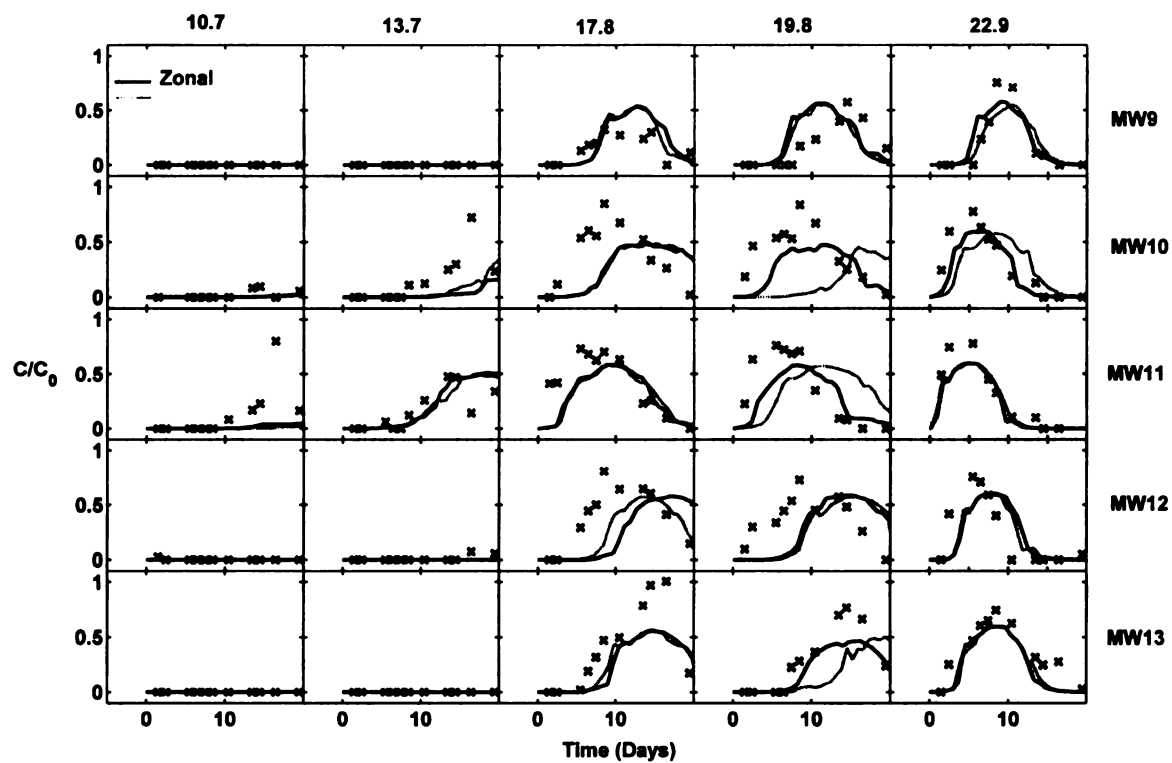


Figure 3.9. Measured tracer test from site (x) with simulated zonal kriging (black line) and simulated non-zonal kriging (gray line).

at 13.7 m and 10.7 m, where the breakthrough occurs a bit earlier in the zonal kriging tracer simulation.

There are a few instances where the two kriging approaches provide similar transport results and a few sites where the traditional kriging breakthrough better matches the measured tracer concentrations. The nonzonal kriging transport simulation better matches the measured tracer at MW12 at 17.8 m depth. This is because the nonzonal kriging interpolated a higher K value than the zonal kriging interpolated at 17.8 m depth.

Conclusions

The addition of stratigraphically significant boundaries into geostatistical interpolation methods helps preserve abrupt changes in K as they occur in the sedimentologic record, thus better honoring the stationarity assumption implicit in the kriging method. The zonal kriging approach requires an understanding of the depositional environment, which can be accomplished by visual analysis of the core material to evaluate stratigraphic units. In locations where core data do not provide enough information, outcrop analogs were used to provide approximate correlation lengths for different facies type.

Kriging K values using the stratigraphic framework identified by the core yields a more realistic aquifer characterization that better matches the true geology of a site. The zonal model of K improved the tracer simulations, most evident where the heterogeneity is the highest or in regions where there is a contrast in K of an order of magnitude or more.

Chapter 4

Transition Probability Geostatistics

Introduction

Transition Probability Geostatistics is an indicator geostatistical method that can be used to estimate the spatial distribution of facies based on geologic information input by the modeler. This is done by first categorizing the data set into three to five geologically distinct facies or hydrofacies. Second, a three-dimensional Markov chain model is fit or developed for the data. Third, this model is used in sequential indicator simulation to simulate the three dimensional facies distributions. Important geological attributes such as 1) volume fraction (proportions), 2) mean lengths (e.g. thickness and lateral extent) and 3) juxtapositional tendencies (how one category tends to locate in space relative to another) are considered in this approach (Carle *et al.*, 1998). Markov chains offer a stochastic model for categorical variables that incorporate all of these geological attributes (Carle and Fogg, 1998). The Markov chain is a model used to mathematically describe the transition probabilities seen in geologic medium. The probability of one facies transitioning directly to another is used to help define the Markov chain model. After the Markov chain models are developed in three principle directions (vertical parallel to flow and perpendicular to flow), conditional simulation followed by simulated annealing was run. Conditional simulation is a process that creates multiple, equally probable spatial distributions of random variables or “realizations” that honor hard data conditioning points at specified locations (Carle *et al.*, 1998). This is a much different method of estimating distribution of K than kriging,

which will only produce one distribution of K (Deutsch and Journel, 1992). Simulated images do not exhibit the characteristic smoothing effect of kriging (Deutsch and Journel, 1992). Therefore, simulated images better preserve abrupt changes in K.

Existing variogram based methods do not provide 1) consideration for asymmetric juxtaposition relationships such as fining upward tendencies; 2) a framework for incorporating geologic interpretation of proportions, lengths, and juxtaposition tendencies into models of spatial variability; or 3) consideration for locally variable anisotropy directions (Carle *et al.* 1998). Incorporating geologic interpretation of proportions, lengths, and juxtaposition tendencies into models of spatial variability, as well as consideration for asymmetric juxtaposition relationships are very important to creating an accurate geologic model at the Schoolcraft site. By enforcing juxtaposition relationships, proportions, and lengths, based on geologic data from the site, geologically plausible simulations of the distribution of facies will be produced even where the data are sparse.

Although the transition probability geostatistical approach produces geologically plausible distributions of heterogeneity, this is only accurate where stationarity can be assumed, or where the mean and standard deviation do not vary spatially (Weissmann and Fogg, 1999). The Schoolcraft site as a whole is not stationary, as described previously in chapter 3. For the transition probability/ Markov chain based simulations, the Schoolcraft site was divided into 2 zones, to better honor stationarity --a coarse grained bottom zone (medial deposits) and a finer grained upper zone (distal deposits). The upper and bottom zones were simulated separately and later combined to create a full aquifer characterization.

Stratigraphic Zones

Two zones were identified at the Schoolcraft Plume A site –a gravely zone at the bottom of the aquifer (22-27 m bgs) that represents intermediate (Donjeck-type) outwash deposits and –a sandy zone at the top of the aquifer (8-22 m bgs) that represents distal (Platte-type) outwash deposits (see Appendix A). The bottom zone was the same as zone 1 used in the zonal kriging (see chapter 3). The top zone was a compilation of zones 2-4 used in the kriging chapter (3). These upper zones were combined since similar hydrofacies are present.

The mean and standard deviation of grain size are significantly different between the two zones (Table 4.1). To show that mean grain size and standard deviation do not depend on location in the top zone of the transition probability geostatistics simulations, the data were divided into the same three zones as the kriging zones from chapter 3 and assessed for mean grain size and standard deviation. Division of the region into two stratigraphic zones for transition probability modeling appears justified since mean and standard deviation are approximately the same for kriging zones 2-4 (Table 4.2). Additionally, the bottom zone consists of predominately medium (46.6%) and coarse sand (23.6%) while the top zone consists of predominately fine sand (74.2%).

Explanation of Hydrofacies from Categories

Within each zone, five distinct hydrofacies were identified by comparing grain size, sorting and K. Mean grain size and standard deviation of grain size were measured from sections of sieved cores (P18, D2, D4, D6, D8, D10, D12 and D14). Core P18 was also described for sedimentologic properties (Appendix A, Figure A.2). Many

| T. P. zones | mean GS | mean GS | mean SD | mean sorting | no. data points | |
|---------------|---------|---------|------------------|--------------|-----------------|----|
| Kriging zones | 1 | 0.11 | very coarse sand | 1.73 | poorly | 29 |
| | 2 | 2.29 | upper fine sand | 0.77 | moderately | 84 |
| | 1 | 0.11 | very coarse sand | 1.73 | poorly | 29 |
| | 2 | 2.28 | upper fine sand | 0.62 | moderately well | 5 |
| | 3 | 2.08 | upper fine sand | 0.78 | moderately | 36 |
| | 4 | 2.48 | fine sand | 0.79 | moderately | 42 |

Table 4.1. Mean grain size (GS) in Phi unit, corresponding Wentworth size class (Boggs, 2001), mean standard deviation (SD), sorting based on standard deviation (Boggs, 2001), and number of data points in each zone for the two transition probability (T. P.) zones and the four zonal kriging zones. Zone one is the same for the transition probability and zonal kriging zones.

| Hydrofacies of the Top Zone | Proportions |
|--|-------------|
| Poorly sorted medium sand (PMS) | 0.065 |
| Poorly sorted coarse sand (PCS) | 0.032 |
| Moderately to well sorted fine sand (MWFS) | 0.742 |
| Poorly sorted fine sand (PFS) | 0.130 |
| Very fine sand (VFS) | 0.032 |
| Hydrofacies of the Bottom Zone | Proportions |
| Pebbles, gravel and very coarse sand (PGVCS) | 0.135 |
| Moderately well to well sorted medium sand (WMS) | 0.115 |
| Poorly sorted coarse sand (PCS) | 0.236 |
| Poorly sorted medium sand (PMS) | 0.466 |
| Moderately to well sorted fine sand (MWFS) | 0.048 |

Table 4.2. Proportions of hydrofacies in the top and bottom zone.

things were considered when choosing categories, including: 1) relationship between grain size and sorting, 2) the interpreted process under which each grain size / sorting combination was deposited and 3) the distribution of K for each grain size / sorting combination. Generally, a relationship exists where, for any grain size, the better a sand is sorted the higher the K value, assuming a normal distribution of grain size (Beard and Weyl, 1973). Measured data indicate from the Schoolcraft site indicate that this assumption is true, even though the sands and gravels from the Schoolcraft site lack normal distribution (Table 4.3 and Table 4.4). Thus, it is believed that this is still reasonable to assume this relationship exists for sands and gravels at the Schoolcraft site.

Top Zone

For the top zone, the five identified categories are: 1) moderately to poorly sorted medium sand (*PMS*), 2) poorly to very poorly sorted coarse sand with pebbles (*PCS*), 3) well to moderately sorted fine sand (*MWFS*), 4) poorly sorted fine sand (*PFS*) and 5) moderately to poorly sorted very fine sand (*VFS*). Mean K decreases from category one to category five. Mean, high and low K values are given in Table 4.3, and plotted in Figure 4.1.

PMS (category 1) is the hydrofacies with highest K in the top zone, and is poorly to moderately sorted. In core, this hydrofacies displayed either faint cross-stratified bedding or massive bedding and grain shape is rounded to subrounded. The sediment color is light olive brown (Munsell 2.5Y 5/4) when wet and pale yellow (Munsell 2.5Y 7/3) when dry. This hydrofacies tends to occur as lenses within the *MWFS* hydrofacies and is interpreted to have been deposited on channel bars.

TOP ZONE

| Category | Hydro facies | average K | high K | low K | no. of points |
|----------|--|-----------|--------|-------|---------------|
| 1 | Poorly sorted medium sand (PMS) | 0.025 | 0.04 | 0.005 | 16 |
| 2 | Poorly sorted coarse sand (PCS) | 0.019 | 0.044 | 0.004 | 4 |
| 3 | Moderately to well sorted fine sand (MWFS) | 0.013 | 0.029 | 0.007 | 51 |
| 4 | Poorly sorted fine sand (PFS) | 0.010 | 0.032 | 0.002 | 6 |
| 5 | Very fine sand (VFS) | 0.008 | 0.012 | 0.002 | 7 |

Table 4.3. Hydrofacies and corresponding assigned category for top zone with high K value, low K value, average K value, and number of points.

BOTTOM ZONE

| Category | Hydro facies | average K | high K | low K | no. of points |
|----------|--|-----------|--------|-------|---------------|
| 1 | Pebbles, gravel and very coarse sand (PGVCS) | 0.057 | 0.103 | 0.024 | 11 |
| 2 | Moderately well to well sorted medium sand (WMS) | 0.043 | 0.066 | 0.018 | 4 |
| 3 | Poorly sorted coarse sand (PCS) | 0.041 | 0.062 | 0.018 | 7 |
| 4 | Poorly sorted medium sand (PMS) | 0.032 | 0.046 | 0.017 | 5 |
| 5 | Moderately to well sorted fine sand (MWFS) | 0.017 | 0.019 | 0.016 | 3 |

Table 4.4. Hydrofacies and corresponding assigned category for bottom zone with high K value, low K value, average K value, and number of points.

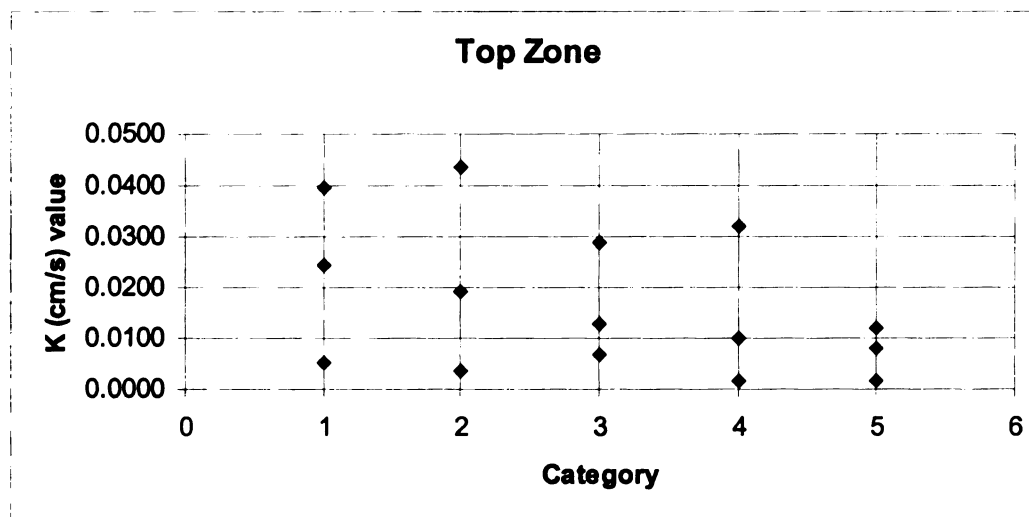


Figure 4.1. Top zone of Schoolcraft site, 1-5 are categories of hydrofacies, corresponds to Table 4.3. Top diamond is high K value, bottom diamond is low K value and middle diamond is mean K value.

The *PCS* hydrofacies (category 2) is poorly to very poorly sorted and contains both pebbly coarse sand and coarse sand without pebbles. These two lithologies were combined because they both display similar K values and represent the coarsest grained sediments in the upper zone. The pebbly sand is matrix supported with rounded pebbles and subrounded grains. The matrix consists of coarse and medium sand. The color is olive brown (Munsell 2.5Y 4/4) when wet, and pale yellow (Munsell 2.5Y 7/3) when dry. The samples of coarse sand without pebbles could not be described for sedimentologic features since only sieve data exists for these samples. This hydrofacies is interpreted to have been deposited on channel bars.

The *MWFS* (category 3) is the most abundant hydrofacies in the top zone (Table 4.2). The moderately to well sorted sand appears to have thicker and more continuous beds than any of the other hydrofacies in this zone (Figure 4.2). In core, *MWFS* displays massive bedding from the base of the zone to about 16 m bgs, above which it becomes cross-stratified (see Appendix A Figure A.2). The color of the sand is generally olive brown (Munsell 2.5Y 4/4) when wet and pale yellow (Munsell 2.5Y 7/3) when dry, and the grain shape is generally subrounded. This hydrofacies is interpreted to have been deposited on channel bars.

The *PFS* (category 4) has a lower K than the moderately to well sorted fine sand due to its poorer sorting. It is generally cross-stratified with either coarser grains along cross-stratified beds or with seemingly randomly placed pebbles composed of sand cemented with calcium carbonate. This hydrofacies appears to be thinner and laterally discontinuous when compared to *MWFS*. This hydrofacies is interpreted to have been deposited on channel bars.

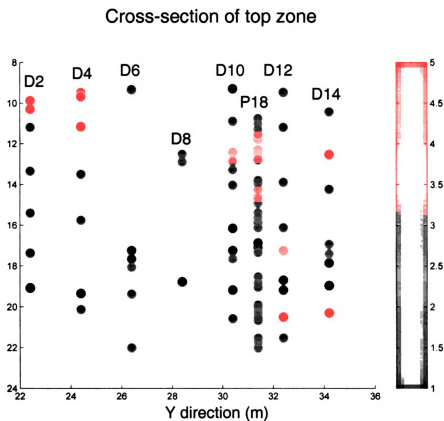


Figure 4.2. Cross-section of categories in top zone. Category 1, poorly sorted medium sand (PMS); category 2, poorly sorted coarse sand (PCS); category 3, moderately to well sorted fine sand (MWFS); category 4, poorly sorted fine sand (PFS); category 5, very fine sand (VFS). X axis is depth (m). Image is presented in color.

The *VFS* (category 5) is the lowest K hydrofacies and it is this facies that forms the “low K zone”, discussed in earlier chapters. In core, the very fine sand is finely laminated, had a high amount of silt and clay (16%), and was well to moderately sorted. The sediment color is olive brown (Munsell 2.5Y 4/4) when wet and pale yellow (Munsell 2.5Y 7/3) when dry. This hydrofacies was interpreted as abandoned channel fill, commonly found in medial and distal outwash facies (Donjeck and Platte type, as described by Miall, 1977). Abandoned channel fills are common in medial and distal outwash facies during flooding where what is commonly referred to as overbank fines infill abandoned channels (Miall 1985; Benn and Evans 1998.)

Bottom Zone

For the bottom zone, the five identified categories are: 1) pebbles, granules, and very coarse sand (*PGVCS*), 2) moderately well to well sorted medium sand (*WMS*), 3) poorly to very poorly sorted coarse sand (*PCS*), 4) poorly to very poorly sorted medium sand (*PMS*) and 5) moderately and moderately to well sorted fine sand (*MWFS*). Mean K decreases from category one to category five. Mean, high and low K values are given in Table 4.4, and plotted in Figure 4.3.

The *PGVCS* (category 1) is the hydrofacies with the highest K in the bottom zone (Figure 4.3, Table 4.4) and is composed of three different mean grain sizes pebbles, gravels and very coarse sand, all of which are poorly or very poorly sorted. These different sub-categories were grouped together because within each there was a high abundance of the other two grain sizes (e.g. the very coarse sand had pebbles and

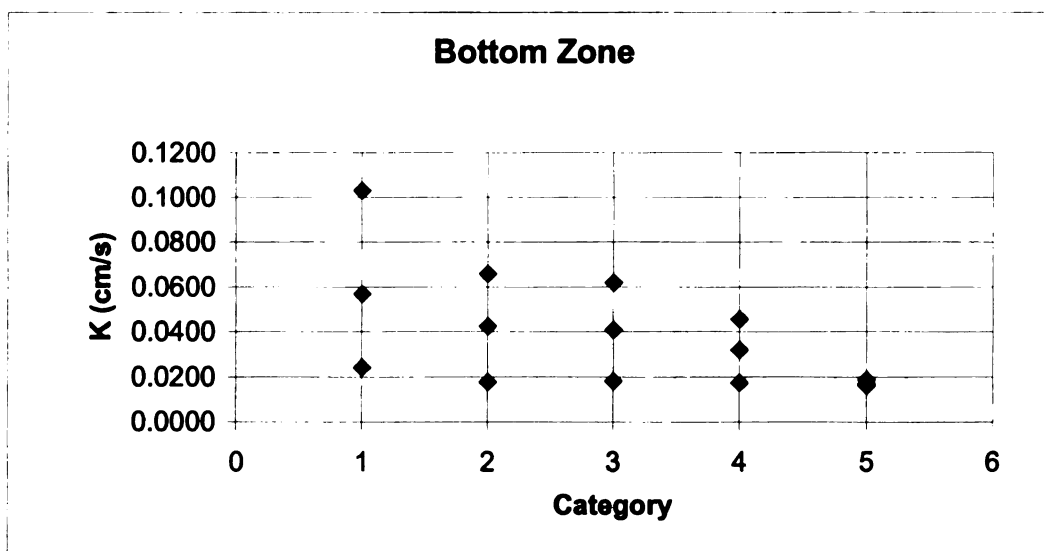


Figure 4.3. Bottom zone of Schoolcraft site, 1-5 categories of hydrofacies, corresponds to Table 4.4. Top diamond is high K value, bottom diamond is low K value and middle diamond is mean K value.

granules present) and all three subcategories had similar K values. In core, the pebbles and granules are rounded and grain supported and display cross-stratified bedding with the coarsest grains tending to occur along cross-stratified beds. The samples of very coarse sand were not described for sedimentologic features since only sieve data exists for these samples. This hydrofacies is present along the base of the aquifer and is interpreted to represent channel lag deposits.

The *WMS* (category 2) is well to moderately well sorted, has rounded grains, and displays cross-stratified bedding. Coarser grains exist along bedding planes. The sediment color is olive brown when wet and light olive brown to pale yellow when dry. This hydrofacies is interpreted to have been deposited on channel bars.

The *PCS* (category 3) is poorly to very poorly sorted. The coarse sand is cross-stratified with subrounded to rounded grains. Coarser grains exist along bedding planes. Grain size ranges from silt to granules. The coarse sand is light olive brown (Munsell 2.5Y 5/4) when wet and pale yellow (Munsell 2.5Y 7/3) when dry. This hydrofacies is interpreted to have been deposited on channel bars. This hydrofacies is very similar to the *PCS* hydrofacies in the upper zone and consequently has the same name.

The *PMS* (category 4) is distinct from category 2 because of differences in average K (Table 4), and sorting. Grain size ranges from silt to granule within this facies. There is a fining upward relationship from *PMS* (category 4) to *WMSM* (category 2). In core, the *PMS* hydrofacies is cross-stratified and displays coarser grains along bedding planes. This hydrofacies is interpreted to have been deposited on channel bars. This hydrofacies is very similar to the *PMS* hydrofacies in the upper zone and consequently has the same name.

The *MWFS* (Category 5) is the lowest K hydrofacies in the bottom zone. This hydrofacies is distributed in very small proportions in the bottom zone. Because of the finer grain size than the rest of the bottom zone, this hydrofacies is interpreted to have been deposited on channel bars under a lower energy than the rest of the sediments in the bottom zone. This hydrofacies is very similar to the *MWFS* hydrofacies in the upper zone and consequently has the same name.

Markov Chain Models

Top Zone Markov Chain Models

The vertical (z)-direction transition probability values for the top zone were measured from core based on a 0.25 m-spacing. Proportions of categories were estimated from the core data (Figure 4.2). In this zone, the *MWFS* hydrofacies has the highest proportions (74.2%) and seems to fill in around all the other categories. Thus *MWFS* was used as the background category (Table 4.2). Unfortunately, the data are very sparse and the addition of more data would have significantly improved the measured and modeled Markov chain models. Moreover, an outcrop analog that closely matched the distribution of grain size and beds to this upper zone was not found, so a Markov chain model could not be developed from analog data. Using the available data, however, a Markov chain model was fit to the measured data (Figure 4.4). The vertical embedded transition probabilities and the mean lengths of the Top zone are given in Table 4.5. Because the *MWFS* hydrofacies is the background category, the vertical (z)-direction embedded transition probabilities are the highest where *MWFS* occurs. The highest embedded

Top Zone Vertical Transition Probability

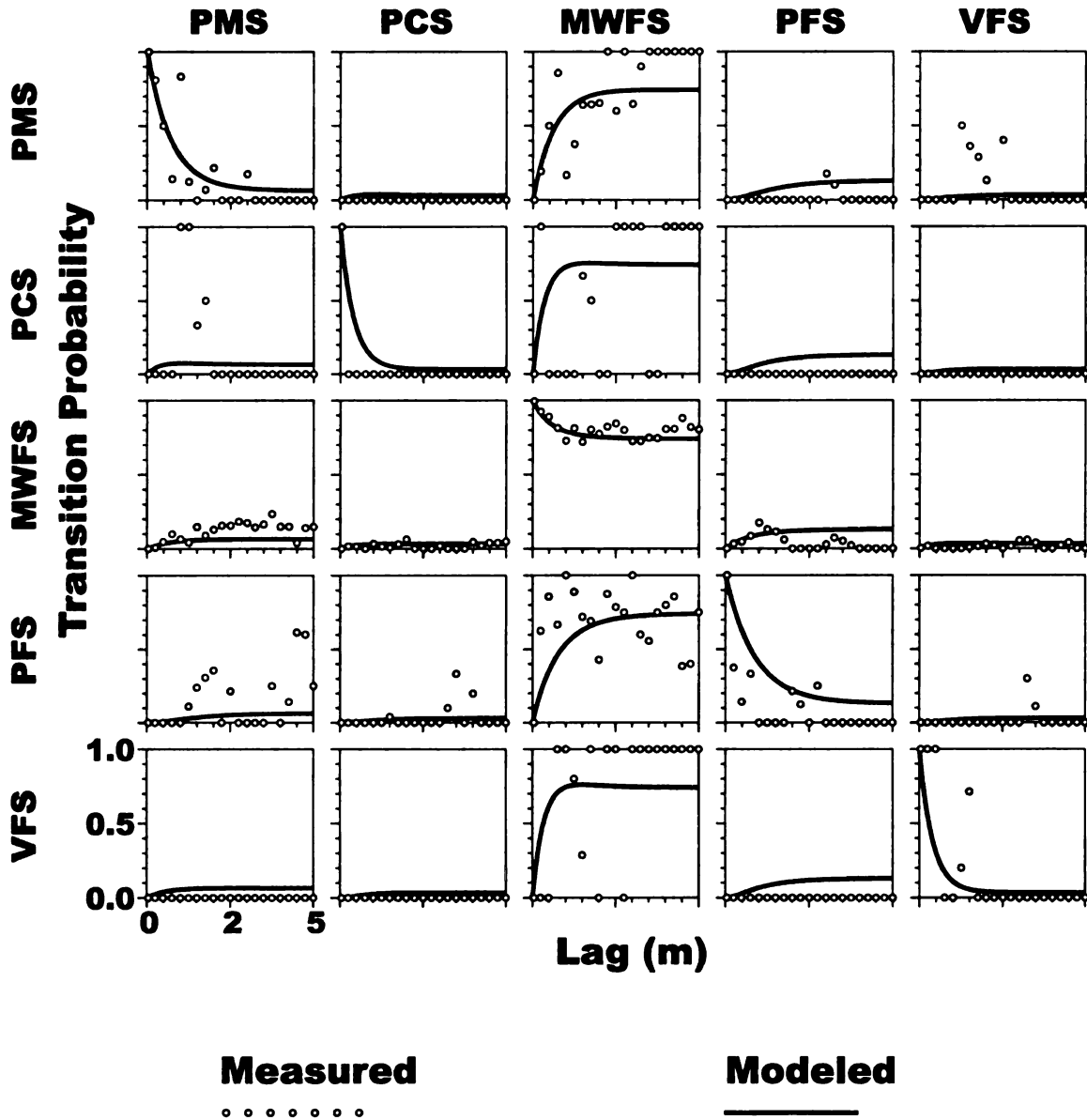


Figure 4.4.
Matrix of vertical (z)-direction transition probabilities showing core data as measurements (open circles) and the Markov chain model (solid line) from the core measurements. The diagonal elements represent auto-transition probabilities within a category, and the off diagonal elements represent transition probabilities between categories.

Vertical (z)-direction

| | PMS | PCS | MWFS | PFS | VFS |
|------|--------------|--------------|----------------|--------------|--------------|
| PMS | L=.750 | 0.100 | 0.889 | 0.010 | 0.001 |
| PCS | 0.100 | L=.400 | 0.898 | 0.001 | 0.001 |
| MWFS | 0.208 | 0.203 | L=2.089 | 0.363 | 0.227 |
| PFS | 0.001 | 0.001 | 0.997 | L=1.000 | 0.001 |
| VFS | 0.050 | 0.001 | 0.948 | 0.001 | L=.400 |

Parallel to flow (x)-direction

| | PMS | PCS | MWFS | PFS | VFS |
|------|--------------|--------------|----------------|--------------|--------------|
| PMS | L=30.0 | 0.100 | 0.799 | 0.100 | 0.001 |
| PCS | 0.100 | L=10.0 | 0.898 | 0.001 | 0.001 |
| MWFS | 0.178 | 0.303 | L=74.74 | 0.414 | 0.104 |
| PFS | 0.001 | 0.001 | 0.997 | L=30.0 | 0.001 |
| VFS | 0.050 | 0.001 | 0.948 | 0.001 | L=31.0 |

Perpendicular to flow (y)-direction

| | PMS | PCS | MWFS | PFS | VFS |
|------|--------------|--------------|---------------|--------------|--------------|
| PMS | L=3.00 | 0.200 | 0.699 | 0.100 | 0.001 |
| PCS | 0.100 | L=1.0 | 0.898 | 0.001 | 0.001 |
| MWFS | 0.182 | 0.288 | L=7.64 | 0.424 | 0.106 |
| PFS | 0.001 | 0.001 | 0.997 | L=3.0 | 0.001 |
| VFS | 0.050 | 0.001 | 0.948 | 0.001 | L=3.1 |

Table 4.5. Embedded transition probability matrices for the top zone. These matrices are read as transition probabilities from the row hydrofacies to the column hydrofacies. (hydrofacies labels: PMS, poorly sorted medium sand; PCS, poorly sorted coarse sand; MWFS, moderately to well sorted fine sand; PFS, poorly sorted fine sand; VFS, very fine sand. Other labels: L, mean length. Bold numbers indicate background category with computed values listed in the table.)

transition probability is from *PFS* to *MWFS* (0.997). This is likely due to the fact *PFS* hydrofacies is often found as an erosional base beneath the *MWFS* hydrofacies and because the proportion of the *MWFS* hydrofacies. The mean lengths were estimated from the core description and the cross-section of categories in the top zone (Figure 4.2).

The parameters used to estimate the perpendicular to flow (y)-direction Markov chain model (Figure 4.5) were estimated from geologic reasoning, juxtaposition relationships and the vertical (z)-direction embedded transition probabilities in an application of Walther's law (Carle *et al.*, 1998). Walther's law states that only those facies that can be found forming side by side in nature can occur in contact with one another in a conformable vertical succession (Miall, 1996). The mean lengths were estimated from the (z)-direction mean lengths. Robinson and McCabe (1997) reported that trough cross bed sets have an average width to depth ratio of 8.5:1 to 10.4:1, depending on unit. A width to thickness ratio of 7.7:1, measured in an outcrop analog which most closely matched the grain size distribution and vertical thickness of beds in this zone, was applied to the mean lengths in the (z)-direction to estimate (y)-direction mean lengths. Even though this outcrop analog was not a close enough analog to add additional information on juxtapositions, based on the similarity of the width to thickness ratio to published data and the fact that it is the best data available, I applied this width to thickness ratio in this zone. However, there is a high amount of uncertainty in the embedded transition probabilities and the mean lengths due to lack of sufficient continuous data.

The parallel to flow (x)-direction Markov chain model were estimated from the perpendicular (y)-direction embedded transition probabilities in an application of

Top Zone Horizontal Transition Probability

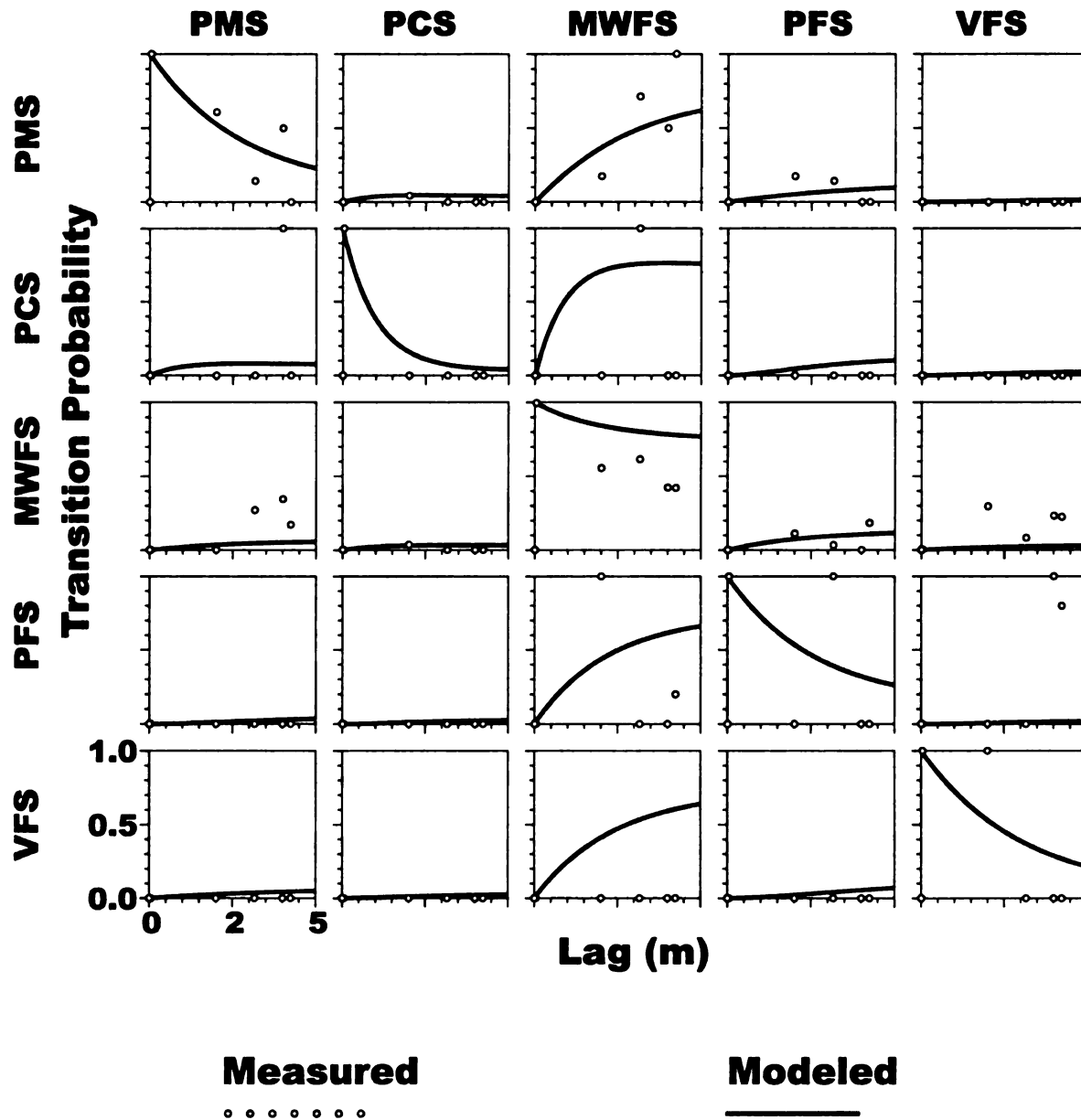


Figure 4.5.
Matrix of perpendicular to flow (y)-direction transition probabilities showing core data as measurements (open circles) and the Markov chain model (solid line) from the core measurements. The diagonal elements represent auto-transition probabilities within a category, and the off diagonal elements represent transition probabilities between categories.

Walther's law (Carle *et al.*, 1998). The mean lengths were estimated from the (y)-direction mean lengths. The embedded transition probabilities are almost the same as the perpendicular to flow (y)-direction embedded transition probabilities (Table 4.5). The mean lengths in the (x)-direction were estimated using the perpendicular to flow mean lengths and multiplying them by 10, an estimate of what the width to length may be off outcrop analogs that were most similar to the characteristics of the top zone. Unfortunately the outcrops were not large enough to measure the length of these units so there is significant uncertainty in the mean lengths in the (x)-direction.

Bottom Zone Markov Chain Models

Vertical (z)-direction transition probability values for the bottom zone were measured from the data, based on a 0.25 m spacing (Figure 4.6). The core data are sparse, and, for that reason, the Markov chain model fit to these measurements was not very good. In an effort to incorporate more data for model development, a 0.25 m grid was overlain on a described outcrop analog which seemed to best fit the facies relationships, proportions, and the thickness of beds in the bottom zone (Figure 4.7). Proportions of categories were estimated based on core data and the outcrop analog (Table 4.2). The additional information on the spatial distribution of facies provided by the outcrop analog helped the Markov chain model, although the addition of more data would further improve the model if the data were available. Figure 4.8 shows the vertical (z)-direction Markov chain model that was fit to the measured data. The embedded transition probabilities and mean lengths used in this model are given in Table 4.6.

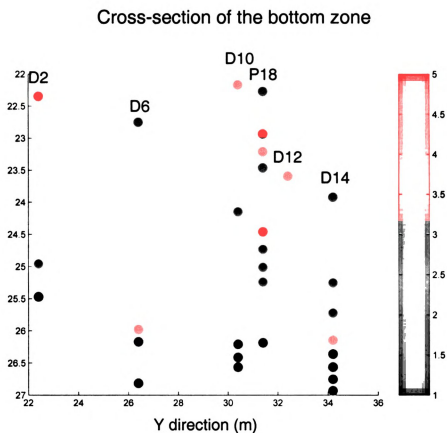


Figure 4.6. Cross-section of category in bottom zone. Category 1, pebbles, granules and very coarse sand (PGVCS); category 2, poorly sorted medium sand (PMS); category 3 poorly sorted coarse sand (PCS); category 4, poorly sorted medium sand (PMS); category 5, moderately and moderately to well sorted fine sand (MWFS). Image is presented in color.

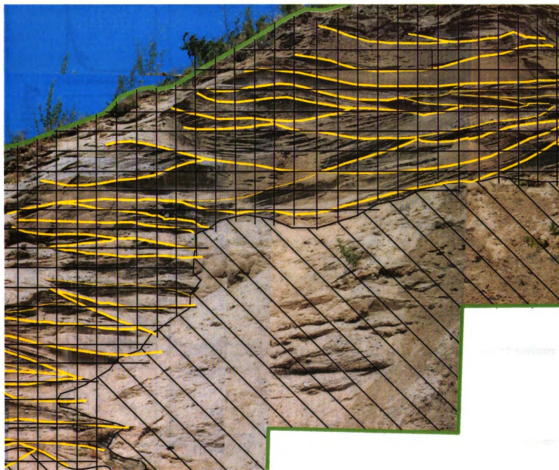


Figure 4.7. Outcrop analog with 0.25 m grid overlay. Image is presented in color.

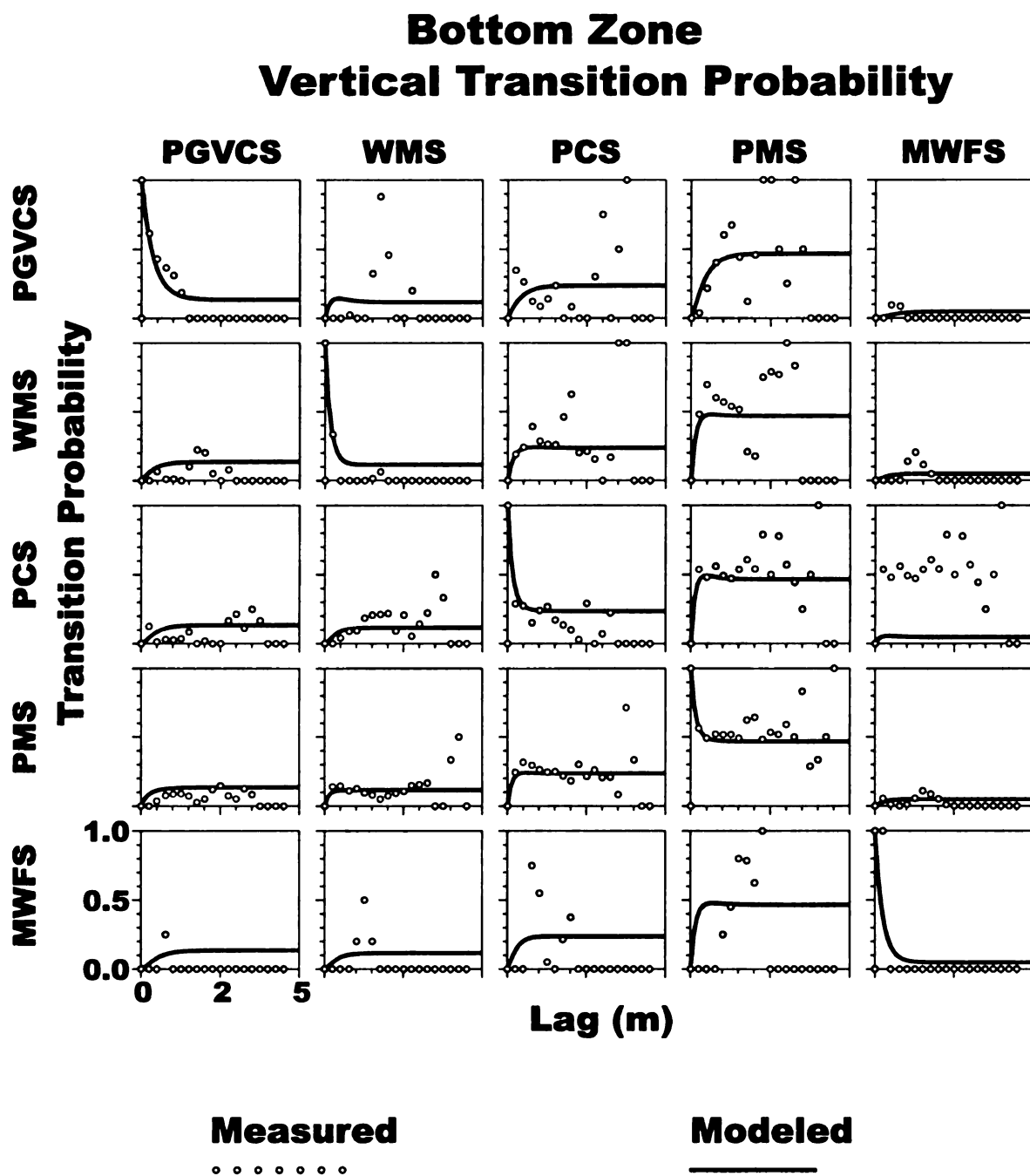


Figure 4.8.
Matrix of vertical (z)-direction transition probabilities showing core data as measurements (open circles) and the Markov chain model (solid line) from the core and outcrop analog measurements. The diagonal elements represent auto-transition probabilities within a category, and the off diagonal elements represent transition probabilities between categories.

Vertical (z)-direction

| | PGVCS | WMS | PCS | PMS | MWFS |
|-------|--------------|--------------|--------------|---------------|--------------|
| PGVCS | L=.420 | 0.500 | 0.240 | 0.250 | 0.010 |
| WMS | 0.050 | L=.190 | 0.250 | 0.690 | 0.010 |
| PCS | 0.010 | 0.005 | L=.200 | 0.885 | 0.100 |
| PMS | 0.162 | 0.257 | 0.542 | L=.273 | 0.038 |
| MWFS | 0.010 | 0.010 | 0.120 | 0.860 | L=.25 |

Parallel to flow (x)-direction

| | PGVCS | WMS | PCS | PMS | MWFS |
|-------|--------------|--------------|--------------|---------------|--------------|
| PGVCS | L=32.0 | 0.250 | 0.450 | 0.290 | 0.010 |
| WMS | s | L=15.0 | 0.250 | 0.603 | 0.010 |
| PCS | s | s | L=15.4 | 0.735 | s |
| PMS | 0.065 | 0.248 | 0.602 | L=25.0 | 0.084 |
| MWFS | s | s | 0.120 | 0.818 | L=25.0 |

Perpendicular to flow (y)-direction

| | PGVCS | WMS | PCS | PMS | MWFS |
|-------|--------------|--------------|--------------|---------------|--------------|
| PGVCS | L=3.20 | 0.250 | 0.450 | 0.290 | 0.010 |
| WMS | s | L=1.50 | 0.250 | 0.603 | 0.010 |
| PCS | s | s | L=1.54 | 0.735 | s |
| PMS | 0.065 | 0.248 | 0.602 | L=2.50 | 0.084 |
| MWFS | s | s | 0.120 | 0.818 | L=2.50 |

Table 4.6. Embedded transition probability matrices for the bottom zone. These matrices are read as transition probabilities from the row hydrofacies to the column hydrofacies. (hydrofacies labels: PGVCS, pebbles, gravel and very coarse sand; WMS, well sorted medium sand; PCS, poorly sorted coarse sand; PMS, poorly sorted medium sand; MWFS, moderately to well sorted fine sand. Other labels: L, mean length. Bold numbers indicate background category with computed values listed in the table.)

Both fining upward and coarsening upward tendencies are present in the bottom zone and preserved in the Markov chain model evident in the w.r.t independent transition frequencies. If the w.r.t values are greater than 1.0 then the transition is more likely to occur and if the w.r.t. values are less than 1.0 then the transition is less likely to occur (Table 4.7). There is a slight fining upward tendency, from *PGVCS* up to *WMS*, from *PGVCS* up to *PCS* and from *PCS* up to *PMS*. However, it is not uncommon to coarsen upward as well. This occurs from *PCS* up to *PGVS*, from *WMS* up to *PCS* and from *MWFS* up to *PMS*.

The perpendicular to flow (y)-direction Markov chain model and mean lengths (Figure 4.9) were estimated from the vertical (z)-direction embedded transition probabilities and vertical (z)-direction mean lengths in an application of Walther's law (Carle *et al.*, 1998). To estimate (y)-direction mean lengths, a 7.7:1 width to thickness ratio, measured in the outcrop analog, was applied to the mean lengths in the (z)-direction. Fining outward tendencies are present in the bottom zone and preserved in the Markov chain model, evident in the w.r.t independent transition frequencies (Table 4.7). The *PGVCS* transitions outward to *WMS* and *PCS*, *WMS* transitions outward to *PMS*, and *PMS* transitions outward to *MWFS*. For the (y)-direction Markov chain model symmetry was forced, noted by an *s* in Table 4.6.

The parallel to flow (x)-direction Markov chain model (Figure 4.5) and mean lengths were estimated from the perpendicular to flow (y)-direction embedded transition probabilities and the (y)-direction mean lengths in an application of Walther's law (Carle *et al.*, 1998). The embedded transition probabilities are the same as for the perpendicular

Vertical (z)-direction

| | PGVCS | WMS | PCS | PMS | MWFS |
|-------|--------------|--------------|--------------|---------------|--------------|
| PGVCS | L=.420 | 5.290 | 1.154 | 0.373 | 0.358 |
| WMS | 1.000 | L=.190 | 1.146 | 0.982 | 0.341 |
| PCS | 0.177 | 0.044 | L=.200 | 1.110 | 3.001 |
| PMS | 1.288 | 1.030 | 0.986 | L=.273 | 0.517 |
| MWFS | 0.215 | 0.108 | 0.588 | 1.310 | L=.25 |

Parallel to flow (x)-direction

| | PGVCS | WMS | PCS | PMS | MWFS |
|-------|--------------|--------------|--------------|---------------|--------------|
| PGVCS | L=32.0 | 2.019 | 1.475 | 0.534 | 0.356 |
| WMS | s | L=15.0 | 0.770 | 1.044 | 0.334 |
| PCS | s | s | L=15.4 | 1.028 | s |
| PMS | 0.534 | 1.044 | 1.028 | L=25.0 | 1.561 |
| MWFS | s | s | 0.407 | 1.561 | L=25.0 |

Perpendicular to flow (y)-direction

| | PGVCS | WMS | PCS | PMS | MWFS |
|-------|--------------|--------------|--------------|---------------|--------------|
| PGVCS | L=3.20 | 2.019 | 1.475 | 0.534 | 0.356 |
| WMS | s | L=1.50 | 0.770 | 1.044 | 0.334 |
| PCS | s | s | L=1.54 | 1.028 | s |
| PMS | 0.534 | 1.044 | 1.028 | L=2.50 | 1.561 |
| MWFS | s | s | 0.407 | 1.561 | L=2.50 |

Table 4.7. W.r.t independent transition frequencies matrices for the bottom zone. These matrices are read as independent transition probabilities from the row hydrofacies to the column hydrofacies. (hydrofacies labels: PGVCS, pebbles, gravel and very coarse sand; WMS, well sorted medium sand; PCS, poorly sorted coarse sand; PMS, poorly sorted medium sand; MWFS, moderately to well sorted fine sand. Other labels: L, mean length. Bold numbers indicate background category with computed values listed in the table.)

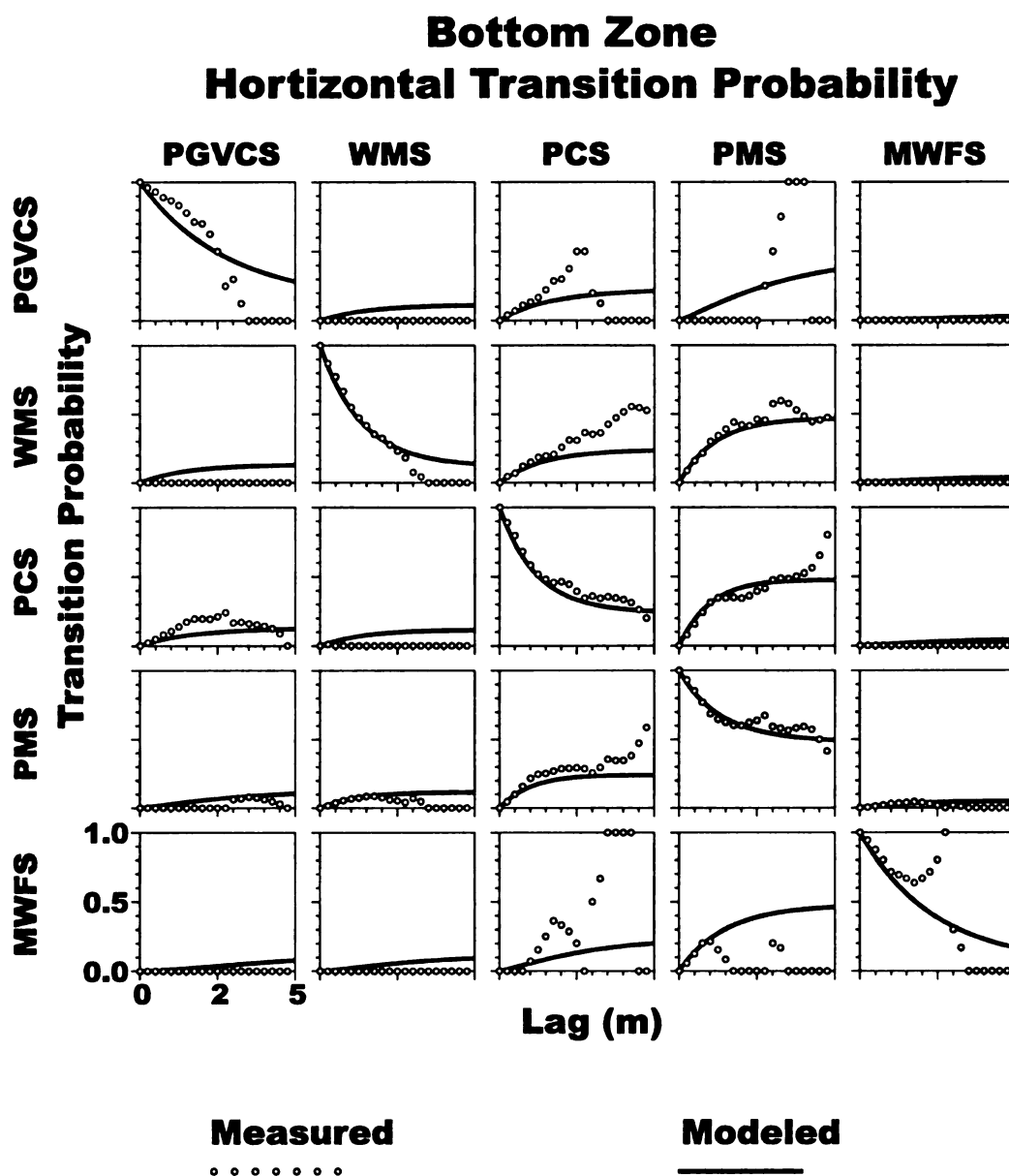


Figure 4.9.
Matrix of perpendicular to flow (y)-direction transition probabilities showing core data as measurements (open circles) and the Markov chain model (solid line) from the core and outcrop analog measurements. The diagonal elements represent auto-transition probabilities within a category, and the off diagonal elements represent transition probabilities between categories.

to flow (y)-direction (Table 4.6). The mean lengths were estimated using the perpendicular to flow mean lengths and multiplying them by 10, an estimate of what the width to length may be based on the outcrop analogs. Unfortunately the outcrops were not large enough to measure the length of these units so there is much uncertainty in the mean lengths in the (x)-direction. For the (x)-direction Markov chain model symmetry was forced, noted by an *s* in Table 4.6.

Conditional Sequential Indicator Simulation

Conditional sequential indicator simulation, followed by simulated annealing (Carle *et al.*, 1998), was run on the top and bottom zones separately using the appropriate Markov Chain model for each zone. The cell size for the realization of the Schoolcraft site was 0.2 m in the lateral directions (x and y) and 0.25 m in the vertical direction (z). This small grid spacing was used so that the realizations simulated here could be input into an existing GMS grid with similar dimensions in the future. Information from core were used as hard conditioning data in the simulations.

Combining the Zones

Once the realizations were complete for the top and bottom zones individually, the results were combined to create a final whole aquifer characterization. There are some categories that occur in both the top and bottom zone. After simulation, these categories were combined to simplify the final product and show similarities between the two zones. Category 5 from the bottom zone (*MWFS*) was combined with category 3 from the top zone (*MWFS*) and on the final plot is called moderately-well sorted fine

sand. Category 4 from the bottom zone (*PMS*) and category 1 from the top zone (*PMS*) were combined and is called poorly sorted medium sand in the final realization.

Category 2 from the top zone (*PCS*) was combined with category 3 from the bottom zone and is called poorly sorted coarse sand in the final realization. The final realizations of the Schoolcraft site are Figure 4.10 and Figure 4.11. Figure 4.11 is separated into five volumetrically equal blocks allowing the inside to be more readily viewed.

The final geostatistical realization reflects juxtaposition tendencies, proportions and the channel orientation used as inputs to the Markov chain model. Fining upward tendencies are preserved in the top zone where *FSP* fines upward to *MWFS*. In the bottom zone, both the fining and coarsening upward tendencies are preserved from *PGVCS* and *PCS* up to *WMSM* and from *WMSM* up to *PCS* and from *MWFS* up to *WMSM*. Channels are orientated perpendicular to Y axis along the maximum correlation direction. In the top zone, the high proportion of *MWFS* is preserved and other hydrofacies are distributed in channel like geometries. The most striking channel like geometry is the *VFS* hydrofacies simulated channel located at about (5, 10, 18) m in Figure 4.10 and Figure 4.11. This is interesting because no conditioning data indicate that a channel is present at this location. Other realizations would likely not simulate a channel at this location. The realization presented here simulated a channel there based on the Markov chain model. By assigning average hydraulic conductivity values (Table 4.3 and Table 4.4) to each hydrofacies, this realization could be used in groundwater flow modeling and contaminant transport simulations. Assigning an average K value to each hydrofacies would preserve abrupt changes in K where other traditional geostatistical tools such as kriging would smooth K values.

Schoolcraft Site

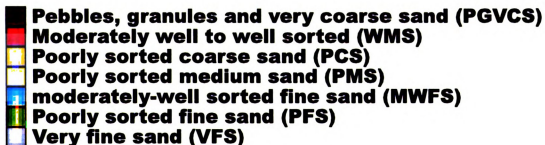
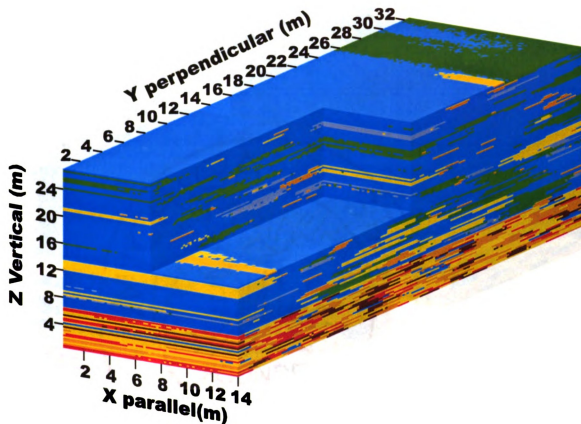


Figure 4.10

A realization of the Schoolcraft plume A site based on transition probability/ Markov chain geostatistics in two zones. This image is presented in color.

Schoolcraft Site

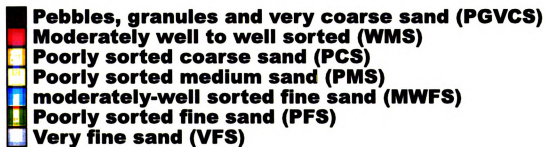
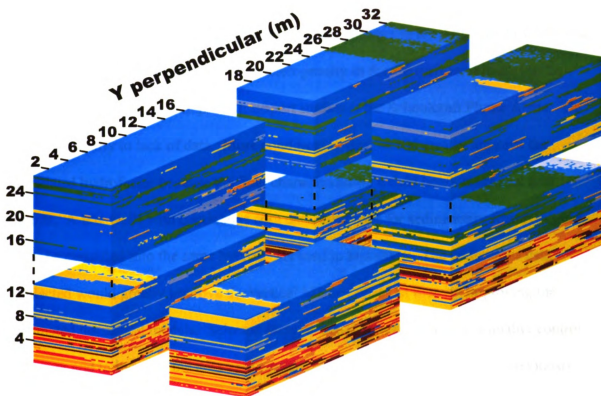


Figure 4.11

A realization of the Schoolcraft plume A site based on transition probability/ Markov chain geostatistics in two zones. This image is presented in color.

Conclusions

Using the transition probability geostatistics and the Markov chain models, a geologically reasonable aquifer characterization was simulated that better honors the stationarity assumption and better preserves abrupt changes in K. Although this is a very reasonable approach to characterizing heterogeneity in the subsurface, it is unclear how much this realization will improve transport studies at the Schoolcraft Plume A site. This is due primarily to lack of data. More conditioning data would greatly improve the simulated hydrofacies because the final characterization would honor more real data points. A few wells with continuous core data, described for sedimentary features could then be classified into the same hydrofacies used in this study. The continuous data collected would greatly improve the vertical Markov chain fit thereby improving the estimated horizontal models. Selected samples could be tested for K as a quality control measure and to increase the data base where only a few samples were tested previously. At a small scale such as this, it is the fine details that are of concern to produce accurate groundwater models and transport simulations. Without closely spaced detailed continuous core descriptions, only general concepts can be obtained from this type of modeling, and at this site accurate detailed aquifer characterizations are the goal.

Chapter 5

Conclusions

Depositional Environment of the Aquifer Below Schoolcraft

Based on grain size data, bedding structures present, location of aquifer and depositional history of Kalamazoo County it was concluded that the base of the aquifer is composed of braided stream deposits located at a position medial (intermediate) the glacier front (Donjeck-type) and the upper portion of the aquifer is composed of braided stream deposits located at a position distal to the glacier front (Platte-type). The grain size of the bottom zone ranges from gravel to medium sand and is primarily gravel to coarse sand. Benn and Evans (1998) stated that a Scott-type stream is composed of greater than 90 percent gravel and a Donjeck-type stream is composed of 10 to 90 percent gravel. Thus, it can be reasoned that a Platte-type stream is composed of less than 10 percent gravel. Benn and Evan's (1998) grain size based divisions of proximal, medial and distal seem realistic upon comparison to Miall's (1977) braided stream facies models. The bottom zone is not classified as proximal to the glacier front (Scott-type braided stream) because it is not composed of more than 90 percent gravel and because the aquifer is located too far away from the Kalamazoo Moraine. Proximal (Scott-type) deposits can be found 0.5 miles from the Kalamazoo Moraine (figure 1). The proximal deposits at this gravel pit are composed almost entirely of gravel. Medial deposits are found 2 miles from the Kalamazoo Moraine at a sand and gravel pit where outcrop analogs were constructed to aid in the interpretation of subsurface geology in this study. An outcrop analog that was interpreted to have been deposited distal to the glacier was

not found. This is likely due to the high water table at distal locations and the fact that the fine sand is not worth as much as gravel and boulders, so it is not as cost effective to have a sand and gravel pit in most distal locations. The top of the Schoolcraft aquifer is interpreted as being deposited distal to the glacier, and is located approximately 6 miles away from the Kalamazoo Moraine. The fining upward sequence from medial to distal braided stream deposits at the Schoolcraft site indicate that a glacial retreat was recorded in this sediments.

Aquifer Characterizations

For all of the geostatistical methods used, lack of data was the biggest problem. With more data, better variograms and Markov chain models could be developed. Increased conditioning data would significantly improve both the zonal kriging and the transition probability simulation because the final characterizations would honor more real data points. A few wells with continuous core described for sedimentologic features, sieved to measure grain size distribution and standard deviation, and tested for K value would accomplish this. Another way to increase continuous core data is to do borehole geophysics (e.g., resistivity and conductivity logs) in boreholes where core was not fully recovered. Geophysical logs could then be compared to core descriptions and interpretations could be made to what type of sediment exist where there was no recovery.

Closely spaced continuous core is critical to further improvement of the small-scale characterization of this aquifer. When focusing on such a small area, fine details in the heterogeneity must be considered, this can not be achieved without sufficient data.

Without close-spaced core data, only general concepts of heterogeneity and facies distribution can be obtained from geostatistical interpolation and simulation methods. At this site, accurate fine scale aquifer characterizations are the goal. Hence, quality close-spaced core data are needed.

Kriging Method

The addition of geologically based zones significantly improved the aquifer characterization as shown by the comparison of simulated to field tracer tests. Stationarity was better honored in the zonal krige characterization because zones were based on K distribution, such that each zone had less of a range of K than all the zones together did. Abrupt changes in K were preserved, especially around the low K zone, with the addition of stratigraphic zones. By understanding the heterogeneity present in the model and how that relates to the simulated versus field tracer tests, predictions can be made of what the geology is where tracer test data are available but no core was recovered.

Transition Probability Method

Stratigraphically based zones used in the transition probability simulation better honors the stationary assumption because the zones were delineated by mean grain size. The top and bottom zone have a mean grain size and a standard deviation of grain size that are more spatially consistent within that zone than across the boundary and into the other zone. Transition probability simulations preserve abrupt changes in K by not smoothing the data, and instead simulating a hydrofacies to every cell. Each hydrofacies

has a distinct K value that can be put into each cell. This is an advantage over kriging which smoothes data and forces the mean of the geostatistical variable at the edge of the model. As with the other geostatistical methods, lack of quality conditioning data limited the use of transition probability modeling. It is unclear how much this characterization method will improve transport studies at the Schoolcraft site, because not enough data was available to do a thorough characterization.

Appendix A

Stratigraphy of the Schoolcraft Plume A Site

Core Data

Core was collected at several wells in the Schoolcraft Plume A site. This core was described for visual grain size, measured grain size by use of sieves, and/or tested for K on a constant head permeameter. For this study, all recovered core from well P18 (see Figure A.1 for location) was described in full for sedimentologic features (Table A.1 and Figure A.2). Portions of core P18 were sieved and measured for vertical K value. Additionally, segments of core from wells P6, P7 and P8 were described for sedimentologic features (Figures A.3-A.8). Core descriptions of wells P18, P6, P7, and P8 and vertical K measurements of P18 were conducted as part of this study. Previous work by Hoard (2002) assessed the grain size distribution and the horizontal K of portions of seven of the 15 delivery wells in the biocurtain (D2, D4, D6, D8, D10, D12 and D14) and wells P6, P7 and P8, located down-gradient of the biocurtain (Table A.2-A.8). Core was collected from approximately 5 m bgs (below ground surface) to 26.5 m bgs. Previous studies indicated that sediment above 8 m bgs did not show evidence of carbon tetrachloride contamination thus, data were not collected above 5 m bgs.

Interpretations of Depositional Environment of the Aquifer Below Schoolcraft

Gravel and sand pits located in Kalamazoo County aid in the interpretation of proximal, medial, and distal location from the glacier at the time the sediments that compose the Schoolcraft aquifer were deposited. Benn and Evans (1998) state that proximal (Scott-type) braided stream deposits are composed of greater than 90 percent

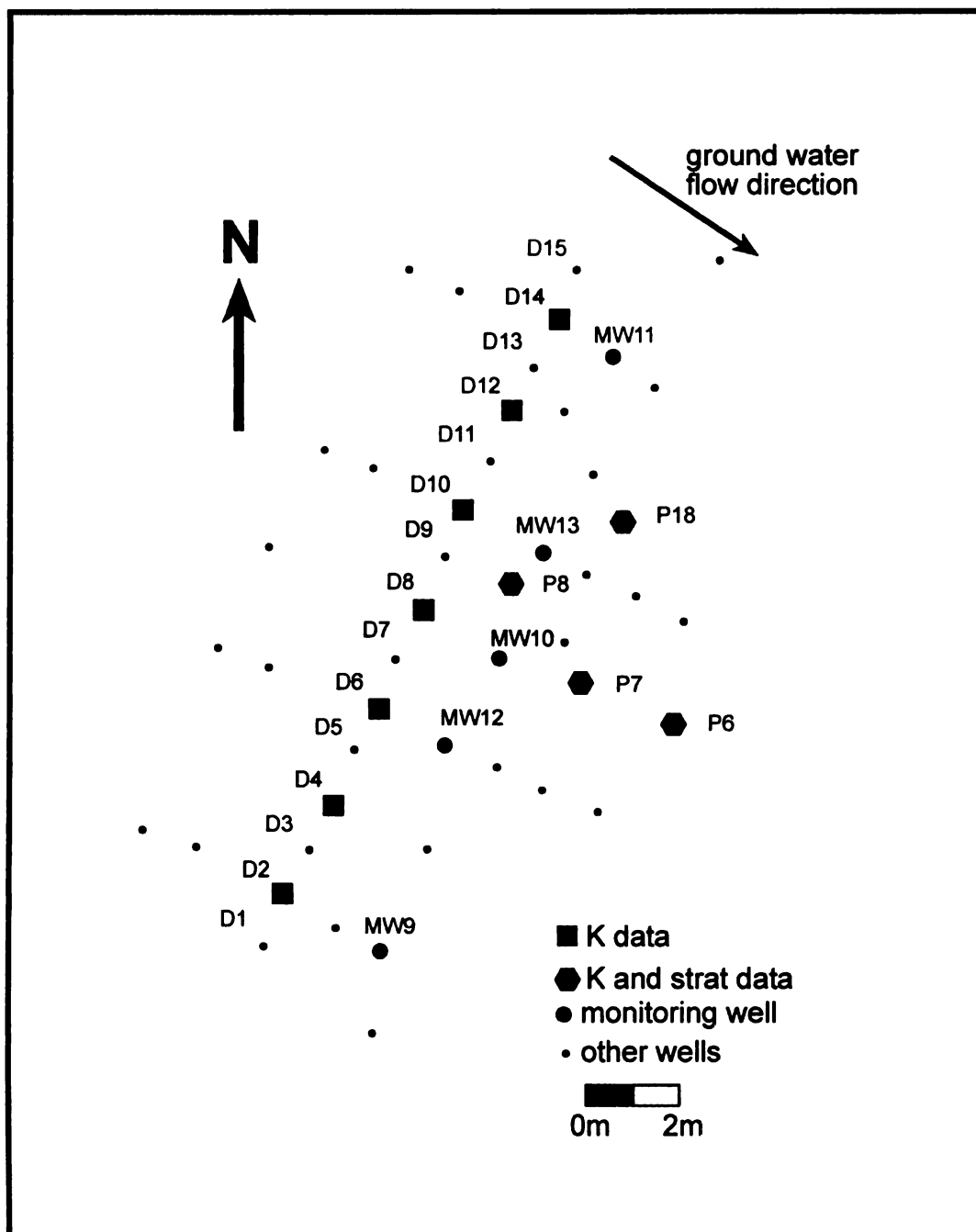


Figure A.1. Location of delivery wells (D), monitoring wells (MW), piezometers (P) and other wells at the Schoolcraft plume A site.

gravel and medial (Donjeck-type) braided stream deposits are composed of anywhere between 10 and 90 percent gravel. It can be further reasoned that distal (Platte-type) braided stream deposits are composed of less than 10 percent gravel.

Along with mean grain size, bedding structures also helped when classifying the outcrop analogs into proximal, medial and distal locations from the glacier. Miall (1977; 1996) stated that proximal braided streams deposits are commonly horizontal gravel sheets displaying weak imbrication. Trough cross-bedded gravels and planar cross bedded gravels are also prominent (Miall 1977; 1996 and Benn and Evans 1996). Medial deposits can be composed of a variety of facies e.g. massive gravels, trough cross-bedded sands and gravels, planar cross-bedded sands and gravels, ripple cross-laminated sand and sand drapes (Miall 1977; 1996 and Benn and Evans 1996). Distal deposits are composed primarily of trough cross-bedded sands, planar cross-bedded sands and horizontally bedded sands. Minor gravel lenses and overbank fines may be present (Miall 1977; 1996 and Benn and Evans 1996).

A gravel pit located approximately 0.5 miles away from the Kalamazoo Moraine on Ravine Road is composed of greater than 90 percent gravel and coarser material with the remaining percent composed of sand. The gravel at this site displays cross-bedding and horizontal bedding with some imbricated clasts indicating minor channel fills or bedforms and channel lag deposits.

Approximately 2 miles from the Kalamazoo moraine on Ravine Road is the gravel and sand pit interpreted as a medial (Donjeck-type) braided stream deposit. This sand and gravel pit, was a site of outcrop analog study for this project. The entire section studied for the outcrop analog was approximately 10 meters in height and generally fined

upward from gravels at the base of the section up to medium sand at the top of the section (Figures B.4- B.7-Appendix B outcrop analogs). This section had less than 90 percent gravel and greater than 10 percent gravel classifying it as a medial (Donjeck-type) deposit. Gravels were cross-bedded to horizontally bedded and some displayed imbrication suggesting minor channel fills, bedforms, and channel lags as locations of deposition. Coarse and medium sands were mainly trough cross-bedded suggesting deposition on linguoid bars, which are common in Donjeck-type streams (Miall, 1977).

No analogs were found to distal (Platte-type) braided stream deposits in Kalamazoo County, likely for the reason that it is not as cost effective to have a sand and gravel pit in distal environments of deposition. This is most likely due to primarily two factors 1) the cost of gravel is much higher than the cost of sand, so less money will be made by the sale of sand and 2) the further from the Kalamazoo Moraine, the lower the elevation and the higher the water table, making excavation of sands difficult and costly when dewatering the area.

The Schoolcraft Aquifer is located approximately 6 miles away from the Kalamazoo Moraine at Paw Paw Lake, which is considered to be the outlet of the river whose sediments compose the Prairie Rhonde Fan and Schoolcraft Aquifer. The bottom of the aquifer (27.5 to 20.5 m bgs) is dominated by gravel fining upward to medium sand, suggesting an intermediate location from the glacier or Donjeck-type braided stream. The medium sands, coarse sands and gravels are cross-stratified with coarser grains deposited along beds.

The upper part of the aquifer (20.5 to 5 m bgs) is dominated by medium and fine sand with some very fine sand, silt and gravel. This corresponds well to the Platte type

braided stream described by Miall (1977). Further evidence for a Platte type braided stream is the presence of cross-stratified sands, massively bedded sands and silt. The cross-stratified sands may have formed in linguoid and transverse bars. The massively bedded sands may have stratification too fine to see at the core scale, or it may have been deposited during high discharge when all of the channels generally merge to create a sheet flow, as described by Krigstrom (1962). The silt described in the core is thought to have deposited during the last stages of waning flow when deposition of thin silt or mud drapes and channel fills occur in inactive areas (Miall, 1977; 1996 and Benn and Evans 1998).





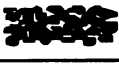
Miall (1977) stated that the Donjeck and Platte types may merge subtly into one another, supporting the degree of difficulty involved in identifying the boundary between medial and distal outwash facies. Although much uncertainty exists when classifying outwash into proximal, intermediate and distal zones, it is believed that the upper portion of the aquifer represents distal outwash (Platte-type) and the bottom portion of the aquifer represent intermediate outwash (Donjeck-type). This conclusion is based on the mean grain size, proportions of grain size, types of bedding, thickness of beds, fining upward cycles and distance from the Kalamazoo Moraine.

Below the outwash, lies a light gray clay that was inferred by Mayotte (1991) to be laterally extensive beneath the Schoolcraft, thus marking the base of the aquifer for this study. This is a till unit that occurs beneath the Village of Schoolcraft and acts to retard the downward migration of plumes A-G (Lipinski, 2002). This till is likely the Ganges till reported by Monaghan *et al.* (1986) to crop out at the Tekonsha moraine and hence underlie sediments between the Tekonsha and Sturgis or Kalamazoo Moraines.

The gray till contains small quantities of sand and silt and was reported by Mayotte (1991) to have been encountered in several test borings at depths ranging from 21.3 to 30.5 m below grade.

Key for core descriptions

Bedding structure symbols and abbreviations

| | |
|---|--|
| Sm | Massively bedded sand |
|  | Cross Stratified bedding |
|  | Faint cross stratified bedding |
|  | Pebbles or granules along cross stratified bedding |
|  | Faint laminar bedding |
|  | Pebbles |
| X-S bedding | cross stratified bedding |
| M bedding | massively bedding |

Sorting abbreviations

| | |
|-------------------|------------------------------|
| vw-sorted | very well sorted |
| w-sorted | well sorted |
| wm-sorted | well to moderately sorted |
| m-sorted | moderately sorted |
| mp-sorted | moderately to poorly sorted |
| p-sorted | poorly sorted |
| pvp-sorted | poorly to very poorly sorted |
| vp-sorted | very poorly sorted |

Grain size abbreviations

| | |
|-----------------------|---|
| VF sand | very fine sand |
| F sand | fine sand |
| M sand | medium sand |
| C sand | coarse sand |
| F-s-c sand | fine sand with high silt and clay content |
| F-m-vf sand | fine sand with high medium and very fine sand content |
| F-msand | fine sand with high medium sand content |
| F-m-c sand | fine sand with high medium and coarse sand content |
| F-m-g sand | fine sand with high medium sand and granule content |
| F-m-p sand | fine sand with high medium sand and pebble content |
| F-m-vf-p sand | fine sand with high medium, very fine sand and pebble content |
| M-f sand | medium sand high fine sand content |
| M-f-c sand | medium sand with high fine and coarse sand content |
| M-c sand | medium sand with high coarse sand content |
| M-c-f sand | medium sand with high coarse and fine sand content |
| M-g sand | medium sand with high granule content |
| C-m sand | coarse sand with high medium sand content |
| C-g sand | coarse sand with high granule content |
| C-p-g sand | coarse sand with high pebble and granule content |
| Pebbles-c sand | pebbles with high coarse sand content |

Other abbreviations

| | |
|------------|-------------------|
| SAA | same as above |
| HCL | hydrochloric acid |

Table A.1. Key for core descriptions.

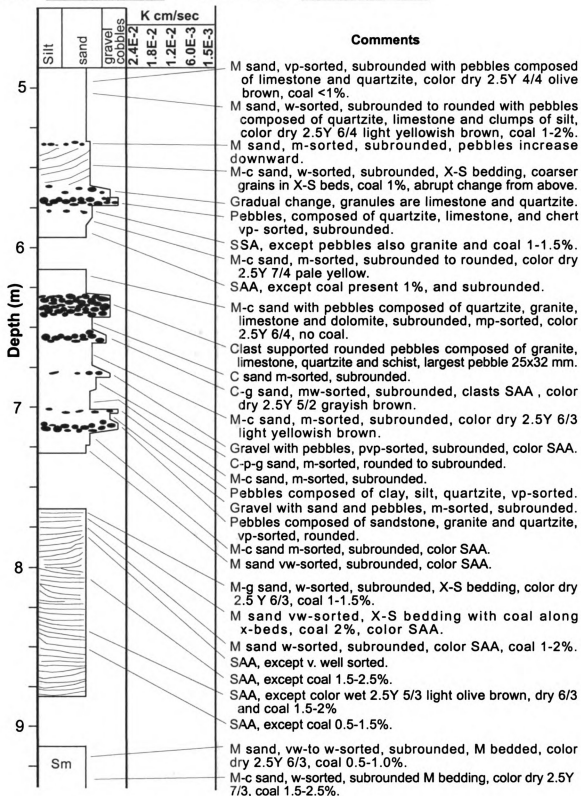
Date: **1-5-01 thru 1-12-01**Described by: **Susanne E. Biteman**

Figure A.2.a. Core description of well P18.

Date: **1-12-01, 7-19-01 thru 8-12-01**

Described by: **Susanne E. Biteman**

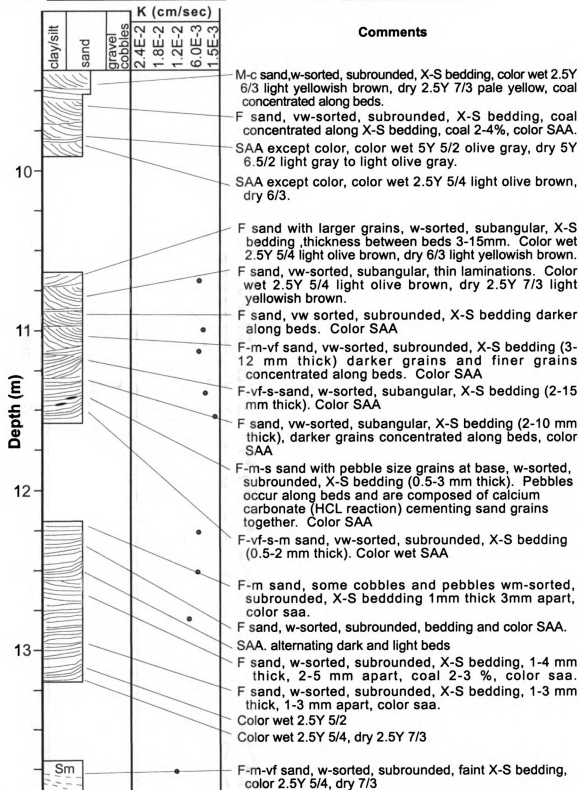


Figure A.2.b. Core description of well P18. Vertical K measurements shown in second column.

Date: **7-23-01 thru 8-17-01** Described by: **Susanne E. Biteman**

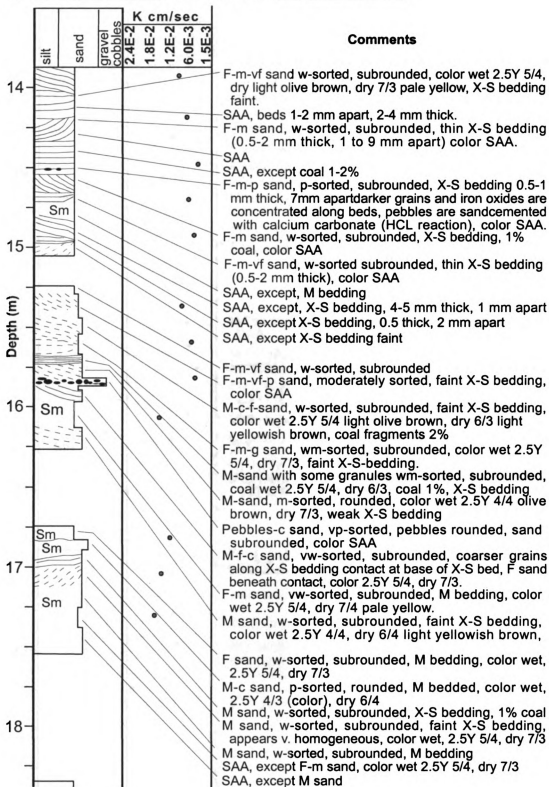


Figure A.2.c. Core description of well P18. Vertical K measurements shown in second column.

Well Name: P-18 Location: Plume A, Schoolcraft, MI Page: 4 of 5

Date: 7-31-01 thru 8-22-01 Described by: Susanne E. Biteman

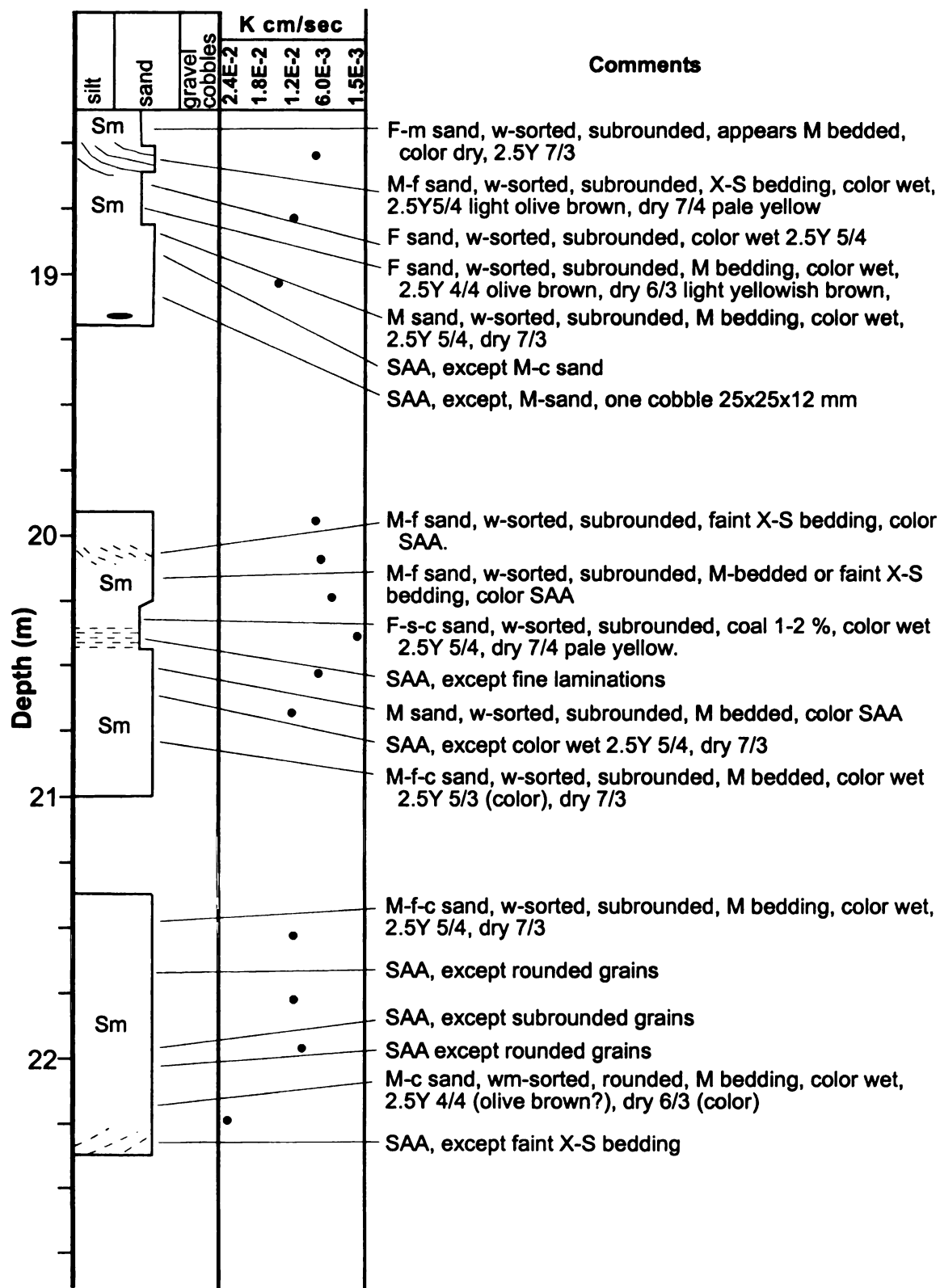


Figure A.9.d. Core description of well P18. Vertical K measurements shown in second column.

Date: **7-18-01, 8-22-01 thru 8-24-01** Described by: **Susanne E. Biteman**

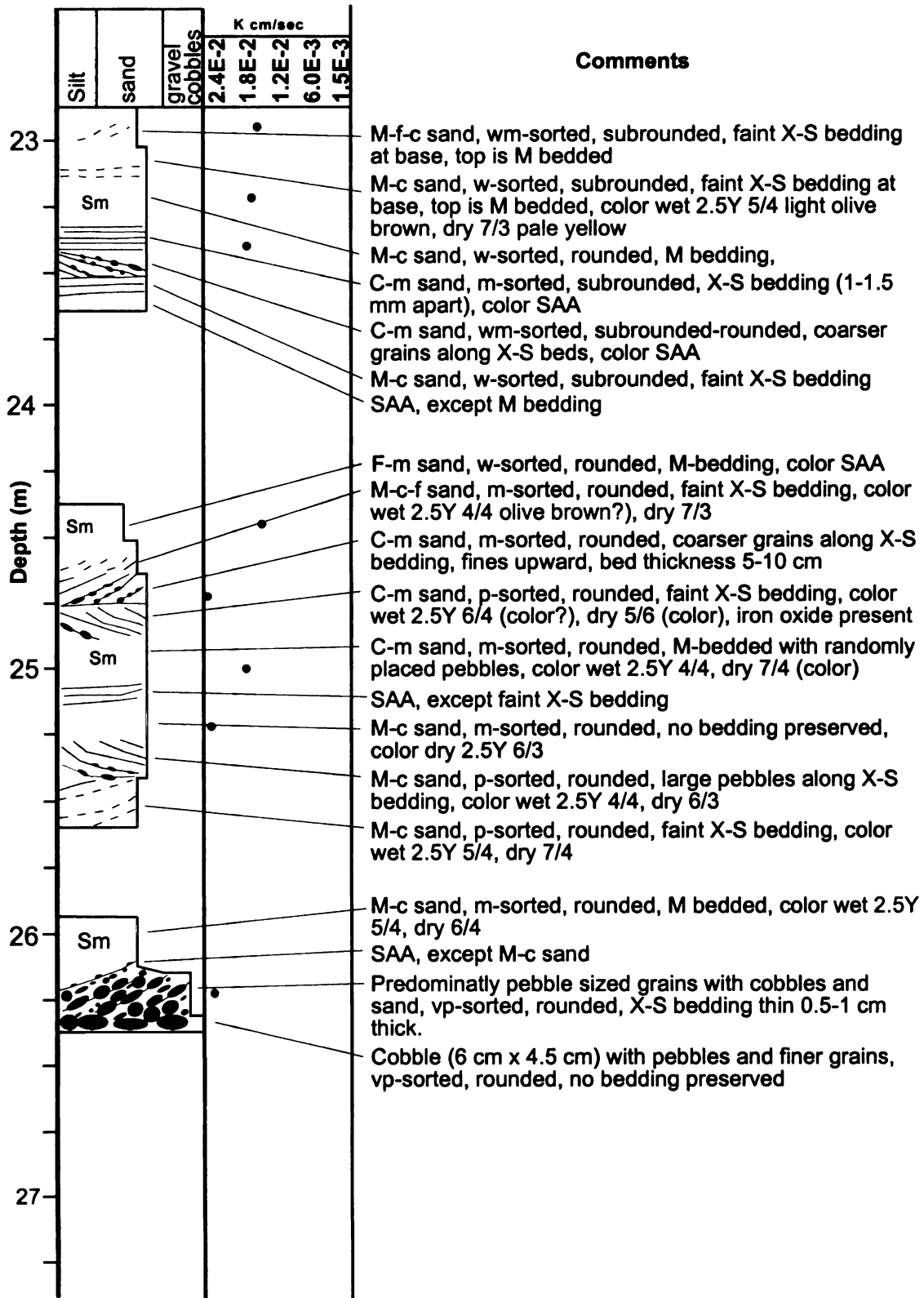


Figure A.9.e. Core description of well P18. Vertical K measurements shown in second column.

Well Name: P-6 Location: Plume A, Schoolcraft, MI Page: 1 of 2

Date: 1-3-01 thru 1-4-01 Described by: Susanne E. Biteman

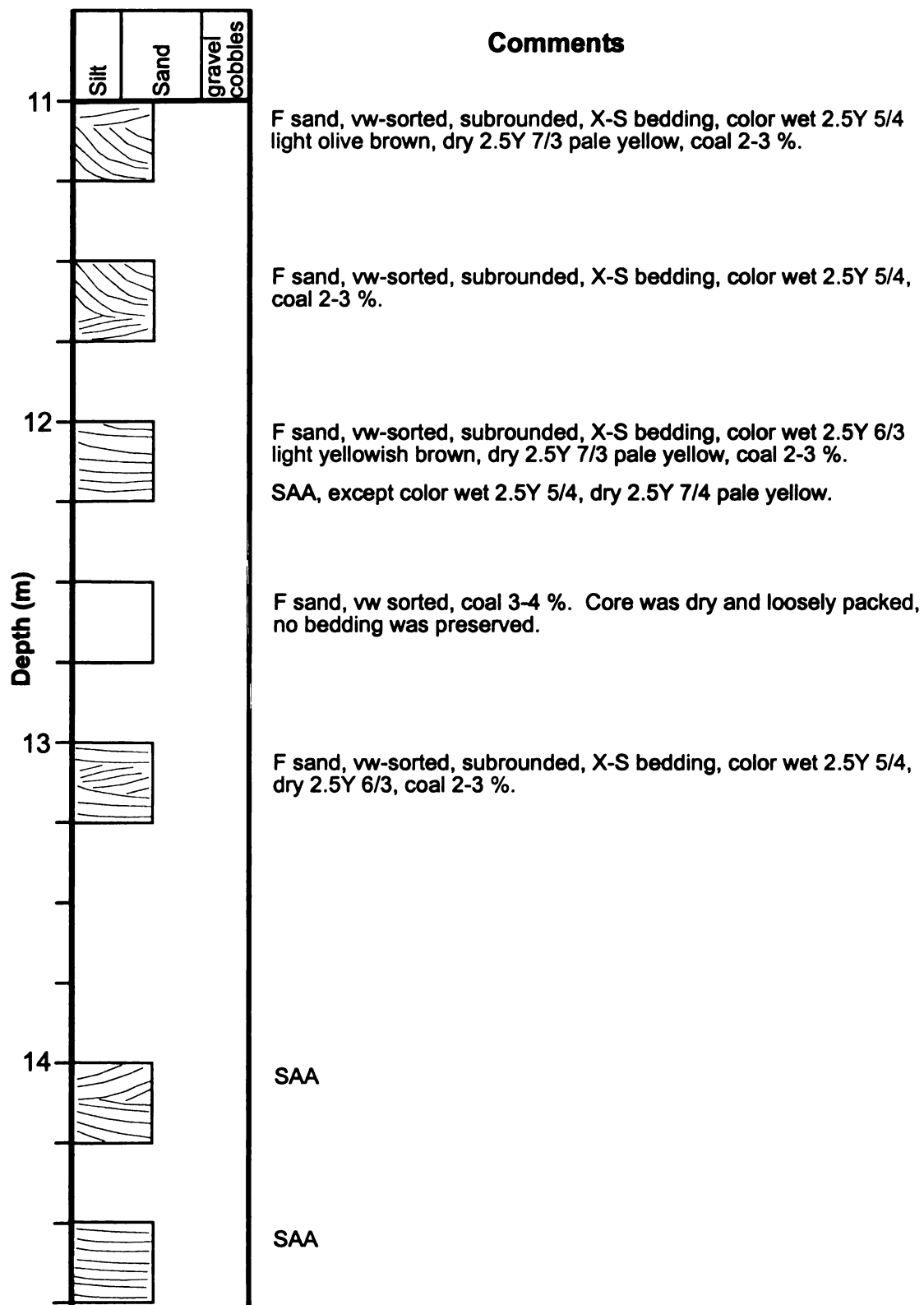


Figure A.3.a. Core description of well P6.

Well Name: P-6 Location: Plume A, Schoolcraft, MI Page: 2 of 2

Date: 1-3-01 thru 1-4-01 Described by: Susanne E. Biteman

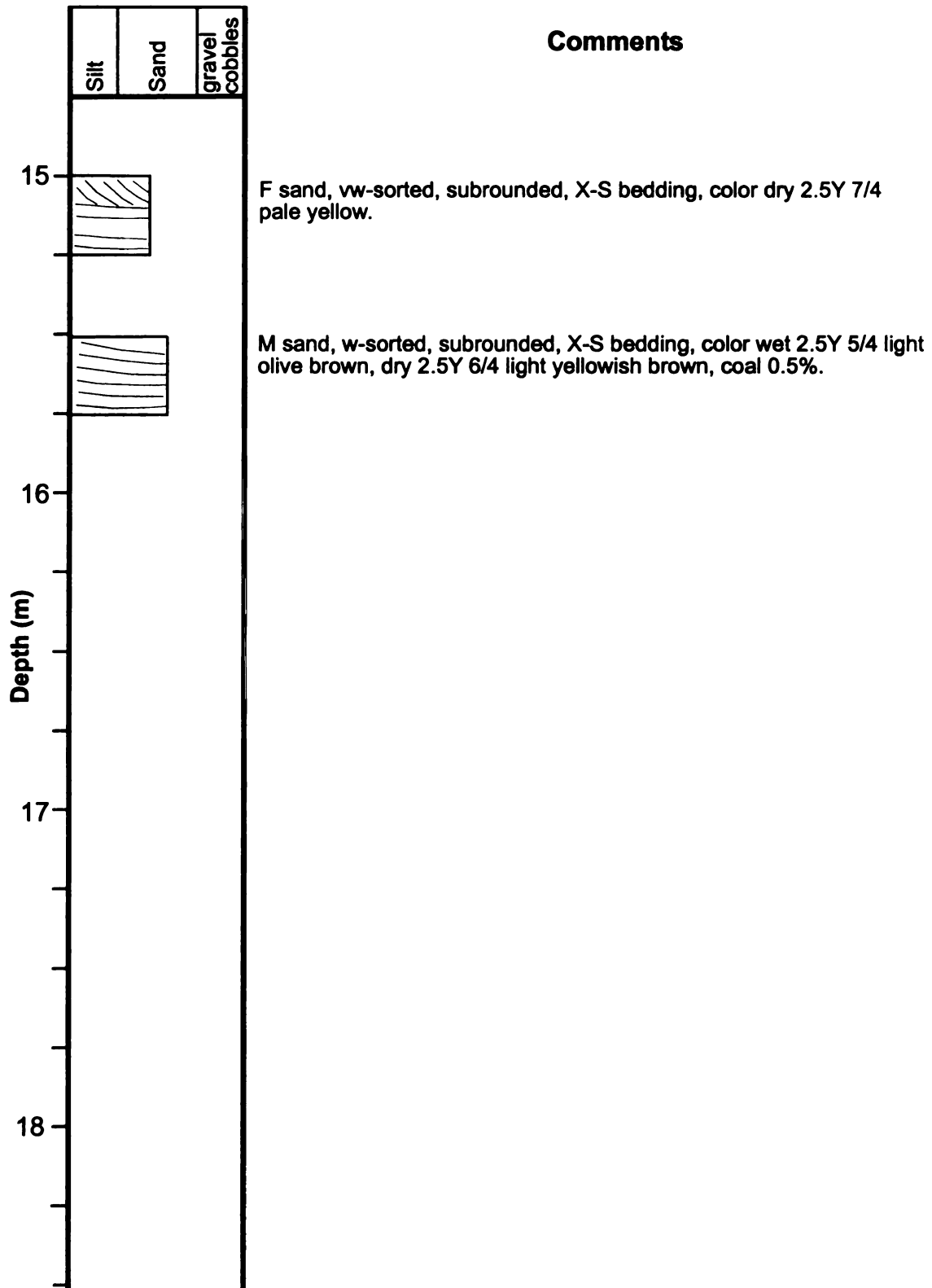


Figure A.3.b. Core description of well P6.

Well Name: PIB-7 Location: Plume A, Schoolcraft, MI Page: 1 of 2

Date: 12-29-00 Described by: Susanne E. Biteman

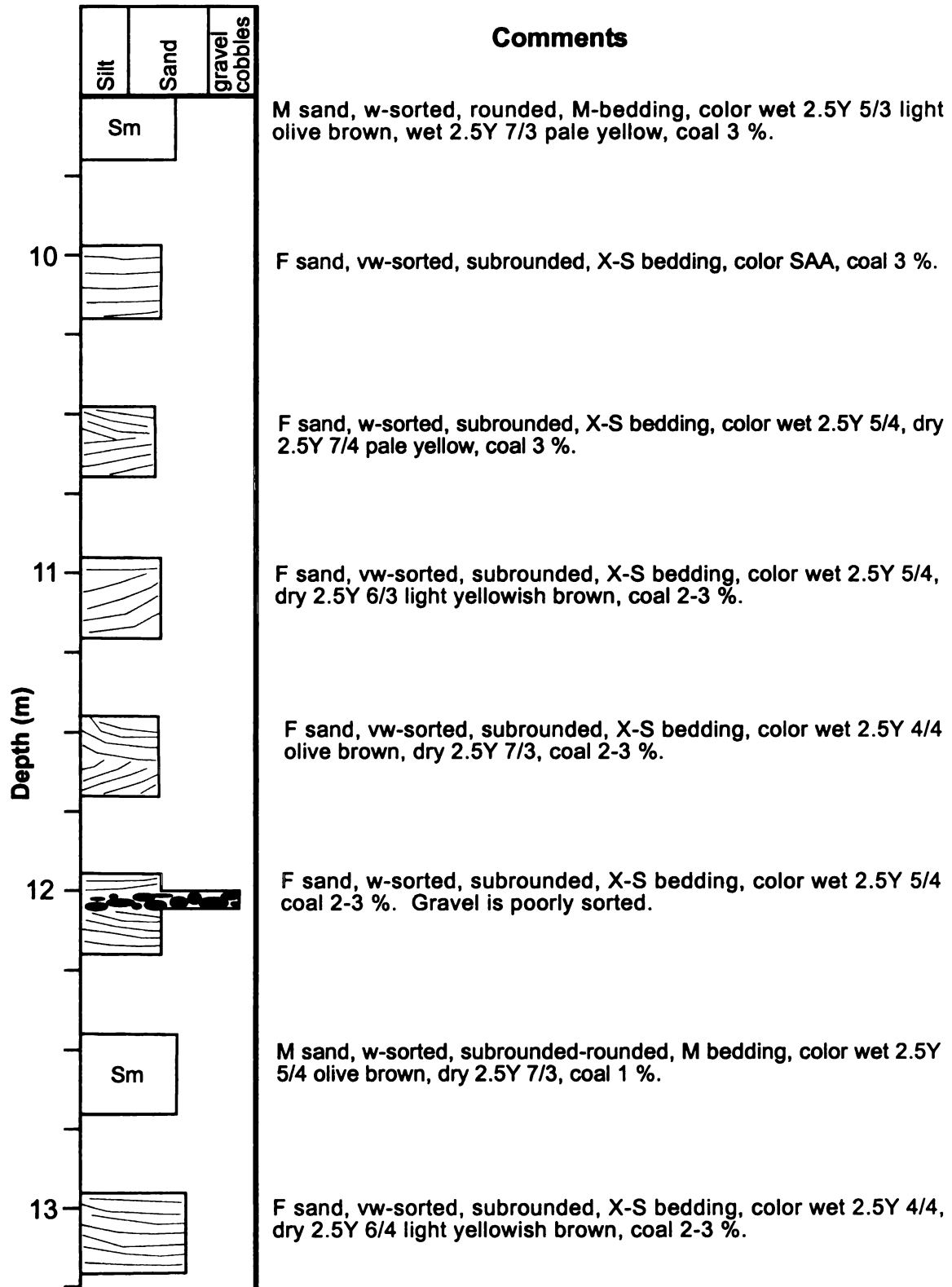


Figure A.4.a. Core description of well P7.

Well Name: PIB-7 Location: Plume A, Schoolcraft, MI Page: 2 of 2

Date: 12-29-01 thru 1-3-01 Described by: Susanne E. Biteman

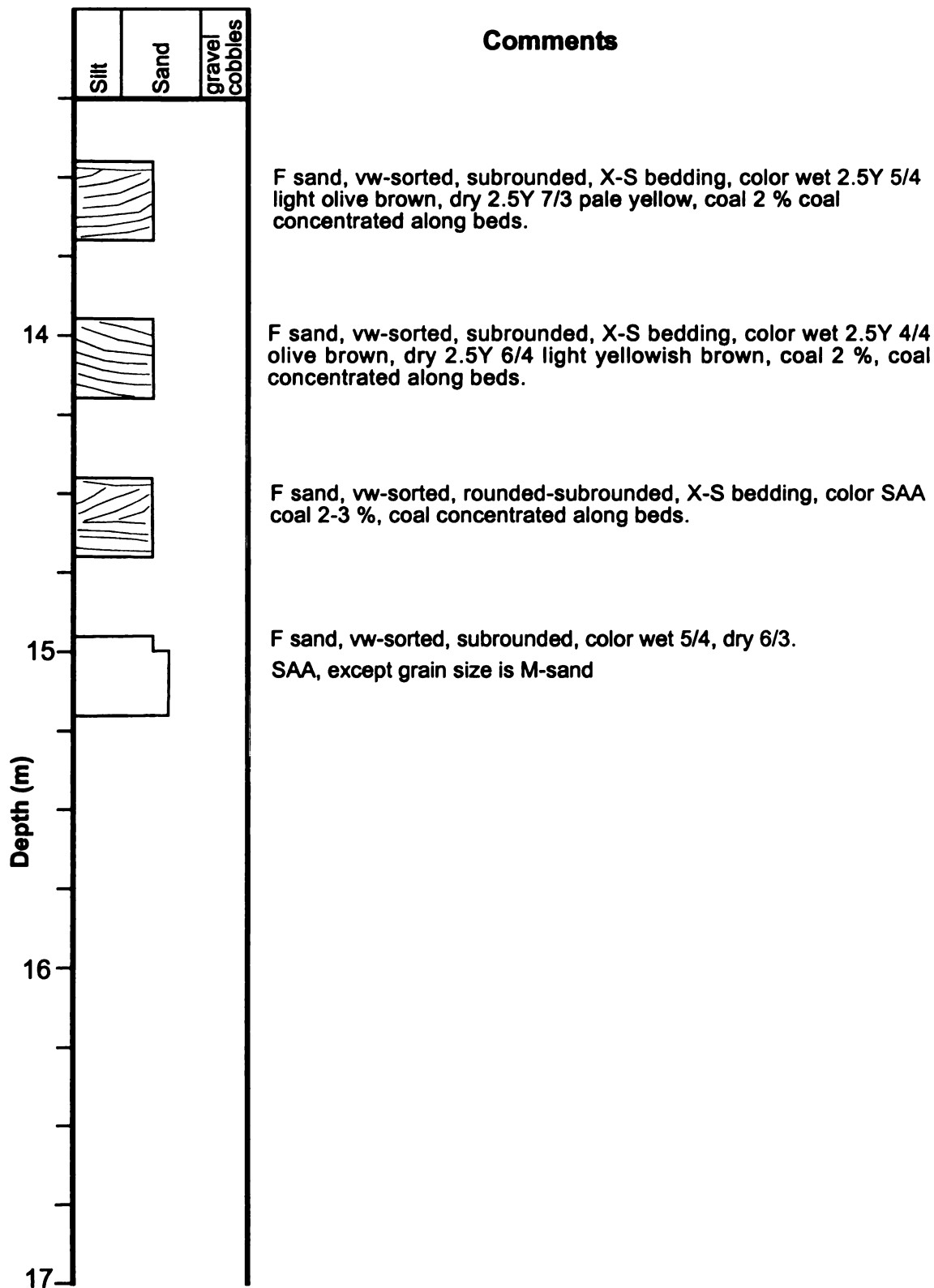


Figure A.4.b. Core description of well P7.

Well Name: PIB-8 Location: Plume A, Schoolcraft, MI Page: 1 of 6

Date: 12-27-00 thru 12-28-00 Described by: Susanne E. Biteman

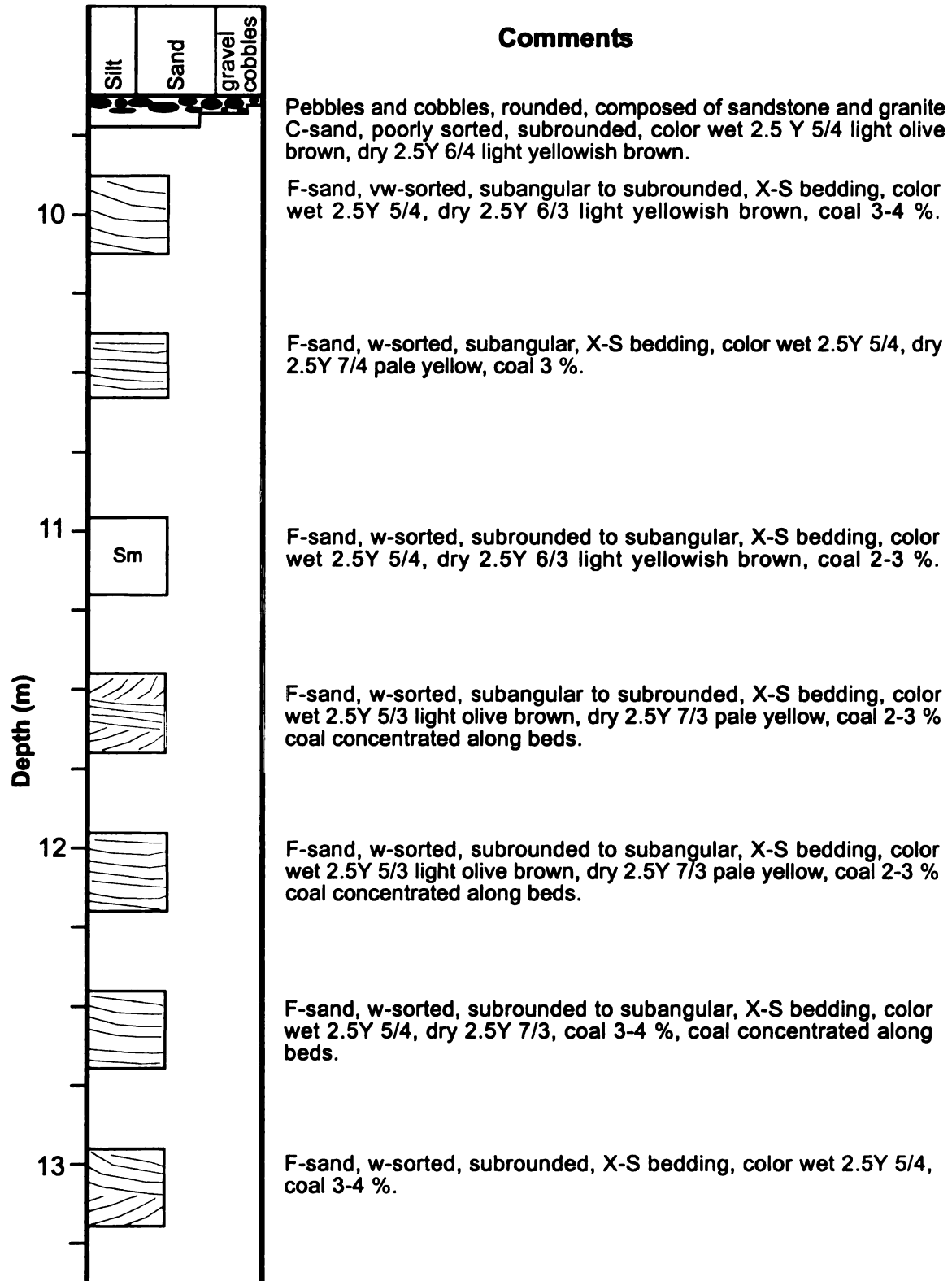


Figure A.5.a. Core description of well P8.

Well Name: PIB-8 Location: Plume A, Schoolcraft, MI Page: 2 of 6

Date: 12-27-00 thru 12-28-00 Described by: Susanne E. Biteman

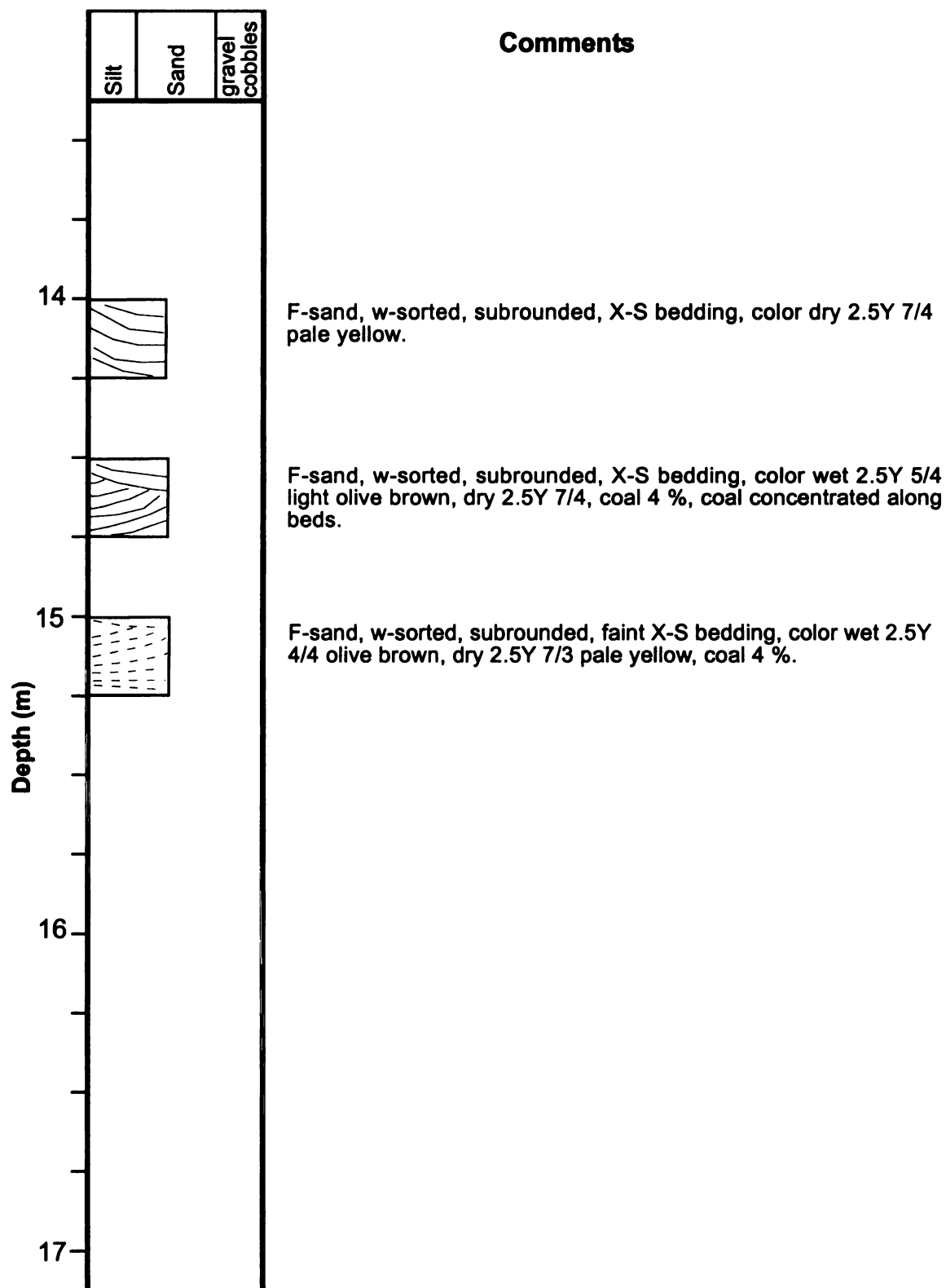


Figure A.5.b. Core description of well P8.

Date: 12-28-00 thru 12-28-00 Described by: Susanne E. Biteman



Well Name: PIB-8 Location: Plume A, Schoolcraft, MI Page: 4 of 6

Date: 12-28-00 thru 12-28-00 Described by: Susanne E. Biteman

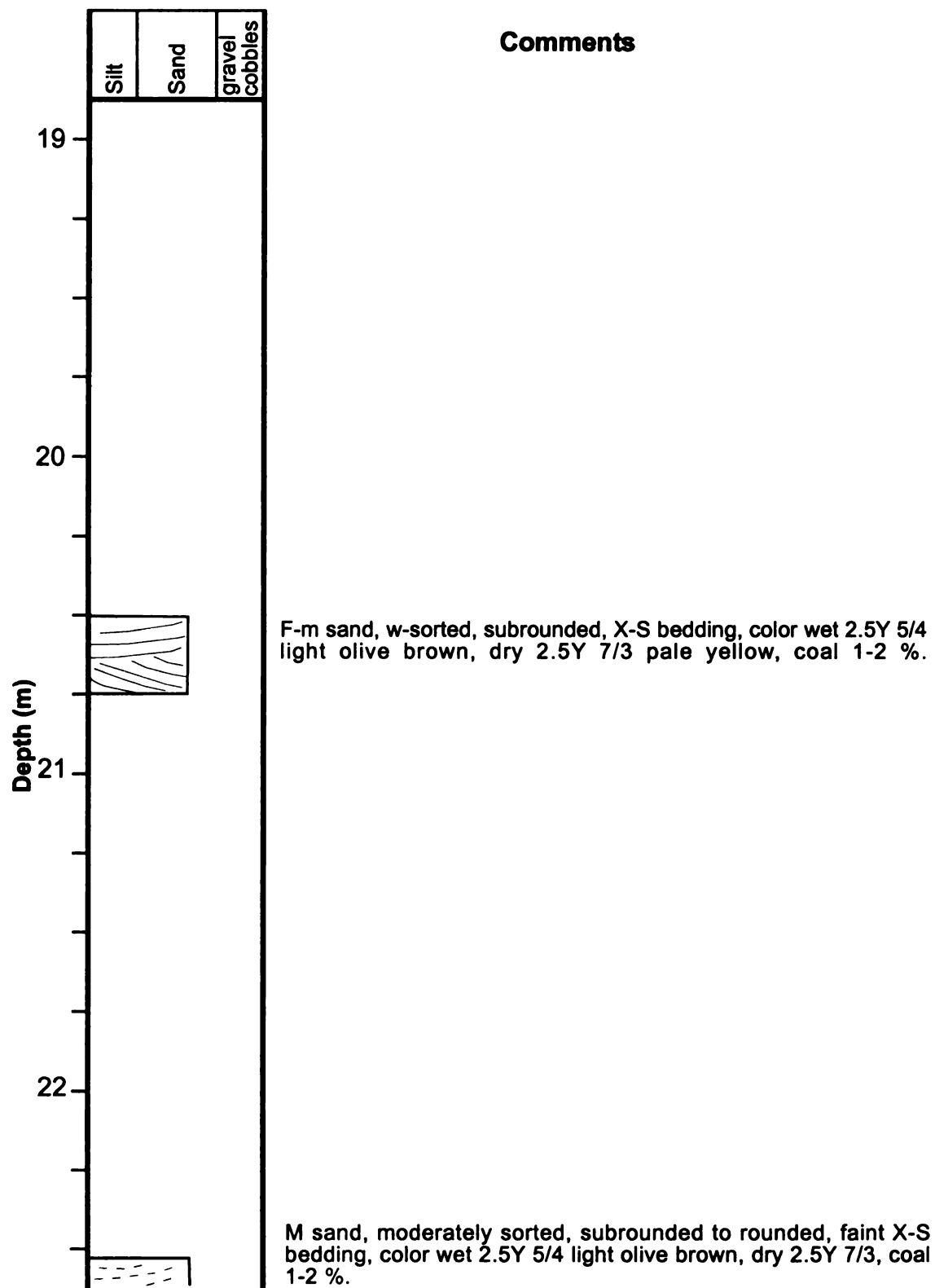


Figure A.5.d. Core description of well P8.

Well Name: PIB-8 Location: Plume A, Schoolcraft, MI Page: 5 of 6

Date: 12-29-00 thru 12-29-00 Described by: Susanne E. Biteman

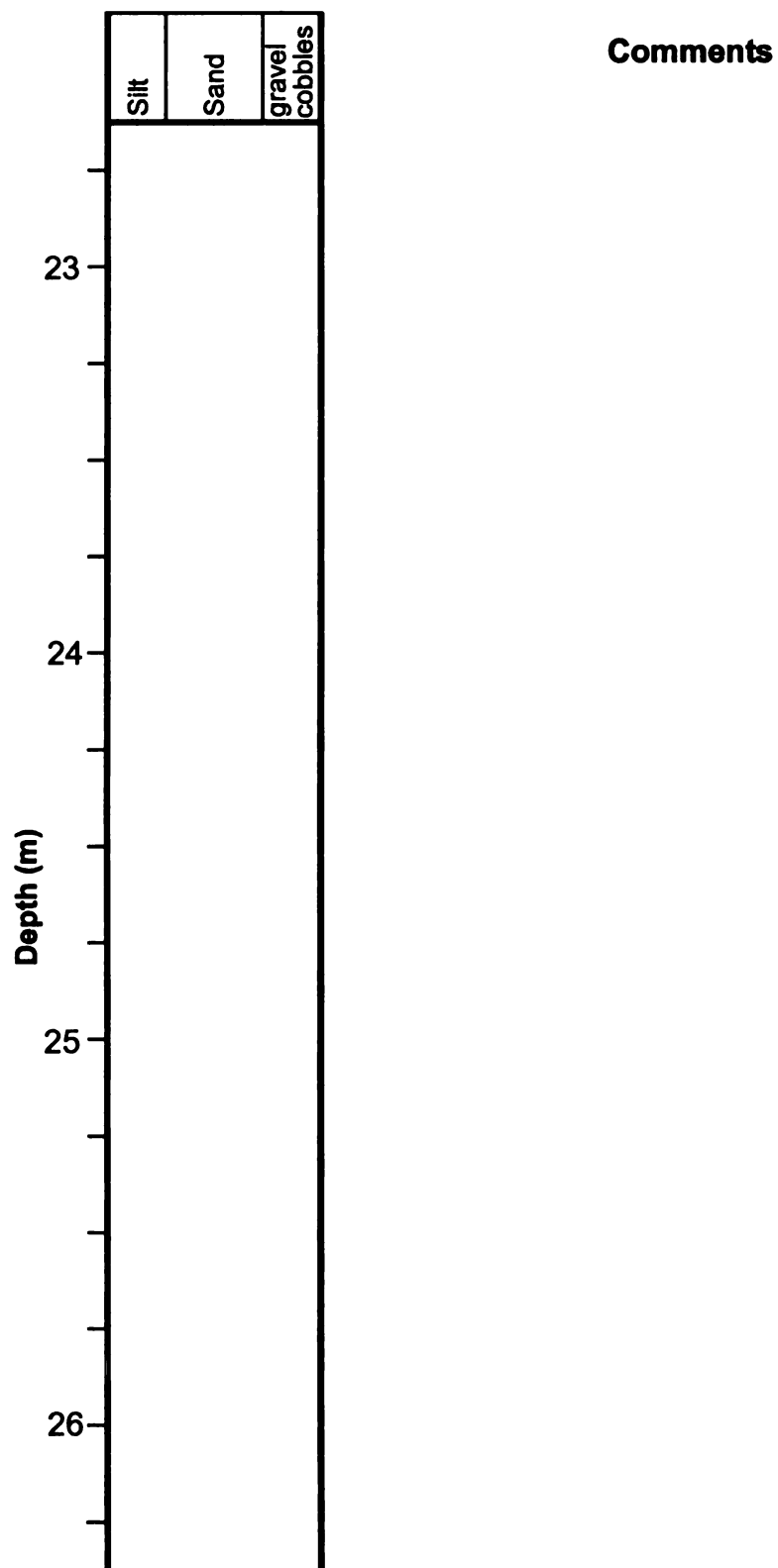


Figure A.5.e. Core description of well P8.

Well Name: PIB-8 Location: Plume A, Schoolcraft, MI Page: 6 of 6

Date: 12-29-00 thru 12-29-00 Described by: Susanne E. Biteman

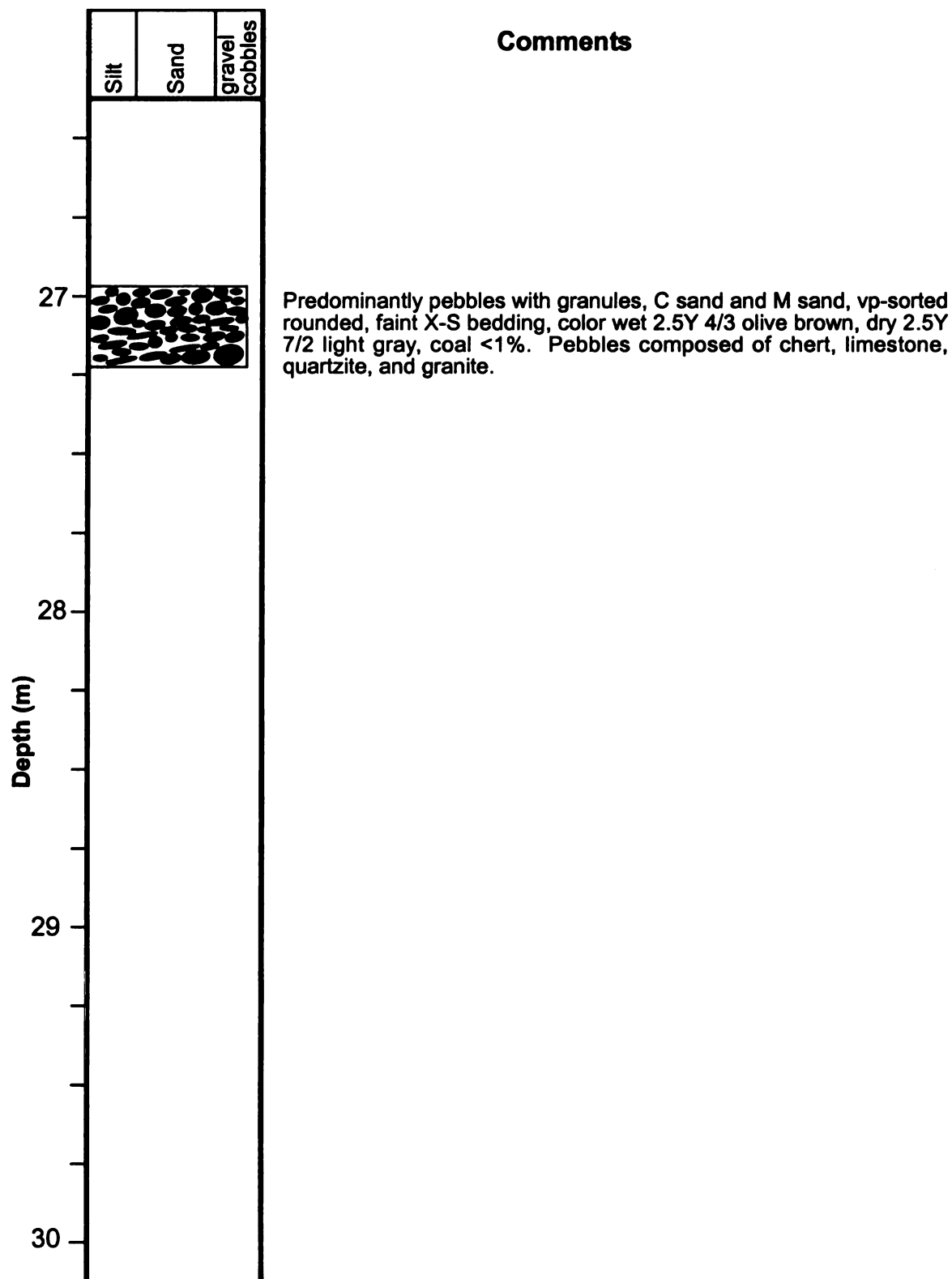


Figure A.5.f. Core description of well P8.

Well Name: PIB-9 Location: Plume A, Schoolcraft, MI Page: 1 of 2

Date: 12-19-00 thru 12-21-00 Described by: Susanne E. Biteman

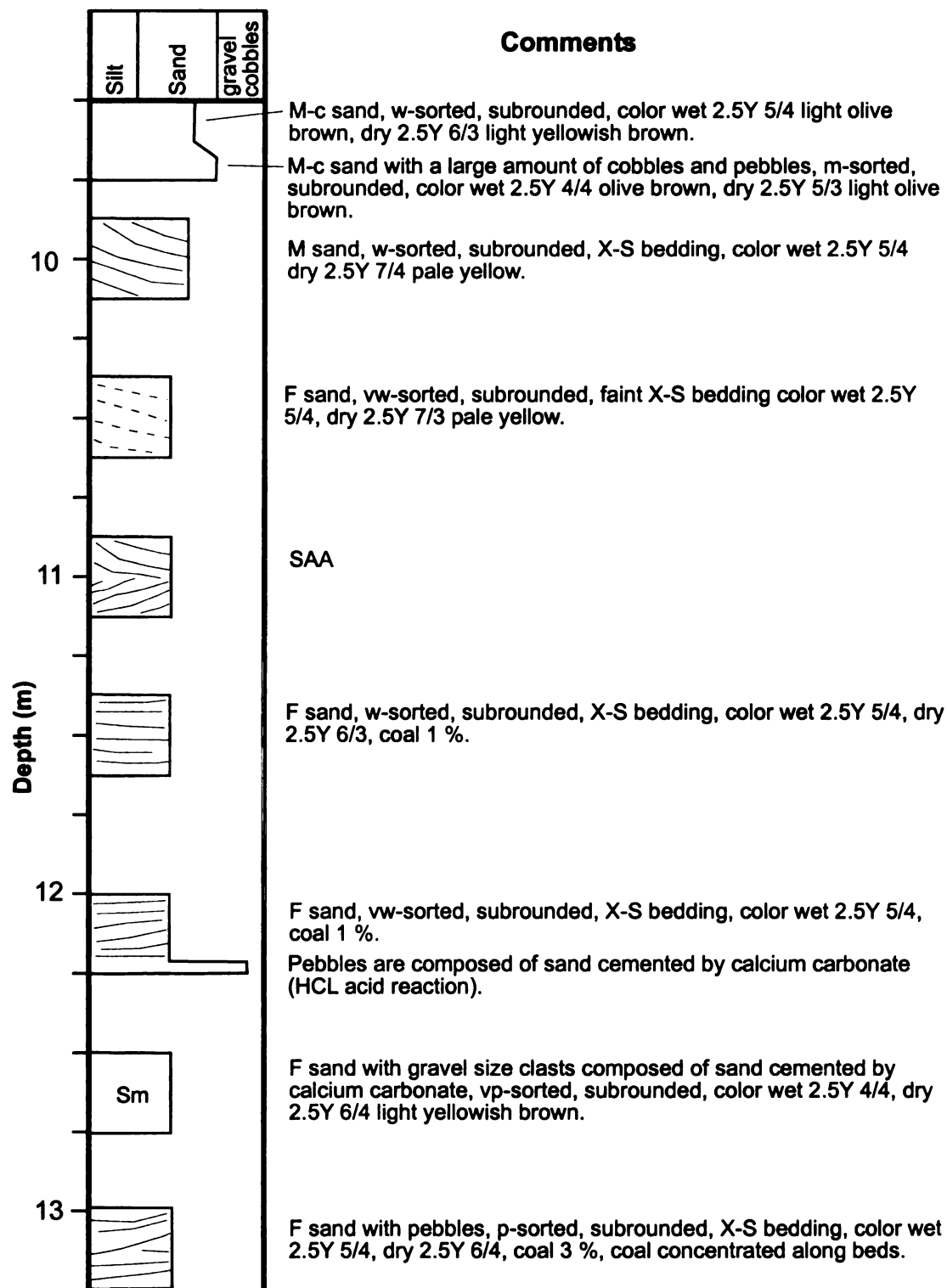


Figure A.6.a. Core description of well P9.

Well Name: PIB-9 Location: Plume A, Schoolcraft, MI Page: 2 of 2

Date: 12-21-00 thru 12-27-00 Described by: Susanne E. Biteman

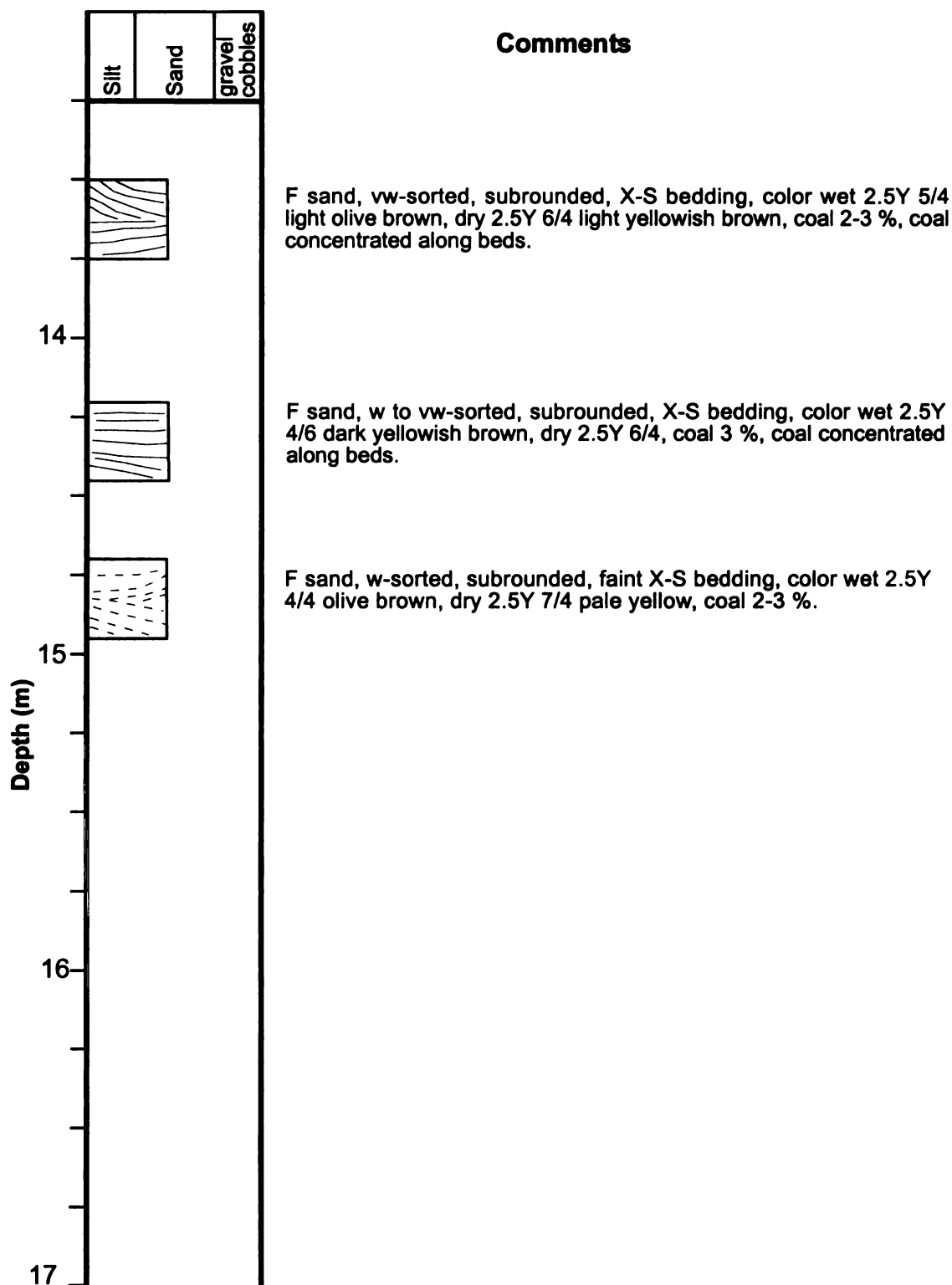


Figure A.6.b. Core description of well P9.

Date: 12-15-00 thru 12-18-00 Described by: Susanne E. Biteman

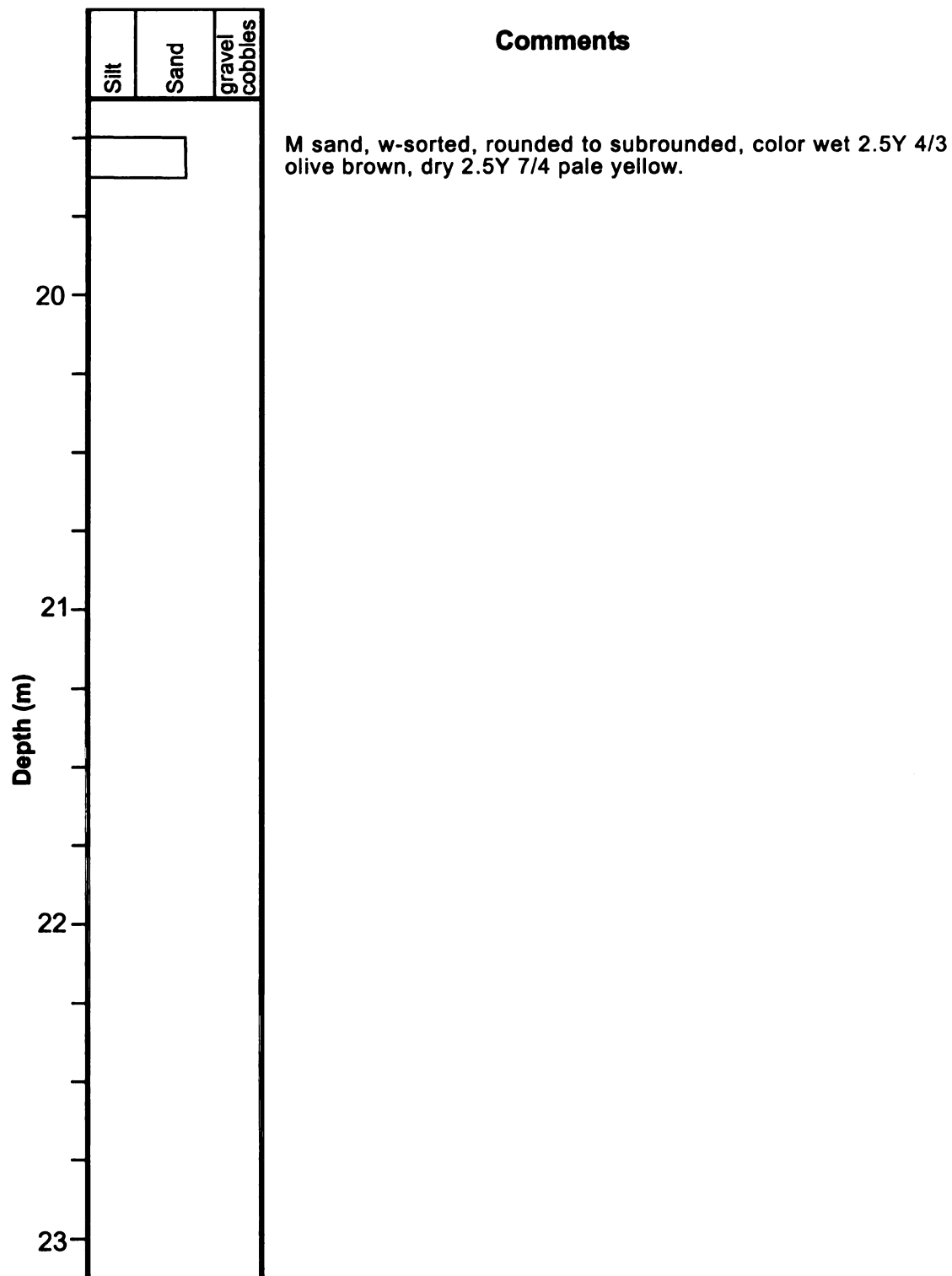


Figure A.7.a. Core description of well P11.

Date: 12-15-00 thru 12-18-00 Described by: Susanne E. Biteman

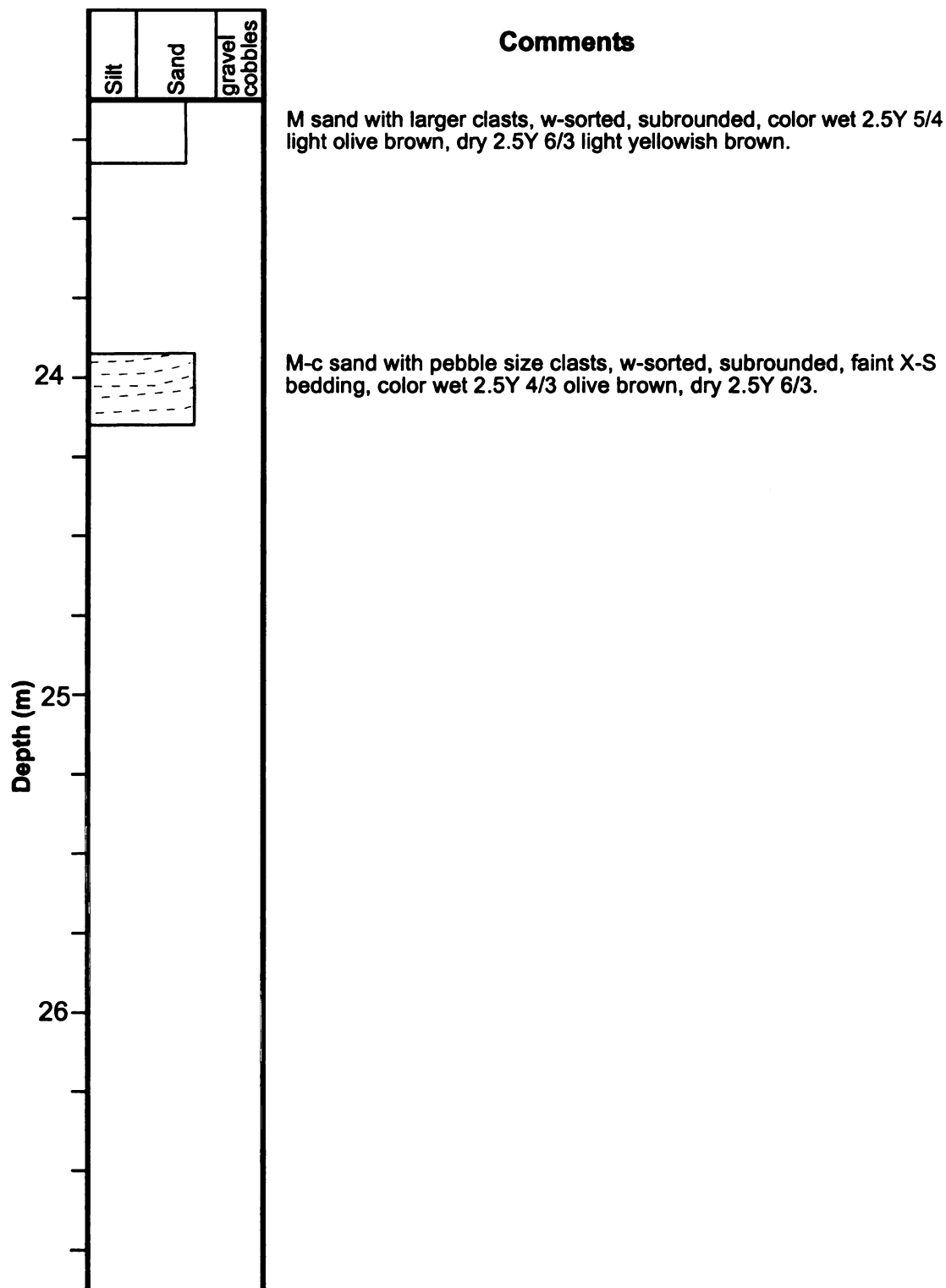


Figure A.7.b. Core description of well P11.

Well Name: PIB-12 Location: Plume A, Schoolcraft, MI Page: 1 of 4

Date: 12-18-00 thru 12-19-00 Described by: Susanne E. Biteman

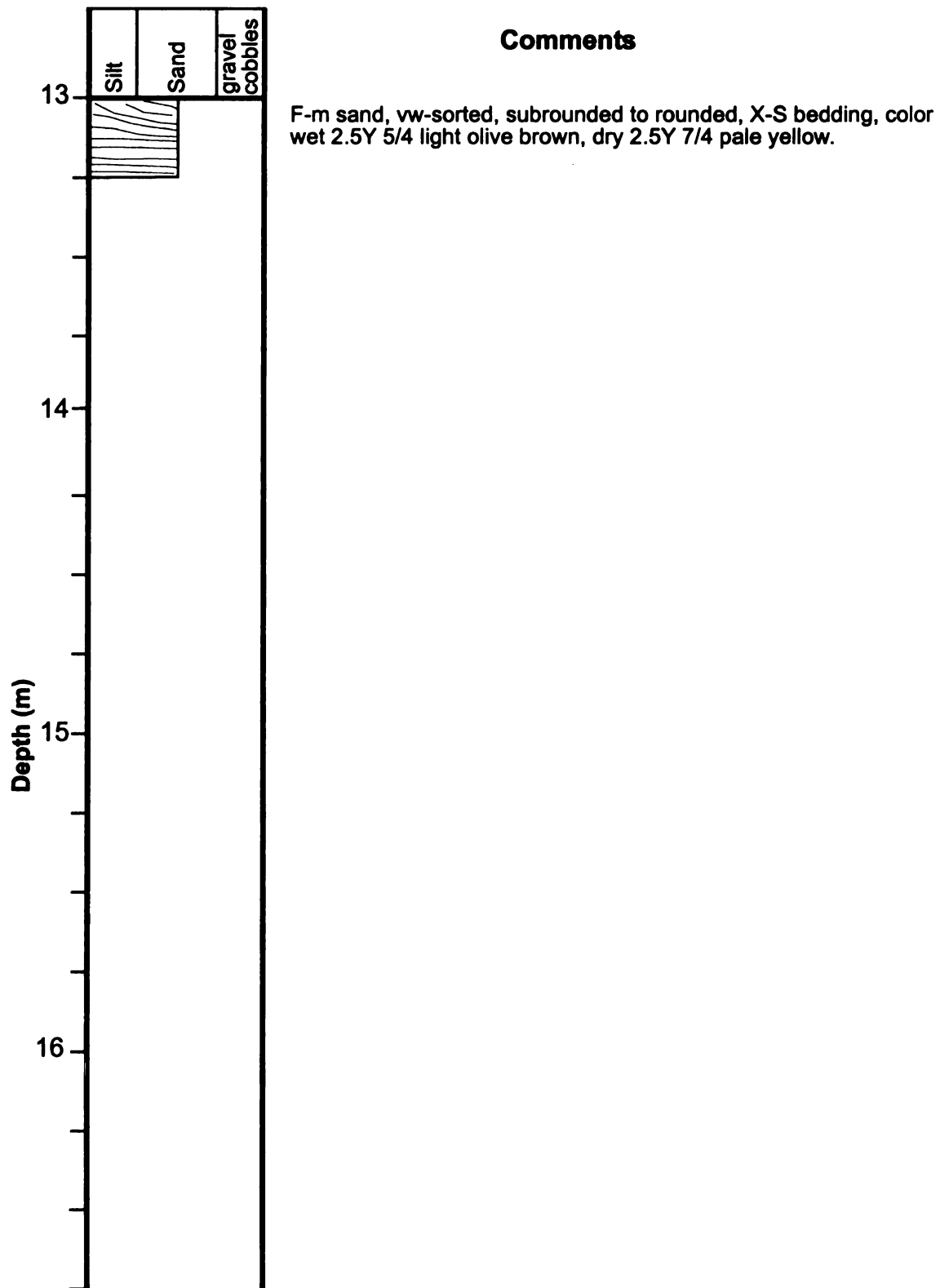


Figure A.8.a. Core description of well P12.

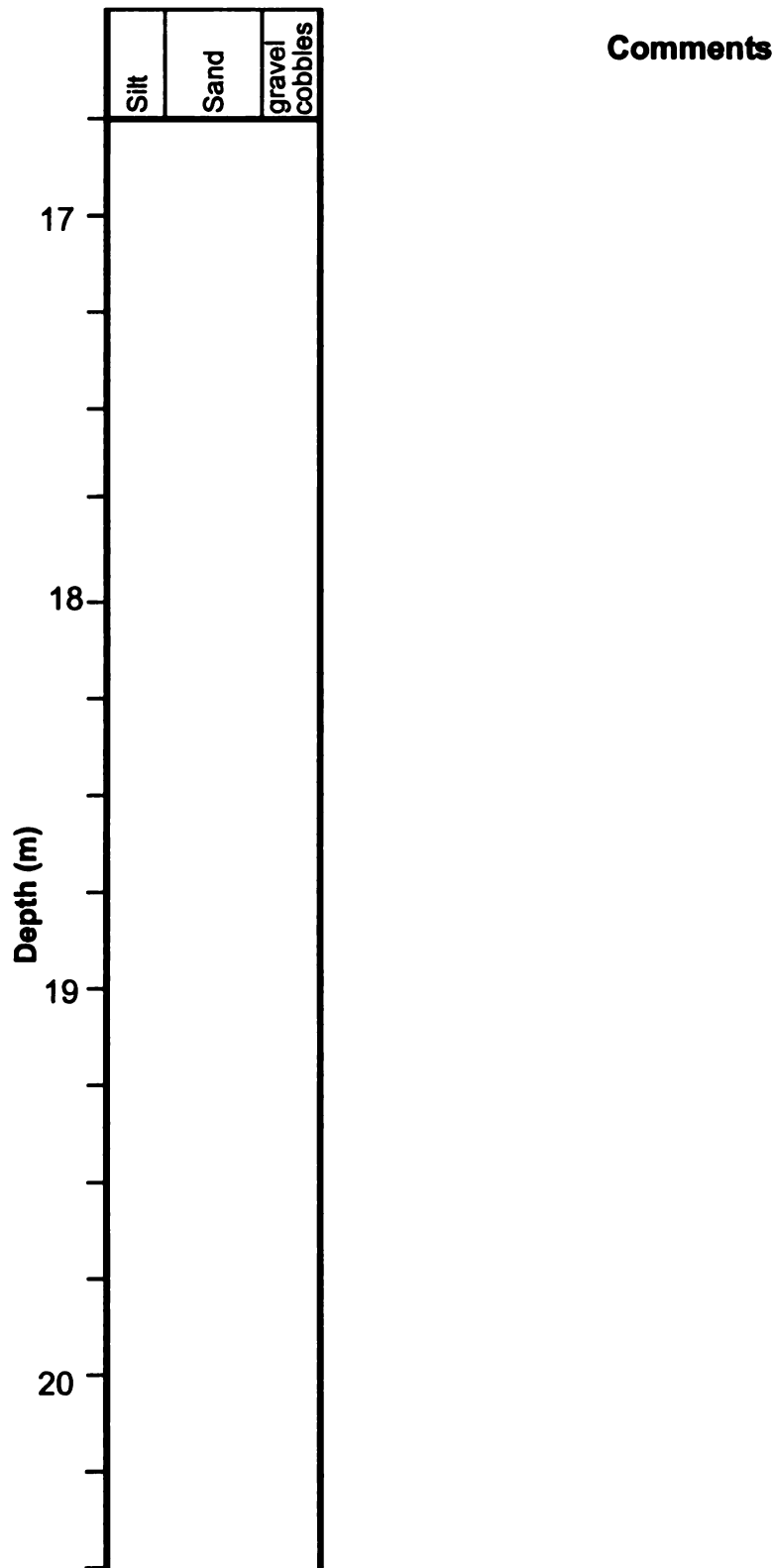


Figure A.8.b. Core description of well P12.

Well Name: PIB-12 Location: Plume A, Schoolcraft, MI Page: 3 of 4

Date: 12-18-00 thru 12-19-00 Described by: Susanne E. Biteman

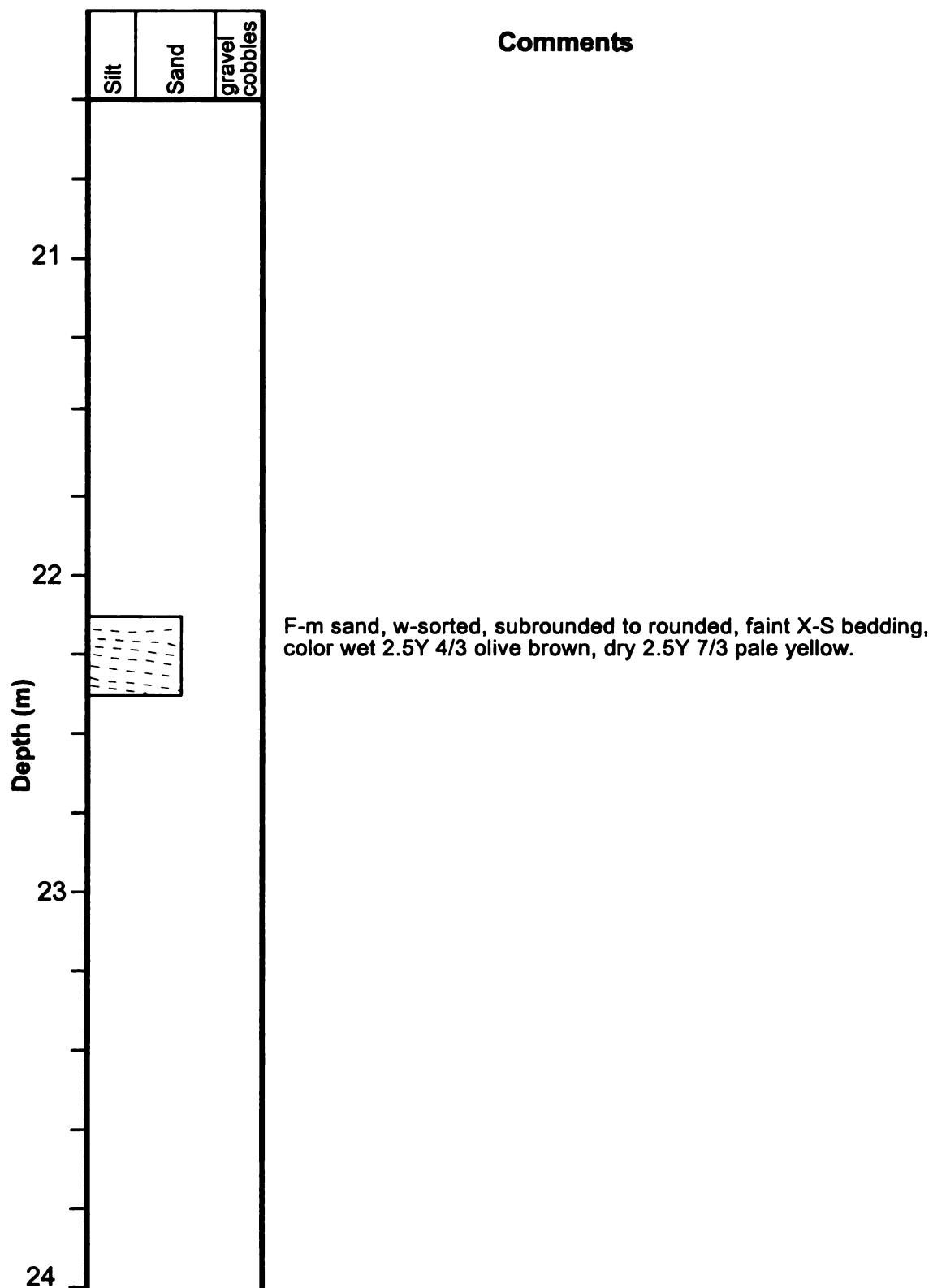


Figure A.8.c. Core description of well P12.

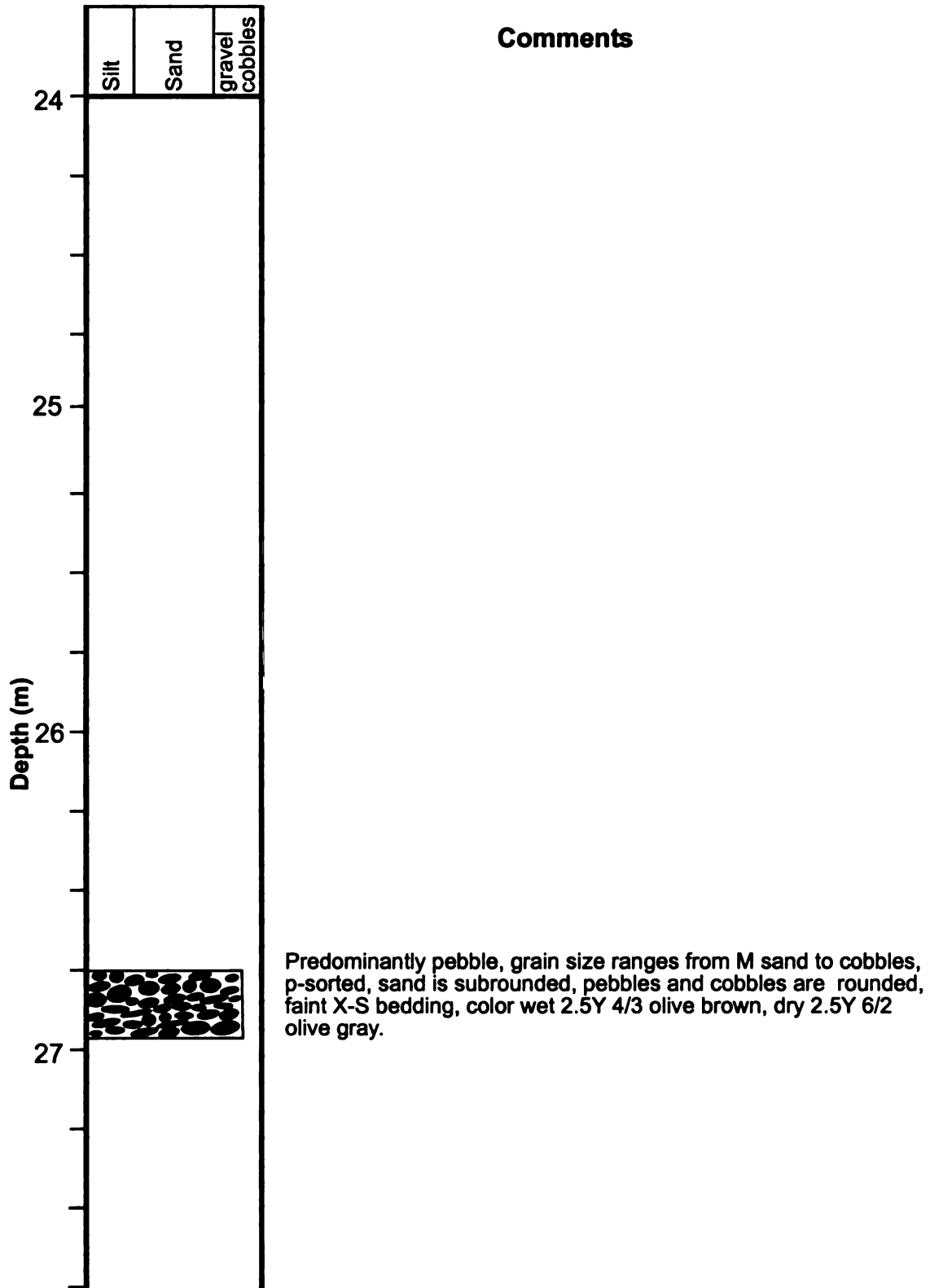


Figure A.8.d. Core description of well P12.

| X | Y | Z | LOG(K) (cm/s) | K (cm/s) | mean grain size | sorting |
|----------|----------|----------|----------------------|-----------------|------------------------|----------------|
| 38.7 | 22.5 | 2.0 | -1.49E+00 | 3.26E-02 | v. fine sand | v-poorly |
| 38.7 | 22.5 | 2.1 | -1.18E+00 | 6.61E-02 | | |
| 38.7 | 22.5 | 2.3 | -1.05E+00 | 8.88E-02 | | |
| 38.7 | 22.5 | 2.5 | -1.21E+00 | 6.20E-02 | coarse sand | poorly |
| 38.7 | 22.5 | 2.9 | -1.35E+00 | 4.42E-02 | | |
| 38.7 | 22.5 | 3.2 | -1.64E+00 | 2.27E-02 | | |
| 38.7 | 22.5 | 3.4 | -1.01E+00 | 9.69E-02 | | |
| 38.7 | 22.5 | 3.6 | -1.16E+00 | 6.98E-02 | | |
| 38.7 | 22.5 | 3.8 | -9.76E-01 | 1.06E-01 | | |
| 38.7 | 22.5 | 4.4 | -1.57E+00 | 2.71E-02 | | |
| 38.7 | 22.5 | 4.9 | -1.17E+00 | 6.75E-02 | | |
| 38.7 | 22.5 | 5.1 | -1.73E+00 | 1.86E-02 | very fine sand | moderately |
| 38.7 | 22.5 | 5.3 | -1.69E+00 | 2.04E-02 | | |
| 38.7 | 22.5 | 5.6 | -1.55E+00 | 2.79E-02 | | |
| 38.7 | 22.5 | 5.9 | -1.55E+00 | 2.79E-02 | | |
| 38.7 | 22.5 | 7.2 | -1.56E+00 | 2.75E-02 | | |
| 38.7 | 22.5 | 7.4 | -1.52E+00 | 3.02E-02 | | |
| 38.7 | 22.5 | 7.8 | -1.42E+00 | 3.84E-02 | | |
| 38.7 | 22.5 | 8.2 | -1.44E+00 | 3.59E-02 | | |
| 38.7 | 22.5 | 8.4 | -1.41E+00 | 3.90E-02 | med sand | moderately |
| 38.7 | 22.5 | 8.6 | -1.27E+00 | 5.38E-02 | | |
| 38.7 | 22.5 | 9.3 | -1.46E+00 | 3.47E-02 | | |
| 38.7 | 22.5 | 9.6 | -1.57E+00 | 2.67E-02 | | |
| 38.7 | 22.5 | 9.9 | -1.20E+00 | 6.28E-02 | | |
| 38.7 | 22.5 | 10.1 | -1.36E+00 | 4.37E-02 | coarse sand | v-poorly |
| 38.7 | 22.5 | 10.5 | -1.53E+00 | 2.98E-02 | | |
| 38.7 | 22.5 | 11.0 | -1.43E+00 | 3.76E-02 | | |
| 38.7 | 22.5 | 11.2 | -1.41E+00 | 3.85E-02 | | |
| 38.7 | 22.5 | 11.4 | -1.35E+00 | 4.51E-02 | | |
| 38.7 | 22.5 | 11.8 | -1.90E+00 | 1.26E-02 | | |
| 38.7 | 22.5 | 12.0 | -1.84E+00 | 1.43E-02 | fine sand | m-well |
| 38.7 | 22.5 | 12.3 | -1.98E+00 | 1.04E-02 | | |
| 38.7 | 22.5 | 12.9 | -1.90E+00 | 1.25E-02 | | |
| 38.7 | 22.5 | 13.9 | -1.94E+00 | 1.15E-02 | | |
| 38.7 | 22.5 | 14.1 | -1.88E+00 | 1.31E-02 | fine sand | well |
| 38.7 | 22.5 | 14.4 | -1.88E+00 | 1.31E-02 | | |
| 38.7 | 22.5 | 14.7 | -1.86E+00 | 1.38E-02 | fine sand | well |
| 38.7 | 22.5 | 15.5 | -1.92E+00 | 1.20E-02 | | |
| 38.7 | 22.5 | 15.9 | -2.07E+00 | 8.60E-03 | | |
| 38.7 | 22.5 | 16.4 | -1.85E+00 | 1.41E-02 | | |
| 38.7 | 22.5 | 16.7 | -2.05E+00 | 8.90E-03 | | |
| 38.7 | 22.5 | 17.2 | -1.97E+00 | 1.06E-02 | v. fine sand | well |
| 38.7 | 22.5 | 17.6 | -1.96E+00 | 1.09E-02 | v. fine sand | well |
| 38.7 | 22.5 | 18.0 | -1.42E+00 | 3.84E-02 | | |

Table A.2. Well D2. X, Y and Z location, Log K value, K value, mean grain size (determined by sieve analysis), and sorting (determined by standard deviation of grain size (Boggs, 2001)).

| X | Y | Z | LOG(K) (cm/s) | K (cm/s) | mean grain size | sorting |
|----------|----------|----------|----------------------|-----------------|------------------------|----------------|
| 38.8 | 24.4 | 3.5 | -1.14E+00 | 7.24E-02 | | |
| 38.8 | 24.4 | 3.9 | -1.37E+00 | 4.23E-02 | | |
| 38.8 | 24.4 | 4.3 | -1.52E+00 | 3.00E-02 | | |
| 38.8 | 24.4 | 5.0 | -1.34E+00 | 4.59E-02 | | |
| 38.8 | 24.4 | 5.4 | -1.73E+00 | 1.86E-02 | | |
| 38.8 | 24.4 | 5.6 | -1.66E+00 | 2.20E-02 | | |
| 38.8 | 24.4 | 7.3 | -1.54E+00 | 2.90E-02 | fine sand | well |
| 38.8 | 24.4 | 8.1 | -1.61E+00 | 2.46E-02 | med sand | m-well |
| 38.8 | 24.4 | 8.5 | -1.55E+00 | 2.83E-02 | | |
| 38.8 | 24.4 | 8.9 | -1.72E+00 | 1.89E-02 | | |
| 38.8 | 24.4 | 10.9 | -1.58E+00 | 2.64E-02 | | |
| 38.8 | 24.4 | 11.3 | -1.53E+00 | 2.98E-02 | | |
| 38.8 | 24.4 | 11.7 | -1.98E+00 | 1.04E-02 | fine sand | moderately |
| 38.8 | 24.4 | 11.9 | -1.88E+00 | 1.32E-02 | | |
| 38.8 | 24.4 | 13.0 | -1.90E+00 | 1.26E-02 | | |
| 38.8 | 24.4 | 13.4 | -1.99E+00 | 1.03E-02 | | |
| 38.8 | 24.4 | 14.0 | -2.09E+00 | 8.20E-03 | fine sand | m-well |
| 38.8 | 24.4 | 14.4 | -1.80E+00 | 1.60E-02 | | |
| 38.8 | 24.4 | 14.7 | -1.80E+00 | 1.60E-02 | | |
| 38.8 | 24.4 | 15.1 | -1.88E+00 | 1.32E-02 | | |
| 38.8 | 24.4 | 16.3 | -1.97E+00 | 1.07E-02 | v. fine sand | well |
| 38.8 | 24.4 | 17.0 | -2.37E+00 | 4.30E-03 | | |
| 38.8 | 24.4 | 17.4 | -1.89E+00 | 1.29E-02 | | |
| 38.8 | 24.4 | 17.8 | -2.13E+00 | 7.40E-03 | v. fine sand | well |
| 38.8 | 24.4 | 18.0 | -1.81E+00 | 1.56E-02 | fine sand | moderately |

Table A.3. Well D4. X, Y and Z location, Log K value, K value, mean grain size (determined by sieve analysis), and sorting (determined by standard deviation of grain size (Boggs, 2001)).

| X | Y | Z | LOG(K) (cm/s) | K (cm/s) | mean grain size | sorting |
|----------|----------|----------|----------------------|-----------------|------------------------|----------------|
| 38.8 | 26.4 | 0.6 | -1.07E+00 | 8.59E-02 | granules | v-poorly |
| 38.8 | 26.4 | 1.0 | -1.18E+00 | 6.62E-02 | | |
| 38.8 | 26.4 | 1.3 | -1.04E+00 | 9.02E-02 | v. fine sand | v-poorly |
| 38.8 | 26.4 | 1.5 | -1.59E+00 | 2.55E-02 | med sand | poorly |
| 38.8 | 26.4 | 3.9 | -1.20E+00 | 6.38E-02 | | |
| 38.8 | 26.4 | 4.2 | -9.91E-01 | 1.02E-01 | | |
| 38.8 | 26.4 | 4.5 | -1.29E+00 | 5.10E-02 | | |
| 38.8 | 26.4 | 4.7 | -1.18E+00 | 6.59E-02 | med sand | moderately |
| 38.8 | 26.4 | 5.0 | -1.21E+00 | 6.19E-02 | | |
| 38.8 | 26.4 | 5.4 | -1.66E+00 | 2.17E-02 | fine sand | moderately |
| 38.8 | 26.4 | 5.9 | -1.60E+00 | 2.54E-02 | | |
| 38.8 | 26.4 | 7.3 | -1.52E+00 | 3.03E-02 | | |
| 38.8 | 26.4 | 7.7 | -1.53E+00 | 2.93E-02 | | |
| 38.8 | 26.4 | 8.1 | -1.59E+00 | 2.59E-02 | fine sand | moderately |
| 38.8 | 26.4 | 8.5 | -1.61E+00 | 2.47E-02 | | |
| 38.8 | 26.4 | 9.4 | -1.49E+00 | 3.22E-02 | fine sand | m-well |
| 38.8 | 26.4 | 9.8 | -1.55E+00 | 2.79E-02 | med sand | moderately |
| 38.8 | 26.4 | 10.2 | -1.40E+00 | 3.95E-02 | med sand | poorly |
| 38.8 | 26.4 | 11.0 | -1.52E+00 | 3.05E-02 | | |
| 38.8 | 26.4 | 11.3 | -1.50E+00 | 3.18E-02 | | |
| 38.8 | 26.4 | 11.7 | -1.63E+00 | 2.33E-02 | | |
| 38.8 | 26.4 | 12.1 | -1.83E+00 | 1.48E-02 | | |
| 38.8 | 26.4 | 13.0 | -1.89E+00 | 1.28E-02 | | |
| 38.8 | 26.4 | 13.4 | -1.84E+00 | 1.44E-02 | | |
| 38.8 | 26.4 | 13.8 | -2.14E+00 | 7.20E-03 | | |
| 38.8 | 26.4 | 14.2 | -1.91E+00 | 1.22E-02 | | |
| 38.8 | 26.4 | 14.6 | -1.81E+00 | 1.55E-02 | | |
| 38.8 | 26.4 | 15.0 | -1.88E+00 | 1.33E-02 | | |
| 38.8 | 26.4 | 15.8 | -2.04E+00 | 9.10E-03 | | |
| 38.8 | 26.4 | 16.2 | -1.90E+00 | 1.25E-02 | | |
| 38.8 | 26.4 | 16.6 | -2.14E+00 | 7.30E-03 | | |
| 38.8 | 26.4 | 17.0 | -2.10E+00 | 7.90E-03 | | |
| 38.8 | 26.4 | 17.4 | -2.04E+00 | 9.10E-03 | | |
| 38.8 | 26.4 | 17.8 | -2.10E+00 | 8.00E-03 | | |
| 38.8 | 26.4 | 18.1 | -1.77E+00 | 1.70E-02 | coarse sand | v-poorly |

Table A.4. Well D6. X, Y and Z location, Log K value, K value, mean grain size (determined by sieve analysis), and sorting (determined by standard deviation of grain size (Boggs, 2001)).

| X | Y | Z | LOG(K) (cm/s) | K (cm/s) | mean grain size | sorting |
|----------|----------|----------|----------------------|-----------------|------------------------|----------------|
| 38.8 | 28.4 | 1.0 | -1.46E+00 | 3.46E-02 | | |
| 38.8 | 28.4 | 1.4 | -1.23E+00 | 5.91E-02 | | |
| 38.8 | 28.4 | 1.8 | -1.23E+00 | 5.90E-02 | | |
| 38.8 | 28.4 | 2.2 | -1.16E+00 | 6.87E-02 | | |
| 38.8 | 28.4 | 2.6 | -1.18E+00 | 6.61E-02 | | |
| 38.8 | 28.4 | 3.0 | -1.45E+00 | 3.55E-02 | | |
| 38.8 | 28.4 | 4.1 | -1.63E+00 | 2.35E-02 | | |
| 38.8 | 28.4 | 4.5 | -1.45E+00 | 3.57E-02 | | |
| 38.8 | 28.4 | 5.1 | -1.73E+00 | 1.85E-02 | | |
| 38.8 | 28.4 | 5.7 | -1.41E+00 | 3.92E-02 | | |
| 38.8 | 28.4 | 7.1 | -2.96E+00 | 1.10E-03 | | |
| 38.8 | 28.4 | 8.3 | -1.77E+00 | 1.70E-02 | | |
| 38.8 | 28.4 | 8.7 | -1.52E+00 | 3.03E-02 | med sand | moderately |
| 38.8 | 28.4 | 10.2 | -1.83E+00 | 1.48E-02 | | |
| 38.8 | 28.4 | 10.6 | -1.94E+00 | 1.14E-02 | | |
| 38.8 | 28.4 | 11.1 | -1.50E+00 | 3.13E-02 | | |
| 38.8 | 28.4 | 11.6 | -1.71E+00 | 1.96E-02 | | |
| 38.8 | 28.4 | 14.6 | -1.79E+00 | 1.61E-02 | fine sand | well |
| 38.8 | 28.4 | 14.9 | -2.00E+00 | 9.90E-03 | fine sand | m-well |
| 38.8 | 28.4 | 15.8 | -1.98E+00 | 1.04E-02 | | |
| 38.8 | 28.4 | 16.2 | -2.39E+00 | 4.04E-03 | | |
| 38.8 | 28.4 | 16.6 | -1.49E+00 | 3.20E-02 | | |

Table A.5. Well D8. X, Y and Z location, Log K value, K value, mean grain size (determined by sieve analysis), and sorting (determined by standard deviation of grain size (Boggs, 2001)).

| X | Y | Z | LOG(K) (cm/s) | K (cm/s) | mean grain size | sorting |
|----------|----------|----------|----------------------|-----------------|------------------------|----------------|
| 38.7 | 30.4 | 0.9 | -1.34E+00 | 4.60E-02 | granules | v-poorly |
| 38.7 | 30.4 | 1.0 | -1.29E+00 | 5.12E-02 | pebble | poorly |
| 38.7 | 30.4 | 1.2 | -9.87E-01 | 1.03E-01 | pebble | v-poorly |
| 38.7 | 30.4 | 3.3 | -1.54E+00 | 2.87E-02 | coarse sand | v-poorly |
| 38.7 | 30.4 | 3.7 | -1.18E+00 | 6.64E-02 | | |
| 38.7 | 30.4 | 4.1 | -1.18E+00 | 6.62E-02 | | |
| 38.7 | 30.4 | 5.3 | -1.34E+00 | 4.56E-02 | med sand | poorly |
| 38.7 | 30.4 | 5.8 | -1.71E+00 | 1.93E-02 | | |
| 38.7 | 30.4 | 6.5 | -2.68E+00 | 2.10E-03 | | |
| 38.7 | 30.4 | 6.9 | -2.60E+00 | 2.50E-03 | fine sand | moderately |
| 38.7 | 30.4 | 7.3 | -2.20E+00 | 6.30E-03 | | |
| 38.7 | 30.4 | 7.9 | -1.59E+00 | 2.59E-02 | | |
| 38.7 | 30.4 | 8.3 | -1.55E+00 | 2.82E-02 | med sand | m-well |
| 38.7 | 30.4 | 8.7 | -1.59E+00 | 2.56E-02 | | |
| 38.7 | 30.4 | 9.0 | -1.83E+00 | 1.49E-02 | | |
| 38.7 | 30.4 | 9.8 | -1.55E+00 | 2.82E-02 | fine sand | well |
| 38.7 | 30.4 | 10.2 | -1.51E+00 | 3.11E-02 | med sand | poorly |
| 38.7 | 30.4 | 11.3 | -1.53E+00 | 2.98E-02 | med sand | moderately |
| 38.7 | 30.4 | 11.7 | -1.53E+00 | 2.96E-02 | | |
| 38.7 | 30.4 | 12.1 | -1.72E+00 | 1.89E-02 | | |
| 38.7 | 30.4 | 13.4 | -2.00E+00 | 1.01E-02 | fine sand | m-well |
| 38.7 | 30.4 | 14.2 | -1.96E+00 | 1.10E-02 | fine sand | m-well |
| 38.7 | 30.4 | 14.6 | -1.81E+00 | 1.56E-02 | fine sand | moderately |
| 38.7 | 30.4 | 15.0 | -1.89E+00 | 1.29E-02 | fine sand | poorly |
| 38.7 | 30.4 | 15.9 | -2.30E+00 | 5.00E-03 | | |
| 38.7 | 30.4 | 16.2 | -1.99E+00 | 1.03E-02 | | |
| 38.7 | 30.4 | 16.6 | -1.91E+00 | 1.24E-02 | fine sand | moderately |
| 38.7 | 30.4 | 17.4 | -2.17E+00 | 6.70E-03 | | |
| 38.7 | 30.4 | 17.7 | -1.95E+00 | 1.12E-02 | | |
| 38.7 | 30.4 | 18.2 | -2.07E+00 | 8.60E-03 | med sand | poorly |

Table A.6. Well D10. X, Y and Z location, Log K value, K value, mean grain size (determined by sieve analysis), and sorting (determined by standard deviation of grain size (Boggs, 2001)).

| X | Y | Z | LOG(K) (cm/s) | K (cm/s) | mean grain size | sorting |
|----------|----------|----------|----------------------|-----------------|------------------------|----------------|
| 38.7 | 32.4 | 3.8 | -1.55E+00 | 2.85E-02 | med sand | poorly |
| 38.7 | 32.4 | 4.2 | -1.19E+00 | 6.49E-02 | | |
| 38.7 | 32.4 | 5.2 | -1.53E+00 | 2.94E-02 | | |
| 38.7 | 32.4 | 5.5 | -1.57E+00 | 2.68E-02 | | |
| 38.7 | 32.4 | 5.9 | -1.61E+00 | 2.47E-02 | fine sand | m-well |
| 38.7 | 32.4 | 7.0 | -2.82E+00 | 1.50E-03 | very fine sand | m-well |
| 38.7 | 32.4 | 7.4 | -1.74E+00 | 1.84E-02 | | |
| 38.7 | 32.4 | 8.3 | -1.41E+00 | 3.92E-02 | med sand | moderately |
| 38.7 | 32.4 | 8.8 | -2.28E+00 | 5.20E-03 | med sand | moderately |
| 38.7 | 32.4 | 9.4 | -1.58E+00 | 2.63E-02 | | |
| 38.7 | 32.4 | 9.8 | -1.54E+00 | 2.90E-02 | | |
| 38.7 | 32.4 | 10.2 | -1.49E+00 | 3.21E-02 | fine sand | poorly |
| 38.7 | 32.4 | 10.9 | -1.52E+00 | 3.00E-02 | | |
| 38.7 | 32.4 | 11.3 | -1.48E+00 | 3.33E-02 | fine sand | m-well |
| 38.7 | 32.4 | 11.7 | -1.54E+00 | 2.86E-02 | | |
| 38.7 | 32.4 | 12.8 | -1.85E+00 | 1.40E-02 | | |
| 38.7 | 32.4 | 13.2 | -1.97E+00 | 1.08E-02 | | |
| 38.7 | 32.4 | 13.6 | -1.94E+00 | 1.14E-02 | fine sand | m-well |
| 38.7 | 32.4 | 14.0 | -2.15E+00 | 7.00E-03 | | |
| 38.7 | 32.4 | 14.4 | -1.74E+00 | 1.82E-02 | | |
| 38.7 | 32.4 | 14.8 | -1.85E+00 | 1.41E-02 | fine sand | poorly |
| 38.7 | 32.4 | 15.4 | -2.09E+00 | 8.10E-03 | | |
| 38.7 | 32.4 | 15.9 | -1.95E+00 | 1.12E-02 | | |
| 38.7 | 32.4 | 16.3 | -1.90E+00 | 1.25E-02 | fine sand | well |
| 38.7 | 32.4 | 16.9 | -1.97E+00 | 1.06E-02 | | |
| 38.7 | 32.4 | 17.2 | -1.83E+00 | 1.48E-02 | | |
| 38.7 | 32.4 | 17.6 | -1.78E+00 | 1.67E-02 | | |
| 38.7 | 32.4 | 18.0 | -1.91E+00 | 1.23E-02 | pebble | poorly |







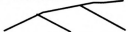
Table A.7. Well D12. X, Y and Z location, Log K value, K value, mean grain size (determined by sieve analysis), and sorting (determined by standard deviation of grain size (Boggs, 2001)).

| X | Y | Z | LOG(K) (cm/s) | K (cm/s) | mean grain size | sorting |
|----------|----------|----------|----------------------|-----------------|------------------------|----------------|
| 38.8 | 34.3 | 0.5 | -1.47E+00 | 3.40E-02 | pebble | v-poorly |
| 38.8 | 34.3 | 0.7 | -1.40E+00 | 3.97E-02 | pebble | v-poorly |
| 38.8 | 34.3 | 0.9 | -1.04E+00 | 9.02E-02 | granules | poorly |
| 38.8 | 34.3 | 1.1 | -1.57E+00 | 2.72E-02 | granules | poorly |
| 38.8 | 34.3 | 1.3 | -1.37E+00 | 4.28E-02 | med sand | poorly |
| 38.8 | 34.3 | 1.7 | -1.38E+00 | 4.17E-02 | coarse sand | poorly |
| 38.8 | 34.3 | 2.2 | -1.24E+00 | 5.77E-02 | coarse sand | poorly |
| 38.8 | 34.3 | 2.6 | -1.17E+00 | 6.76E-02 | | |
| 38.8 | 34.3 | 3.1 | -1.25E+00 | 5.58E-02 | | |
| 38.8 | 34.3 | 3.3 | -1.25E+00 | 5.67E-02 | | |
| 38.8 | 34.3 | 3.5 | -1.21E+00 | 6.24E-02 | med sand | m |
| 38.8 | 34.3 | 3.9 | -1.15E+00 | 7.03E-02 | | |
| 38.8 | 34.3 | 6.8 | -1.64E+00 | 2.28E-02 | | |
| 38.8 | 34.3 | 8.1 | -1.58E+00 | 2.64E-02 | fine sand | m |
| 38.8 | 34.3 | 8.5 | -1.43E+00 | 3.70E-02 | med sand | moderately |
| 38.8 | 34.3 | 9.0 | -1.57E+00 | 2.67E-02 | | |
| 38.8 | 34.3 | 9.6 | -1.65E+00 | 2.25E-02 | med sand | poorly |
| 38.8 | 34.3 | 10.0 | -1.36E+00 | 4.34E-02 | fine sand | m-well |
| 38.8 | 34.3 | 10.5 | -1.69E+00 | 2.04E-02 | fine sand | m-well |
| 38.8 | 34.3 | 10.9 | -1.68E+00 | 2.08E-02 | | |
| 38.8 | 34.3 | 11.1 | -1.71E+00 | 1.96E-02 | | |
| 38.8 | 34.3 | 11.9 | -1.94E+00 | 1.15E-02 | | |
| 38.8 | 34.3 | 13.2 | -2.10E+00 | 7.95E-03 | fine sand | m-well |
| 38.8 | 34.3 | 13.6 | -1.90E+00 | 1.27E-02 | | |
| 38.8 | 34.3 | 14.9 | -1.92E+00 | 1.20E-02 | very fine sand | moderately |
| 38.8 | 34.3 | 15.7 | -2.01E+00 | 9.70E-03 | | |
| 38.8 | 34.3 | 16.1 | -2.06E+00 | 8.70E-03 | | |
| 38.8 | 34.3 | 16.6 | -1.91E+00 | 1.22E-02 | | |
| 38.8 | 34.3 | 17.0 | -1.80E+00 | 1.58E-02 | fine sand | well |
| 38.8 | 34.3 | 17.4 | -2.03E+00 | 9.30E-03 | | |
| 38.8 | 34.3 | 17.8 | -1.91E+00 | 1.24E-02 | | |

Table A.8. Well D14. X, Y and Z location, Log K value, K value, mean grain size (determined by sieve analysis), and sorting (determined by standard deviation of grain size (Boggs, 2001)).

APPENDIX B:
OUTCROP ANALOGS

Symbol abbreviation

| | |
|---|------------------------------|
|  | high order bounding surface |
|  | low order bounding surface |
|  | approximate bounding surface |
|  | bed number |
|  | fining upward trends |
|  | measurements (cm) |
|  | talus |

Facies abbreviation

| | |
|------------|---|
| St | trough cross bedded sand |
| Sm | massively bedded sand |
| Sr | sand with ripple marks |
| Fsm | massively bedded silt or clay |
| Gt | trough cross bedded gravel |
| Gh | horizontally laminated gravel |
| Gu | gravel undifferentiated (no distinct bedding evident) |

Insert Key for Outcrop analogs

Table B.1. Key for Photomosaics

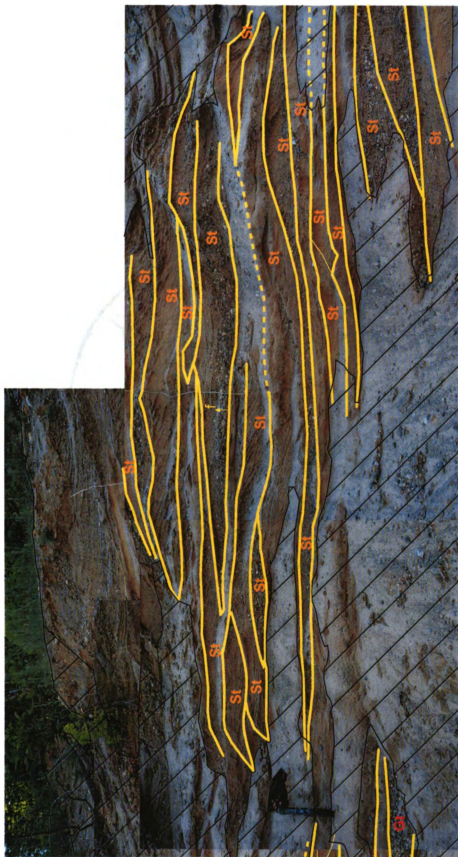


Figure B.1. Photomosaic of outcrop analog at Azon pit. Yellow lines represent bounding surfaces. Thinner lines represent lower order bounding surfaces. Shovel for scale. Image is presented in color.



Figure B.2. Photomosaic of outcrop analog at Azon Pit. Yellow lines represent bounding surfaces. Thinner lines represent lower order bounding surfaces. Shovel for scale. Image is presented in color.

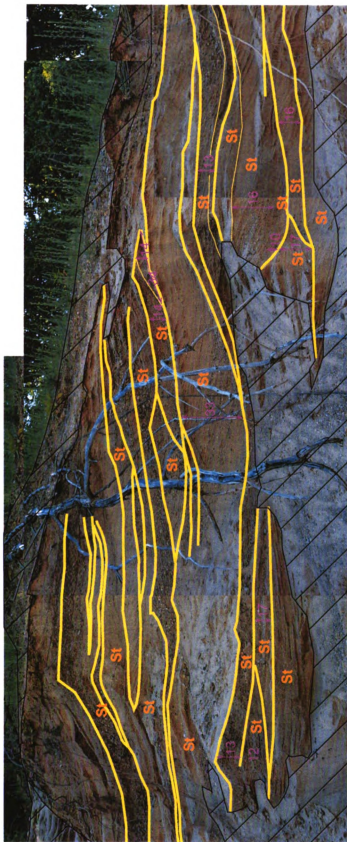


Figure B.3. Photomosaic of outcrop analog at Azon pit. Yellow lines represent bounding surfaces. Thinner lines indicate lower order bounding surfaces. All measurements are in centimeters and are shown by pink arrows. Image is presented in color.

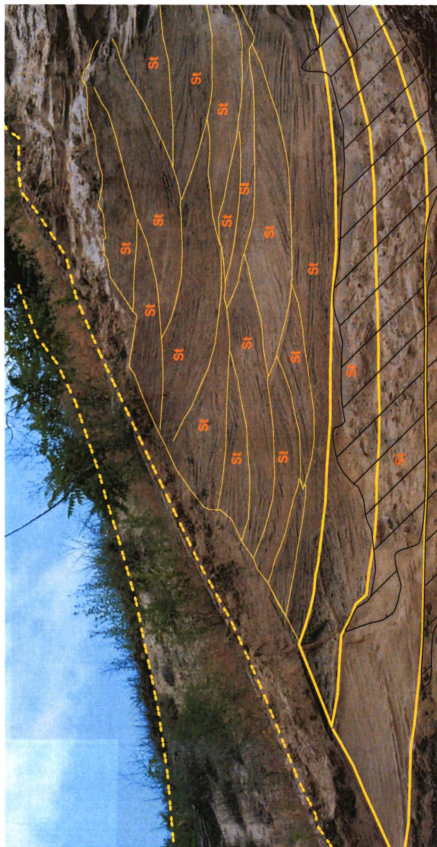


Figure B.4. Photomosaic of outcrop analog at Stadler sand and gravel pit. Yellow lines represent bounding surfaces. Thinner lines represent lower order bounding surfaces. Height of outcrop is approximately 12 meters. Image is presented in color.

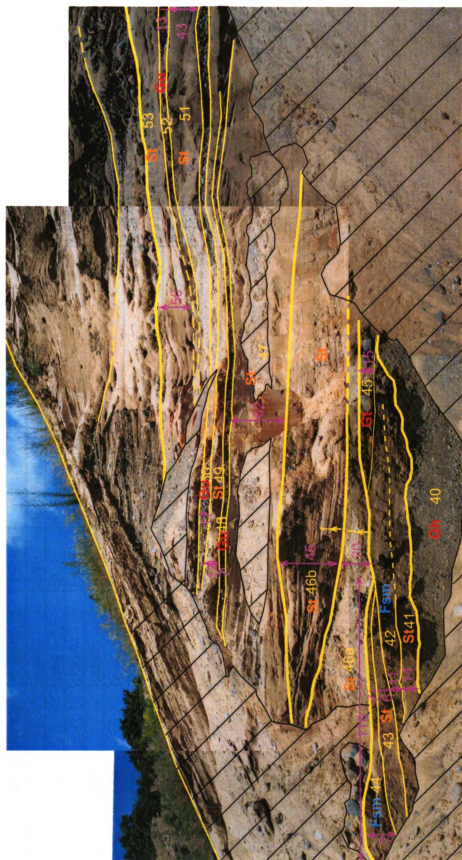


Figure B.5. Photomosaic of outcrop analog at Stadler sand and gravel pit. Yellow lines represent bounding surfaces. Thinner lines represent lower order bounding surfaces. Measurements are in centimeters and are shown by pink arrows. Bed numbers correspond to descriptions given in Table B.2. Image is presented in color.

| bed | mean grain size | sorting | facies | other | grain size range |
|-----|-----------------|------------|--------|------------------------------------|-----------------------------|
| 40 | gravel | poorly | Gm | no internal bedding, homogenous | M-sand to cobbles |
| 41 | M-sand | well | St | finest to left of photo | M-sand to F-sand |
| 42 | silt | poorly | Fsm | cobbles and pebbles at top of unit | clay to cobbles and pebbles |
| 43 | F-sand | poorly | St | | VF-sand to pebbles |
| 44 | clay-silt | well | Fsm | | clay-silt |
| 45 | cobble | V-poorly | Gt | | M-sand to boulder |
| 46a | M-sand | moderately | St | fining upward | silt to boulders |
| 46b | M-sand | moderately | St | fining upward | F-sand to cobbles |
| 47 | M-sand | well | St | no internal bedding, homogenous | F-sand to C-sand |
| 48 | gravel | moderately | Gu | partially cemented | M-sand to cobbles |
| 49 | M-sand | well | St | no internal bedding, homogenous | F-sand to C-sand |
| 50 | gravel | moderately | St | internal bedding, heterogeneous | F-sand to cobbles |
| 51 | M-sand | well | St | internal bedding, heterogeneous | F-sand to C-sand |
| 52 | cobble | poorly | Gu | | F-sand to cobbles |
| 53 | M-sand | well | St | | M-sand to F-sand |

Table B.2. Descriptions of outcrop analog shown in Figure B.5. Bed number, mean grain size, sorting, facies, other trends, and grain size range is given.

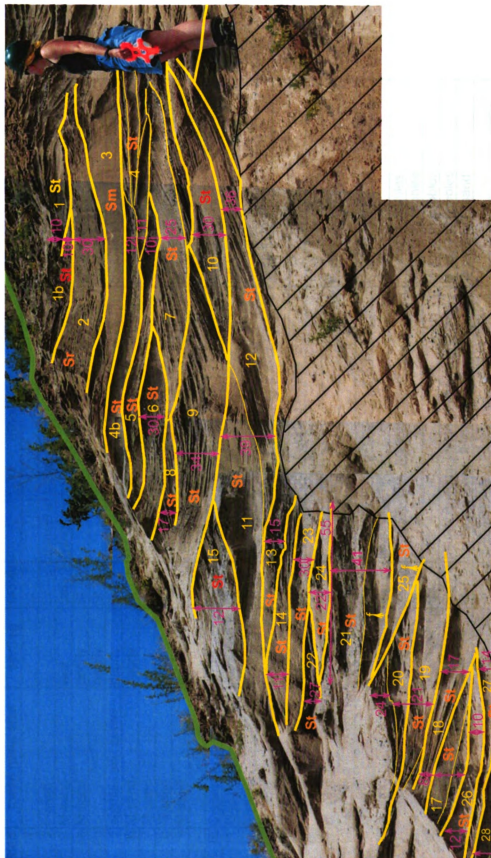


Figure B.6. Photomosaic of outcrop analog at Stadler sand and gravel pit. Yellow lines represent bounding surfaces. Thinner lines represent lower order bounding surfaces. Measurements are in centimeters and are shown by pink arrows. Bed numbers correspond to descriptions given in table B.4. Image is presented in color.

| bed | mean grain size | sorting | facies | other | grain size ranges |
|-----|--------------------|------------|--------|--|-----------------------------|
| 1 | | | St | | |
| 2 | F-sand | | Sr | coarser at bottom | |
| 3 | M-sand | well | Sm | fining upward | |
| 4a | M-sand | poorly | St | | silt to gravel |
| 4b | | poorly | St | | silt to gravel |
| 5 | pebbles and gravel | poorly | St | | cobbles to F-sand |
| 6 | M-sand | poorly | St | pebbles in layers heterogeneous | cobbles to F-sand |
| 7 | M-sand | | St | left side of bed heterogeneous | cobbles to F-sand |
| 8 | M-sand | well | St | heterogeneous, layers of coarse and fine | at right, pebbles to gravel |
| 9 | M-sand | moderately | St | heterogeneous, layers of coarse and fine | at left silt to pebbles |
| 10 | C-sand | | St | | silt to pebbles |
| 11 | M-sand | moderately | St | | silt to gravel |
| 12 | M-sand | moderately | St | | |
| 13 | M-sand | poorly | St | homogenous | M-sand to cobbles |
| 14 | M-sand | | St | | |
| 15 | | | St | heterogeneous, layers of coarse and fine | |
| 16 | | | St | | |
| 17 | M-c sand | poorly | St | homogenous | M-sand to cobbles |
| 18 | M-c sand | well | St | homogenous | |
| 19 | M-sand | well | St | homogeneous with random pebbles | M-sand to pebbles |
| 20 | M-sand | moderately | St | pebbles at base | silt to pebbles |
| 21 | M-sand | moderately | St | fining upward, heterogeneous | F-sand to cobbles |
| 22 | M-sand | mod-well | St | | M-sand to cobbles |
| 23 | M-sand | mod-well | St | | M-sand to cobbles |
| 24 | M-c sand | poorly | St | heterogeneous, layers of coarse and fine | M-sand to cobbles |
| 25 | C-sand | mod-well | St | pebbles at base, fining upward | M-sand to C-sand |
| 26 | M-sand | well | St | homogenous | |

Table B.3. Descriptions of outcrop analog shown in Figure B.6. Bed number, mean grain size, sorting, facies, other trends, and grain size range is given.

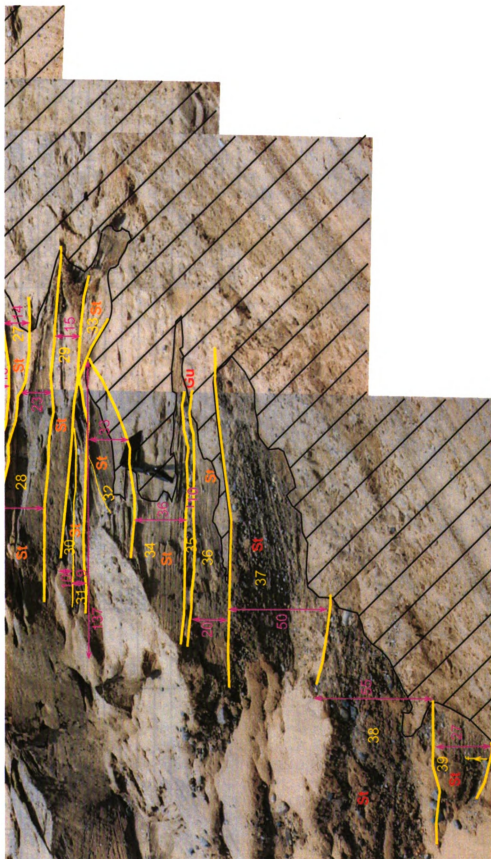


Figure B.7. Photomosaic of outcrop analog at Stadler sand and gravel pit. Yellow lines represent bounding surfaces. Thinner lines represent lower order bounding surfaces. Measurements are in centimeters and are shown by pink arrows. Bed numbers correspond to descriptions given in Table B.4. Image is presented in color.

| bed | mean grain size | sorting | facies | other | grain size ranges |
|-----|---------------------|------------|--------|------------------------------------|-------------------------------|
| 27 | M-f sand | well | St | mostly homo., some coarse lay. | med-fines |
| 28 | M-sand | moderately | St | random pebbles throughout | fine-pebbles and cobbles |
| 29 | C-sand | | St | hetero | cobbles- v fine sand |
| 30 | gravel to C-sand | moderately | St | hetero | med sand-cobbles |
| 31 | C-sand | mod-well | St | hetero | med sand-cobbles |
| 32 | M-sand | well | St | hetero | fine-pebbles |
| 33 | M-sand | well | St | hetero | fine-pebbles |
| 34 | M-sand | well | St | hetero | fine-pebbles |
| 35 | cobbles | | Gu | thick boulder/cobble layer | matrix is med. s little fines |
| 36 | M-sand | poorly | St | | fine-pebbles and cobbles |
| 37 | cobbles | | St | hetero | boulders (70cm) to fine sand |
| 38 | gravel | | St | hetero | med-boulders, a lot of coarse |
| 39 | pebbles and cobbles | | St | boulders at top, and fining upward | fine-boulders |

Table B.4. Descriptions of outcrop analog shown in Figure B.7. Bed number, mean grain size, sorting, facies, other trends, and grain size range is given.

REFERENCES

- Adams, E. E., and Gelhar, L., 1992, Field study of dispersion in a heterogeneous aquifer, 2. Spatial moments analysis: *Water Resources Research*, v. 28, no. 12, p. 3293-3307
- Anderson, M. P., Aiken, J. S., Webb, E. K., and Mickelson D. M., 1999, Sedimentary and hydrogeology of two braided stream deposits: *Sedimentary Geology*, v. 129, p. 187-199.
- Ashley G. M., 1990, Classification of large scale subaqueous bedforms; a new look at an old problem: *Journal of Sedimentary Petrology*, v. 60, no. 1, p. 161-172
- Barrese, P. G., 1991, A Hydrogeochemical Characterization of a Glacial Drift Aquifer System in Southwest Michigan: Master's Thesis, Western Michigan University, Kalamazoo, MI.
- Beard, D. C., and Weyl P. K., 1973, Influence of Texture on Porosity of Unconsolidated Sand: *The American Association of Petroleum Geologists*, v. 57, no. 2, p. 349-369.
- Benn D. I., and Evans, D. J. A., 1998, *Glaciers and Glaciation*: New York, Oxford University Press Inc., 734 p.
- Boggs, M. J., Yound, S. C., Beard, L. M., Gelhar, L. W., Renfeldt, K. R., and Adams E. E., 1992, Field study of dispersion in a heterogenous aquifer, 1., Overview and site description: *Water Resources Research*, v. 28, no. 12, p. 3281-3291.
- Boggs S. Jr., 2001, *Principles of Sedimentology and Stratigraphy* 2nd edition, Prentice Hall, Upper Saddle River, New Jersey.
- Brigham Young University, 2000, Department of Defense Groundwater Modeling System (GMS) Version 3.1., Salt Lake City, UT.
- Carle, S. F., LaBolle, E. M., Weissmann, G. S., Van Brocklin, D., and Fogg, G. E., 1998, Conditional Simulation of hydrofacies architecture: a transition probability approach, In: Fraser, G.S., Davis, J.M., (Eds.). *Hydrogeological Models of Sedimentary Aquifers, Concepts in Hydrogeology and Environmental Geology* No. 1 Society for Sedimentary Geology Special Publication, p. 147-170.
- Carle, S. F., and Fogg, G. E., 1998, TPMOD: A transition probability/ Markov approach to geostatistical modeling and simulation, User Documentation, University of California, Davis.

- Clement, T. P., 1997, A modular computer model for simulating reactive multispecies transport in three-dimensional groundwater systems: PNNL-SA-11720, Pacific Northwest National Laboratory, Richland, Washington.
- Clement, T. P., and Jones, N. L., 1998, RT3D Tutorials for GMS Users, PNNL-11805, Pacific Northwest National Laboratory, Richland, Washington.
- Davis, M. J., Wilson, J. L., Phillips, F. M., and Gotkowitz, M. B., 1997, Relationship between fluvial bounding surfaces and the permeability correlation structure: *Water Resources Research*, v. 33, no. 8, p. 1843-1854.
- Deutsch, C. V., and Journel, A. G., 1992, *GSLIB: Geostatistical Software Library and User's Guide*, Oxford University Press, London.
- Dorr, J. A. Jr., and Eschman, D. F., 1970, *Geology of Michigan*, Ann Arbor, Michigan, University of Michigan Press, p. 476.
- Davis J. M., Lohman, R. C., Phillips, F. M., Wilson, J. L., Love, D. W., 1993, Architecture of the Sierra Ladrones formation, central New Mexico: Deposition controls on the permeability correlation structure: *Geological Society of America Bulletin*. V. 105, p. 998-1007.
- Eschard, R., Lemouzy, P., Bacchiana, C., Desaubliaux, J., Parpant, J., and Smart B., 1998, Combining sequence stratigraphy, geostatistical simulations and production data for modeling a fluvial reservoir in Chaunoy Field (Triassic, France): *American Association of Petroleum Geologists Bulletin*, v. 82, p. 545-568.
- Finbeiner, K. 1994. *Subsurface Glacial Geology of the Area Between the Tekonsha and Kalamazoo Moraines, Kalamazoo County, Michigan: Master's Thesis*, Western Michigan University, Kalamazoo, MI.
- Forstat, D. W., and Sorensen, H. O., 1982, *Bedrock Geology of Kalamazoo County, County Geologic Map Series*, Michigan Geological Survey Division, Lansing, MI.
- Hess, K. M., Wolf, S. H., and Celia M. A., 1991, Estimation of Hydraulic Conductivity in a sand and Gravel Aquifer, Cape Code, Massachusetts: USGS Water Resources Investigation report 91-4034, p. 15-22.
- Hoard, C. J., 2002, *The value of Hydraulic Conductivity Data in Groundwater Flow and Transport Models of Schoolcraft Plume A. Master's Thesis*, Michigan State University, East Lansing, MI.
- Hoeksema, R. J., and Kitanidis, P. K., 1985, Analysis of the spatial structure of properties of selected aquifers: *Water Resources Research*, v. 21, no. 4, p. 563-572.

- Howell, P. D., and van der Pluijm, B. A., 1990, Early history of the Michigan Basin: Subsidence and Appalachian tectonics: *Geology* v. 18, p. 1195-1198.
- Howell, P. D., and van der Pluijm, B. A., 1999, Structural Sequences and Styles of subsidence in the Michigan Basin: *Geological Society of America Bulletin*, v. 111, no. 7 p. 17
- Hyndman, D. W., Dybas, M. J., Forney, L., Heine, R., Mayotte, T., Phanikumar, M. S., Tatara, G., Tiedje, J., Voice, T., Wallace, R., Wiggert, D., Zhao, X., and Criddle, C. S., 2000, Hydraulic characterization and design of a full-scale biocurtain: *Groundwater*, v. 38, no. 3, p. 462-474.
- Kehew, A. E., Straw, W. T., Steinmann, W. K., Barrese, P. G., Passarella, G., Peng, W., 1996, Ground-Water Quality and Flow in a Shallow Glaciofluvial Aquifer Impacted by Agricultural Contamination: *Groundwater*, v. 34, no. 3, p. 491-500.
- Klingbeil, R., Klieneidam, S., Asprion, U., Ainger, T., and Teutsch, G., 1999, Relating lithofacies to hydrofacies: outcrop-based hydrogeological characterization of Quaternary gravel deposits: *Sedimentary Geology*, v. 129, p. 299-310.
- Kolterman, C. E., Gorelick, S. M., 1996, Heterogeneity in sedimentary deposits: A review of structure-imitating, process-imitating, and descriptive approaches: *Water Resources Research*, v. 32, no. 9, p. 2617-2658.
- Krigstrom, A., 1962, Geomorphological studies of sandur plains and their braided rivers in Iceland: *Geology Annaler*, v. 44, p. 238-346.
- Leopold, L. B., and Wolman, M. G., 1957, River channel patterns: braided, meandering, straight: United States Geological Survey. Professional Paper, 282-B, p. 39-85.
- Lipinski, B. A., 2002, Estimating Natural Attenuation Rates for a Chlorinated Hydrocarbon Plume in a Glacio-fluvial Aquifer, Schoolcraft, Michigan: Master's Thesis, Michigan State University, East Lansing, MI.
- Martin, H. 1957, Outline of the Geological History of Kalamazoo County: Michigan Geological Survey Division, Open File Report.
- Mayotte, T. J., 1991, Village of Schoolcraft Kalamazoo County, Michigan Final Remedial Investigation and Feasibility Study of Remedial Alternatives, Plume A and Plume F: Halliburton NUS Environmental Corporation Project Number 4M84.
- McDonald, G., and Harbaugh, A. W., 1988, A Modular Three-dimensional Finite Difference Groundwater flow model: U.S. Geological Survey Techniques of Water-Resources Investigations, Book 6, chapter A1, Reston, VA.

- Miall A. D., 1997, A Review of the Braided-River Depositional Environment: *Earth Science Reviews*, v.13, p. 1-62.
- Miall A.D. 1996. *The Geology of Fluvial Deposits*. Springer-Verlag, Berlin.
- Miall, A. D., 1985, Architectural-Element Analysis: A New Method of Facies Analysis Applied to Fluvial Deposits: *Earth Science Reviews*, v. 22, p. 261-308.
- Moltzaner, G.L., R.W.D. Killey. 1988. The Twin Lake tracer tests: longitudinal dispersion. *Water Resources Research* v. 24 no. 10 p. 1613-1627.
- Monaghan, G. W., and Larson, G. J., 1982, Surficial Geology of Kalamazoo County: County Geologic Map Series, Michigan Geological Survey, Lansing MI.
- Monaghan, G. W., Larson, G. L., Gephart, G. D., 1986, Late Wisconsinan Drift Stratigraphy of the Lake Michigan Ice lobe in Southwestern Michigan: *Geological Society of America Bulletin*, v. 97, p. 329-334.
- Rehfeldt, K. R., Boggs, M. J., and Gelhar, L., 1992, Field study in a heterogeneous aquifer, 3., Geostatistical analysis of hydraulic conductivity: *Water Resources Research*, v. 28, no. 12, p. 3281-3291.
- Robinson J. W, and McCabe, P. J., 1997, Sandstone-Body and Shale-Body Dimensions in a Braided Fluvial System: Salt Wash Sandstone Member (Morrison Formation), Garfield County, Utah: *American Association of Petroleum Geologists*, v. 81, no. 8, p. 1267-1291.
- Sleep, N. H., and Sloss, L. L., 1978, A deep borehole in the Michigan Basin: *Journal of Geophysical Research*, v. 83, p. 5815-5819.
- Smith N. D., 1985, Proglacial Fluvial Environment: *Glacial Sedimentary Environments SEPM short course* eds. G.M. Ashley, J. Shaw, N.D. Smith, no. 16, p. 85-134.
- Steinmann, W. K., 1994, The Geological and Hydrogeological Characterization of the Schoolcraft Aquifer, Schoolcraft, Michigan: Master's Thesis, Western Michigan University, Kalamazoo, MI.
- Sudicky, E. A., 1996. A natural gradient experiment on solute transport in a sand aquifer: spatial variability of hydraulic conductivity and its role in the dispersion process: *Water Resources Research*, v. 22, no. 13, p. 2069-2082.
- Weissmann, G. S., and Fogg, G. E., 1999, Multi-scale alluvial fan heterogeneity modeled with transition probability geostatistics in a sequence stratigraphic framework: *Journal of Hydrology*, v. 226, p. 48-65.

MICHIGAN STATE UNIVERSITY LIBRARIES



3 1293 02372 6957